SPECTRAL REDUNDANCY: BROAD OVERLAPPING-BAND IMAGING WITH SIMULATED RESPONSE COMPRESSION

by

John Patric MacDonald

B.A. Simon Fraser University 1987

M.Sc. Simon Fraser University 1990

THESIS SUBMITTED IN PARTIAL FULFILLMENT OF THE REQUIREMENTS FOR THE DEGREE OF DOCTOR OF PHILOSOPHY

in the Department

of

GEOGRAPHY

SIMON FRASER UNIVERSITY

December 1995

ISBN 0-612-16988-X

PARTIAL COPYRIGHT LICENSE

Title of Thesis/Project/Extended Essay

Spectral Redundancy: Broad Overlapping-Band Imaging With Simulated Response Compression

Author:

(signature)

John Patric MacDonald
(name)

December 18, 1995
(date)

APPROVAL

Name: John Patric MacDonald

Degree: Doctor of Philosophy

Title of Thesis: Spectral Redundancy: Broad Overlapping-Band Imaging With Simulated Response Compression

Examining Committee:

Chair: R.C. Brown, Associate Professor

A.C.B. Roberts, Associate Professor
Senior Supervisor

B. Beyerstein
Associate Professor, Psychology Department

R.B. Horsfall
Assistant Professor

T.K. Poiker, Professor,
Department of Geography
Simon Fraser University
Internal Examiner

S.E. Franklin, Associate Professor and Head,
Department of Geography, University of Calgary,
External Examiner

Date Approved: December 18, 1995

Abstract

Multispectral video has been widely used in environmental remote sensing. Applications commonly employ a three camera configuration with optical filtration. Filter selection is generally determined by the spectral features being mapped. Filter combinations tend to consist mainly of discrete narrow wavebands, intended to optimize spectral resolution. Narrow band configurations of this sort are extremely sensitive to illumination changes and surface signal fluctuations over the area being mapped. Scene irradiance can vary over mapped areas to the extent that like target areas will not statistically classify as the same cover type. In an attempt to overcome this problem an analogue model of between band gain control has been tested for its utility in improving image classification and interpretation.

The model tested employed a broadly overlapping waveband configuration designed for spectral redundancy. Under induced illumination changes, in a laboratory setting, between band manual gain adjustments were employed as a brightness adaptive process. The induced illumination changes, while affecting the raw digital number (DN) values substantially, did not result in an unacceptable classification performance. While subsequent image classification failed to show a substantial improvement in classification accuracy, with the method as employed, success in restoring the relative reflectance characteristics of the target was achieved, for a subset of the conditions.

The experimental results indicate that filter selection was the critical factor affecting method performance. The overlapping range of sensitivities afforded by the spectral redundancy of the configuration, proved very useful in monitoring between band gain responses under the experimental conditions.

To my wife, Kirstie Louise Overhill, M.D., without whose unselfish support and encouragement this work would not have been possible. And to my mother, Hattie B. MacDonald, who always said "you can do whatever you put your mind to".

ACKNOWLEDGEMENTS

The author wishes to express sincere appreciation to the Natural Sciences and Research Council of Canada for supporting this research. Special thanks is extended to Arthur C.B. Roberts, Ph.D. for his assistance throughout my residency and to R.B. Horsfall, Ph.D., and to B. Beyerstein, Ph.D., for their encouragement and assistance in preparing this manuscript.

TABLE OF CONTENTS

List of Tables

Page

Tables Included in Text

Tables of Appendix A

List of Figures

Page

Figures Included in the Text

Figures and Charts Included in Appendix B

I

Introduction

Remote sensing is the science, art and technology of extracting earth's resources information, remote from the subject of investigation. A variety of imaging techniques are employed for this purpose. Methods of extracting the desired information include both visual interpretation and quantitative approaches to spectral pattern recognition. Both methods have inherent strengths and weaknesses. Much remote sensing research explores ways in which each of these methods synergistically complements the other. Spectral pattern recognition performed by human interpreters tends to be product rather than process intensive. Examples would include object recognition by color or pattern of reflectivity, such as specular reflectance from water surfaces. Many human cognitive processes appear to be shaped by training and life experience. A desire to better understand the processes underlying cognitive output has led researchers to examine the perceptual processes behind the product. Whether this approach will prove fruitful has yet to be determined; it may be akin to exploring the clockworks in an attempt to understand the nature of time.

Of the growing number of tools (sensors and analytical methods) employed by the remote sensing community, none has as yet displaced the requirement for human interpretation. Technology has provided us with tools with powerful capabilities, different than those we possess. Among these capabilities is wavelength discrimination. The ability to record and analyze discrete wavelength information is the factor separating remote sensing from its origins in aerial photographic interpretation. Target objects may be identified by their spectral reflectance properties within discrete wavebands or spectral regions defined by wavelength limits. The spectral reflectance properties of many of nature's objects are very similar within the visible portion of the spectrum. In such instances, the human eye - brain combination may see such objects as being essentially the same hue or color and confuse their identity. While other spatial cues can be employed in determining an object's identity, discrimination may still be confounded.

The task of delineating boundaries between object types in an automated procedure is what remote sensing data analysis schemes attempt to do (Lillesand and Kiefer, 1994). Once delineated by target cover types, earth's surface features can be mapped. In order to achieve success with such a scheme the features must be spectrally separable (Lillesand and Kiefer, 1994).

Both computational techniques and the devices which we employ continually improve. Video surveillance equipment, in the form of black and white or color video cameras, is widely available, inexpensive, and when configured as a multisensor array (two or more cameras, configured for different spectral wavebands viewing the same target region), can provide a valuable source of multispectral information. Used in a suitable spectral combination, multispectral information provides the remote sensing specialist with a powerful mapping tool.

Unlike electronic sensors, humans are incapable of wavelength discrimination. While apparent contradictions to this statement can be found among painters, color printers and others who work intensively with color mixture and color processes, who have developed a keen sense of color recognition, it is generally agreed that those of us considered to have normal color vision, do not posses wavelength discrimination.[1] Humans do, however, posses the ability to consistently discriminate object color under a wide variety of illumination conditions. This ability, while sometimes confounded by atmospheric effects which generate for us blue distant mountains or fiery red landscapes under the fading light of sunset, has few other natural failures.

An understanding of how the human visual system is able to effectively discount spectral variations in ambient light is yet to be determined. The continued search for an answer has revealed much about the mechanisms believed, at least in part, responsible. Among the functions involved in discounting the illuminant, is photoreceptor adaptation. The human visual

---

[1] One apparently convincing exception to this statement was reported by the clinical neurologist Oliver Sacks (1995), in The Case of the Colorblind Painter, wherein the author accounts the perceptions of an artist patient who having lost all color vision resulting from an accident, exhibited some degree of wavelength discrimination under narrow band illumination conditions.

system possesses two classes of photoreceptors, each named for its shape. The most ubiquitous of these, rods, are used primarily for dark adapted vision, the other class, cones, are tuned to broadly overlapping waveband sets for color discrimination.

The similarity between the multispectral sensors used in remote sensing and the photoreceptor sets of the eye is that both have imaging capabilities tuned to discrete spectral regions. The main difference between these two sensor types is in waveband width and degree of overlap in spectral sensitivity. Separation in spectral sensitivity is normally desirable from a photographic or electronic imaging perspective to achieve spectral separability between either photo emulsion layers or sensor products. Yet the human observer is capable of discriminating some five million colors and two hundred shades of gray, with an incredible degree of redundancy in spectral sensitivity (fig. 1.1). Each of the three sets of cones records spectrally redundant information within the regions of waveband overlap. In what seems a completely contradictory approach, we in the remote sensing community continue to design imaging configurations which avoid spectral redundancy, in pursuit of finer wavelength discrimination.

This design course is not without its vagaries. These highly sensitive devices require signal amplification which does not discriminate between system noise and signal. They also tend to be extremely sensitive to abrupt surface reflectance changes and changes in ambient light fluctuations, resulting in considerable variation in signal amplitude for a given target. Where sensor amplitude fluctuations are assumed to relate to target reflectance characteristics only, comparison between spectral waveband sets may also include spectral energy shifts, (illumination changes). When analytical comparisons between waveband sets are confounded by illumination changes, target reflectance properties must somehow be separated from scene irradiance.

A multiband radiometer is normally employed in separating target spectral reflectance from scene irradiance. Computing spectral reflectance is normally a three part process (Lillesand and Kiefer, 1994). The sensor (radiometer) is aimed at a calibration target of known stable (benchmark) reflectance. This permits the measurement of incoming radiation or irradiance at

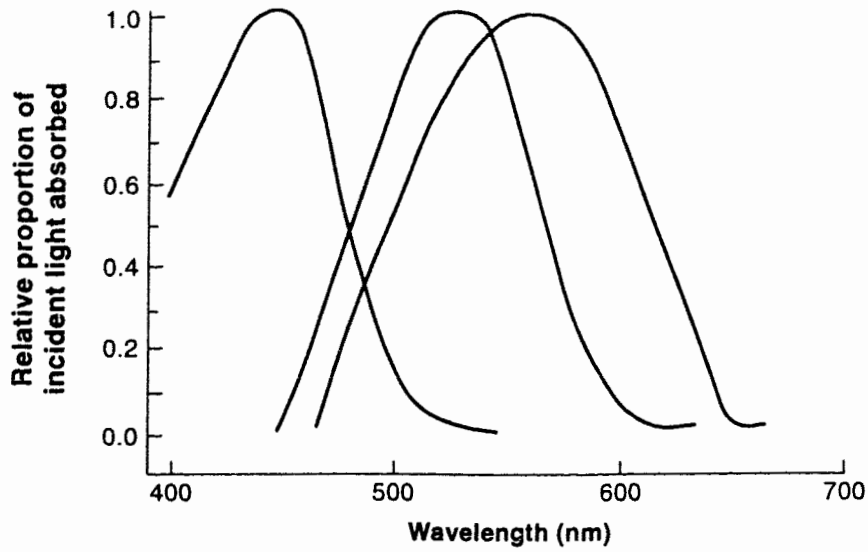

Fig. 1.1 Absorption spectra for the three classes of cones found in the human retina. Heights have been adjusted to have maxima at 1.0. [According to Cornsweet, (1970)]

the target site, as a function of wavelength. The instrument is then suspended over the target and the radiation reflected by the target is measured. The spectral reflectance of the target object is computed by ratioing the reflected energy to the incoming energy in each waveband. The result is termed the reflectance factor. Without this type of ground based measurement, target reflectance cannot be separated from scene irradiance. Measurements of this sort permit the remote sensing analyst to discount the illuminant when mapping the spatial distribution of target elements by their reflectance.

The ability of the human visual system to discount the illuminant is called chromatic adaptation. A subject of continued investigation, the physical processes believed responsible have been scrutinized by many. Just how the human visual system obtains information needed to regulate the adaptive mechanisms has been the focus of many computational approaches to chromatic adaptation and its product, color constancy. Emphasis has been placed upon theories of light sense wherein brightness constancy is considered the primary regulatory mechanism of chromatic adaptation. Speculation is offered herein regarding aspects of redundancy in human spectral sensitivity, to adaptive mechanisms.

This thesis outlines an analogue approach to chromatic adaptive imaging, based upon a spectrally redundant waveband configuration. The experiment is designed to test the ability to maintain a relative degree of sensor excitation between broadly overlapping waveband sets. The method employs between-band gain control, as a simulation model for a photoreceptor adaptation function known as response compression. The experiment is intended to evaluate the robustness of the simulation to changes in illumination quality. The method tested assumes that the spectral redundancy of the configuration affords some control over maintaining the relations of sensitivity between waveband sets, by simple gain adjustments. In doing so, an internal white region is employed as a calibration benchmark target to which between-band gain adjustments are set. The principal thesis relies upon maintaining the relative degree of sensitivity between the three waveband sets, employing the white target region within the sensor field of view, as a benchmark.

It is expected that this technique will obviate the need for computing the difference in scene irradiance between image sets, by maintaining a relative degree of sensor excitation between image wavebands and improve classification accuracy. It is further expected that the color rendition produced by the waveband configuration will also be maintained. The results of the imaging experiment are evaluated both quantitatively by image classification and graphic representations of spectral data, and qualitatively.

II

Theory

The theoretical basis underlying this thesis is addressed by component. Chromatic adaptation and its adjunct mechanisms, are the departure point for the experimental approach taken and will be discussed first. An early and fairly accurate account of the facts of chromatic adaptation was postulated by von Kries in 1878 (MacAdam, 1985). Von Kries's coefficient law states that " visual responses are proportional to the physical stimulation of each of the three sets of spectrally different sensitive receptors in the eye and that only the ratios of the coefficients of proportionality change from one chromatic adaptation to another" (MacAdam, 1985). In other words, according to the von Kries law, the relative sensitivities of the individual classes of photoreceptors remain constant as a result of adaptation (MacAdam, 1985). Since that time investigators have concentrated on determining the relative sensitivities of the three classes of photoreceptors and the mechanisms associated with adaptation.

The consequence of the attribute of color vision called chromatic adaptation is color constancy. Color constancy is the term given to the collective effects of brightness and hue constancy. Hue is the aspect of perception commonly called color (Cornsweet, 1970). Object hue tends to remain constant when the spectral composition of the source illuminant is varied over a wide range (Cornsweet, 1970). As a result the apparent brightness and color of an object remain approximately constant because the three receptor set (rgb) ratios, of object intensities within the field of view, tend to remain constant (Cornsweet, 1970).

Of the one hundred and twenty-five million photosensitive cells in the human eye, approximately six to seven million are cones (Brown and Wald, 1963:64; Leibovic, 1990), so named because of their cone shape. Due to their shape and slight differences in the refractive index inside and outside the cell, photoreceptors act as light guides

(Leibovic, 1990). The one hundred and twenty-five million rods and cones converge on one million ganglion cells, beneath the bipolar and horizontal cell layers (Leibovic, 1990). Photoreceptor diameter and spacing are ideally matched to the optical limits of resolution, with the distance between cones varying between 3 μm in the center to 5 or 6 μm in the surrounding macula (Leibovic, 1990).

Thomas Young was the first to propose that the three primary colors, red, green and blue, corresponded to the sensitivity of our cone photoreceptors, with his proposition being demonstrated by Rushton (1961), Marks *et al* (1964), Brown and Wald (1964), Paritsis and Stewart (1983). While not corresponding as we might expect to the three primary colors, the cones' broadly overlapping bands have absorption spectra with peaks near 440, 535, and 565 nm (Land, 1977). In examining color vision differences and variation in spectral position of cone photopigments Neitz *et al.*, (1991), found that long wave sensitive pigments may differ in spectral peak by 5 to 6 nm in populations with normal color vision.

Visual processing begins when light reflected from objects enters the eye. Upon absorbing photons, photopigment bleaching produces neural signals which ultimately result in the visual sensation (Cornsweet, 1970). The rate at which the photopigment bleaching occurs is protected by the depletion effects of bleaching, changing the degree of sensitivity in proportion to the fraction of unbleached pigment (Boynton, 1979). Cones can alter their range of responses to different intensities, depending on average long term brightness (Mahowald and Mead, 1991). Boynton, (1979) points out that after bleaching and pupil size are accounted for, the cones still must handle light inputs covering a three thousand-fold range and to suppose that they do so without adapting is to imply that their responses should be linearly related to their rate of photon absorption.

Boynton and Whitten, (1970) determined by electropsyiological experiment that a nonlinear relation between light input and receptor output exists, in the receptor potentials of macaque monkeys, whose vision is very similar to that of man. Boynton, (1979), concluded that the three factors combined in shrinking the range of cone responses included (1) dilation of the

pupil; (2) bleaching of the cone photopigments; (3) nonlinear cone response. Boynton, (1979) identified other temporal characteristics of photoreceptor potential that are not dealt with by the response compression model. He noted that as adaptation level increased, the light intensity required to elicit a response also increased and acknowledged that this is the prime manifestation of adaptation (Boynton, 1979).

Boynton (1979), noted that adaptation is selective within receptors and their associated pathways and points out that if the eye were neutrally adaptive the appearance of chromatic materials of different colors would not be resistant to moderate changes of the source illuminant. For example, if the source illuminant is dominated by the long wavelengths, an object's reflectance would, in comparison with white light, affect the longwave (red) cones more than the middlewave (green) cones, making those objects appear more reddish than normal (Boynton, 1979). Instead, objects in the environment, reflecting more of the long wavelengths than they would under white light (broadspectrum illumination), will mediate the selective adaptive effect, of the red cones relative to the green cones, restoring the appearance of such surfaces, to the same hue that would have prevailed under white light (Boynton, 1979). Many lateral pathways are known to exist between cones and cone pathways, making it possible that the absorption of light in red cones might also alter the sensitivities of the green and blue (shortwave) cones, even if the two do not absorb a single photon (Boynton, 1979).

Much research has followed regarding the influence of chromatic adaptation upon color discrimination. Hita *et al.*, (1989), found that an overall worsening of discriminatory capacity occurs under red adaptation conditions, and with adaptation to green a marked improvement in discrimination followed. This marked improvement in discrimination was no doubt due to the fact that the peak sensitivity of the human visual system is in the green-yellow spectral region at approximately 555 nm (MacAdam, 1985). Hita *et al.*, (1989) determined, that for pairs of stimuli, a particular adaptation altered the response of the corresponding chromatic channel, without producing any significant change in the others.

While adaptation to ambient light levels is generally acknowledged as playing a role in both color and brightness constancy, the nature of the adaptive transforms and contributing mechanisms is poorly understood (Hayhoe and Wenderoth, 1991). There is, however, a general level of agreement that the adaptive transformations involve gain control mechanisms (Barlow, 1965; Barlow and Levick, 1969; 1976; Andelson, 1982; Geisler, 1981; Walraven and Valeton, 1984; Hayhoe *et al.*, 1987; Hayhoe and Wenderoth, 1991). Hayhoe and Wenderoth (1991) propose that following the absorption of quanta, the photoreceptor signal is attenuated by a multiplicative gain control mechanism, which they attribute to some kind of feedback. The signal is then further reduced by subtractive lateral inhibition, followed by another subtractive mechanism, which slowly removes most of the original signal (Hayhoe and Wenderoth, 1991). Hayhoe and Wenderoth (1991), note, however, that it is not very clear where the gain control mechanisms reside or if one mechanism alone could perform the different functional requirements for both brightness and color adaptation. Hayhoe and Wenderoth (1991), propose two separate mechanisms for brightness and color constancy, wherein color constancy only requires compensation for changes in the distribution of excitation across the three cone types.

Land (1964; 1977; 1983), asserted that color sensation results from a comparison of excitation between cone sets, affected by each point in a scene, including a reference point. The reference point is the point in the scene with the highest "integrated reflectance" in all three receptor sets and may be considered analogous to a benchmark to which the lightness of all other perceived objects is calibrated (MacDonald, 1989). In most, if not all images, objects having the highest integrated reflectance in all three receptor sets will result in the perception of white (MacDonald, 1989). Land's (1959;1977), theory asserts that the final perceptual response of the visual system is lightness. Experiments conducted by Land and McCann (1971), indicated that color perception is partially independent of electromagnetic energy flux (changes in the rate of energy flow across and object or scene), and wavelength (MacDonald, 1989). These observations were further supported in similar experiments by Arend *et al.*, (1991).

Unlike other imaging sensors, only the eye is capable of this type of chromatic adaptive performance. Photographic film is not as versatile and is highly affected by shifts in wavelength. When one uses daylight color film indoors under tungsten light, the resulting photograph appears saturated by yellow light, resulting from the dominant wavelength of the source illuminant.

How does the human visual system record true object lightness? According to Land (1977), each photoreceptor set (red, green and blue) integrates for each point in a given scene the influence of the light of all wavelengths to which the cone set is sensitive, then compares the degree of excitation of the cone sets that encode the same color at the reference point. Land (1977), speculated that the human visual system arrives at a given color sensation, through the comparison of the three (rgb) lightness sensations, and provided several arithmetic models, illustrating how the comparison could be made.

Of key importance is the similarity of performance between the theoretical mechanisms believed responsible for chromatic adaptation. It is generally believed that at some point early in the visual process, the ratios of the outputs of the three cone types are measured in maintaining chromatic adaptation. This widely embraced view, that object color depends on the relative degree of excitation between receptor sets rather than the absolute amount of reflected light, dates as far back as Ernst Mach (Marr, 1982). This view persists among modern color vision theorists (Helson, 1938; Judd, 1940; Cornsweet, 1970; Land and McCann, 1971; Boynton, 1979; Marr, 1982; Hayhoe and Wenderoth, 1991).

Computational Approaches to Color Constancy

Hilbert (1987), noted "The existence of color constancy establishes the lack of correlation between perceived color and any characteristic of light but at the same time suggests another possibility for the objective basis of color". Hilbert's principal thesis: color is surface spectral reflectance. "If this identification can be successfully defended, then the objectivity of colors will be established". ..."If color is reflectance, then it is possible in principal to determine the colors of objects without making use of the characteristics of human color experience". Probably unknown

to many researchers reported herein, Hilbert's (1987) assertion forms the basis for many computational approaches to color constancy.

Computational approaches to achieving color constancy have been in the forefront of color research for most of this past decade. Approaches have varied as differing degrees of success have been accomplished. Some models are based upon determining the specifications of a surfaces spectral reflectance functions and ambient light spectral power distributions, from which the expected color signal is calculated (Wandell, 1987). The underlying assumption of this model type is that the spatial variation of the ambient light is slower than the spatial variations of the surface's reflectance function (Wandell, 1987). The underlying implication is that the spectral power distribution remains constant over a local region of the image, within which there is significant spatial variation in the surface spectral reflectance function (Wandell, 1987). The calculation of photoreceptor responses, based upon a calculation advocated by Cornsweet (1970), must be made for every image point, after which display device intensities can then be adjusted, with the synthesized colors having the same visual effect as if the observer had been in the same position as the camera (Wandell, 1987). Models of this type reportedly work well for rendering color constant the images recorded by color video cameras. Remote sensing applications requiring standard three color images for reconnaissance purposes would no doubt benefit from corrective models of this type.

Finite-dimensional linear models, such as that proposed by Gershon *et al.*, (1987), have been among the more successful models. The idea behind the model is to describe surface reflectances by estimating the illuminant and using the estimated illuminant, obtain color descriptors. The method incorporates the use of a finite-dimensional linear model which represents light sources and reflectances (Gershon *et al.*, 1987). An assumption common to the above mentioned color constancy models is that the color of the illuminant is constant throughout the imaged scene.

Finlayson *et al.*, (1995), have more recently produced a color constancy algorithm which defines color descriptors for a set of possible illuminants. This algorithm exploits the constraint

inherent in the fact that illumination is usually spectrally varying rather than constant and outperforms the aforementioned otherwise constrained models (Finlayson *et al.*, 1995). The producers of image processing software have yet to adopt and distribute software incorporating any of the aforementioned color constancy models for use in every day remote sensing applications. Software generation and distribution is hopefully forthcoming.

Recent advancements in computational approaches to color constant imaging show much promise, however, their utility in applied remote sensing has yet to be determined. Within the remote sensing community, color composite imaging of the type to which the outlined computational approaches could be applied, remains only a small part of the total imaging performed. One common factor shared by the aforementioned approaches is that each method is applied *a posteriori.* The only disadvantage with this application, from a remote sensing perspective, is that a remote sensing specialist must perform a number of existing permutations between data collection and map accuracy assessment; increasing this by a significant amount will eventually affect productivity. For this reason alone, approaches toward chromatic adaptive imaging requiring little *a posteriori* processing, should be pursued.

Photoreceptor chromatic adaptation is a complex process and research is ongoing as to what the adaptive mechanisms are and exactly where the processes take place. While the implications of various research findings and their relation to color vision theory go much further than what is reviewed herein, the relative selective adaptive effect and between band sensitivities, carry important implications for multispectral digital imaging. The experimental procedure herein is designed to determine to what degree, overlapping range (band) sensitivities would provide the between-band gain responses required of a feedback mechanism for a multiband video imaging system. Finally, would between-band gain control produce chromatic adaptive video imaging?

Brightness Constancy and Chromatic Adaptation

Brightness constancy means that the apparent lightness sensation of an object tends to remain constant despite changes in illumination falling upon it (Cornsweet, 1970). For example, when viewed in ordinary room light, an ordinary piece of white paper reflects about 90% of the light incident upon it, while a piece of black paper reflects about 10%. When viewed in direct sunlight the increase in intensity may be 1000- fold, yet the papers retain the same apparent relative brightness as when viewed indoors (Cornsweet, 1970). Various researchers have confirmed this phenomenon (Land, 1959;1977; Graham, 1965; Cornsweet, 1970; Boynton, 1979; Brou *et al.*, 1986; Arend *et al.*,1991). Arend *et al.*, (1991), found that in subjects tested, lightness matches were remarkably invariant over a nineteen to one (19:1) luminance range. Luminance is the technical term referring to the intensity per unit area of light incoming from a surface towards the eye (Boynton, 1979). Most subjects show only minor departures from perfect brightness constancy. Exceptions arise when illumination is confined to small illuminated patches which exclude the background and surrounding areas (Cornsweet, 1970).

Upon examining data collected by Heinemann (1955), Cornsweet (1970), concluded that an object's lightness or apparent brightness depends not only on the intensity of light falling on the retinal image of a point, but on the relations between the intensities within the entire field of view of the region including both the point and its surround.

It is widely accepted that the three retinal cell layers, photoreceptors, horizontal, and bipolar cells, adapt to widely varying amounts of incoming light and in doing so, adapt their response to produce a signal with a much narrower dynamic range. Some of the functions presumed to be performed by these three cell layers have been reproduced electronically to model each cell layer's role in response compression. Mahowald and Mead (1991), produced an elegant example of the adaptive functions of the first three cell layers, revealing how the retina copes with varying inputs by stages. The following account of cell structure and performance to which they modelled their design, describes the performance of their silicon retina. The first layer of rods (hypersensitive photoreceptors used mainly after dark adaptation) and cones convert

incoming light to electrical signals. The second layer makes connections to both photoreceptors and bipolar cells through the triad synapse. Each horizontal cell is connected to its neighbour by gap junctions through which ions diffuse. The potential of any horizontal cell is determined by the spatially weighted average of the potentials of its surrounding cells, with nearby cells contributing more than distant ones.

Bipolar cells receive inputs from photoreceptors and a horizontal cell then produces a signal proportional to the difference between the two. Bipolar cells have an even narrower dynamic range than rods and cones. Bipolar cell responses are enhanced by the triad synapse which mediates, by reducing response to a uniform intensity, to provide feedback between horizontal cells and cones. The bipolar cells do not respond to absolute scene brightness but to the difference between the photoreceptor signal and the local average computed by the horizontal cell network. Both photoreceptors and horizontal cells produce logarithmic signals, thus the output of the bipolar cells corresponds to the ratio of the local light intensity to the background intensity, regardless of absolute light level (bipolar o/p = local intensity / background intensity). Mahowald and Mead (1991), postulate that local intensity includes response compression and the background intensity is the local average computed by the horizontal cells. The intensity ratios enable the retina to see detail in shaded and bright areas within the same scene. They report that their silicon retina behaved remarkably similar to the biological system in terms of response compression and optical illusions (simultaneous contrast, Mach bands, and Herring grid).

Similar to human visual processes, the digital retina entirely lost an image without constant scanning motion, further indicating that only changes and differences convey information (Mahowald and Mead, 1991).

To what degree and indeed whether or not the same mechanisms are responsible for both color and brightness constancy is yet to be determined. For some theoretical models, a brightness constancy mechanism alone would provide color constancy. Land's (1964; 74; 77; 86) color vision theory asserts that the final perceptual response of the visual system is lightness.

Land (1977), postulated that the human visual system arrives at a given color sensation, through the comparison of the three cone system (blue (440nm), green (535nm), and red (565nm)) lightness sensations on a point by point basis, with the process taking place somewhere between the retina and cerebral cortex of the brain. Land (1977) termed the comparator systems retinexes. The point by point comparison was made by ratioing the reflected brightness between neighbouring points and scaling the resulting quotient to a reference point (MacDonald, 1989).

While proposing two separate mechanisms for brightness and color constancy Hayhoe and Wenderoth (1991), postulate that the requirement for color constancy only demands compensation for changes in the distribution of excitation across the three cone types. They speculate that some type of gain control mechanism, operating on receptor set ' feedback ' would fulfill this requirement. Under the conditions of a theoretical model such as Land's (1977) retinex model, some form of between band gain control could satisfy the requirement set out by Hayhoe and Wenderoth (1991) and Land's (1977) model. Using this type of model, the requirement for a feedback mechanism may not be completely necessary. The degree of band overlap between photoreceptor sets proposed by Brown and Wald (1963:64) and adopted by Land (1977), could provide sufficient overlap in sensitivity to minimize feedback requirements. Overlapping range of band sensitivities, should produce overlapping responses to shifts in radiant energy flux. If this were the case, Boynton's (1979), postulated depletion effects of bleaching, would provide somewhat of a between-band gain control and in effect, provide the capability for changing the relative degree of sensitivity between receptor sets at least within a portion of the range of overlap.

Brightness Constancy and Chromatic Adaptive Imaging

While much research interest has been focused on separating and identifying mechanisms of brightness and color constancy in human color vision, the problem can be simplified somewhat in terms of a multiband elector- optical imaging system. The question to be answered is, in terms of a multiband video imaging system, whether brightness constancy alone

would provide chromatic adaptive imaging capabilities, given sufficient overlap in band range sensitivities? The signal output from a single black and white (panchromatic) video camera can be considered analogous to the signal output by a single photoreceptor set. Both the video sensing array and the photoreceptors convert the incoming light to electrical signals.

The video gain control performs a function analogous to Boynton's (1979), theorized response compression. Video gain control sets the gain of the output video device to produce a signal of a fixed dynamic range of one hundred standard divisions, over one volt, peak to peak (1V p-p). In doing so, video gain is capable of adapting the output signal to widely varying amounts of incoming light. In terms of raw gain (voltage), the manual gain adjustments used for the experiments conducted herein represent a luminance range of compression/expansion of approximately eight-to-one (8:1). The range of luminances tested herein represent less than half the range capabilities of human subjects of nineteen-to-one, (Arend *et al.*, 1991), . The Sony XC-75 cameras used for these experiments are, however, capable of handling an overall luminance range equal to or greater than that of humans. The video gain control can, therefore, be considered approximately analogous to the much hypothesized "gain control" function of response compression.

By monitoring the output voltage of three panchromatic video cameras, with broadly overlapping band configurations, and controlling their output voltages by manual gain adjustments, an approximate analogue of response compression may be achieved.

Broad vs Narrow Band Sensor Configurations

Broad band imaging has been the most widely used method of imaging for mapping and reconnaissance purposes. One method of broad band imaging commonly used is that of panchromatic photography. The decade before the launch of the first satellite remote sensing systems (ca. 1970), saw the most experimentation with broad band photographic imaging, primarily for underwater photographic applications such as water column penetration (Boller and

McBride, 1974). Non-photographic broadband imaging clearly has advantages over narrow band configurations in terms of higher signal to noise performance, reducing background electronic noise or the extraneous unwanted responses associated with any electronic system (Lillesand and Kiefer, 1994). As well, broadband configurations tend to produce a greater range in the levels of signal sensed. Spectral resolution, or the ability to discriminate fine spectral differences is sacrificed somewhat by increasing bandwidth.

This sacrifice can be compensated for statistically in many cases. One has to realize that fine spectral differences are not necessarily lost using broad band configurations, they are merely aggregated within the overall information. In other words, broad band sensor configurations covering the same spectral peaks as narrow band sensor configurations are capable of collecting the same spectral information reflected from a target. That information must be separately differentiated from the aggregate of information captured. Narrow band configurations, on the other hand, are designed to capture only the reflected information characteristic of one target or cover type within the scene, excluding the aggregate of adjacent target reflectances. The overall objective of narrow band sensing is to capture what is commonly referred to in remote sensing as the "spectral signature" of a target. Target spectral signature implies that the spectral response patterns of given targets are unique or in some way absolute. In the natural world, however, spectral response patterns may not be as distinctive and are not necessarily unique.

Experiments conducted by Dekker *et al.*, (1992) on the effect of spectral bandwidth on spectral signature analysis of inland waters using imaging spectrometer measurements, suggested a minimum bandwidth of 10 nm. Dekker *et al.*, (1992), concluded that, for the reasons of expense associated with increased data handling, longer integration times as absolute radiance levels decrease, the occurrence of shifts in spectral features within and between target areas, and decreased signal to noise performance, bandwidths narrower than 10 nm should be avoided. Frequently, the range of values (variance) captured by narrow band sensors, lacks sufficient breadth for reliable discrimination by classification algorithms.

For example, Zacharias *et al.*, (1992), using a set of bandwidths ranging between 3.6 to 27.8 nm, selected for their ability to differentiate between intertidal vegetation types, were unable to obtain reliable classifications. They reported that the only reliable classifications obtained were those created using Principal Components Analysis (PCA) images as input bands. This technique amounts, in effect, to creating a set of broad band images by aggregating a set of narrow band images to improve classification.

Principal Components Analysis, also referred to as factor or Karhunen-Loeve analysis, can be used to identify those image components which represent the greatest contribution in terms of total variance contributed, as designated by output component images (Jensen, 1986). The technique is intended to decrease the dimensionality or number of bands in a data set that must be analyzed to produce reliable results. The application of a PCA transformation to correlated remote sensor data will result in an uncorrelated multispectral data set, having ordered variance properties wherein the transformed data contain as much information as those from the original data set (Jensen, 1986).

In examining the relations between the derivatives of remotely sensed data when correlated with known spectral features, Philpot (1991) found that second and third derivatives are most sensitive to spectral features of about 30 to 40 nm bandwidths. Philpot (1991) noted that there are no pronounced reflectance features with a characteristic bandwidth less than 30 nm for water and none less than 20 nm for certain vegetation types with the exception of the "high slope" region around 700 nm. Philpot (1991) further noted that large bandwidths are required to avoid high frequency atmospheric spectral fluctuations. He concluded that reliable correlations with detectable features, tended to be within broader bandwidths.

With the advent of charge-couple devices (CCDs) used in both one dimensional linear arrays such as the Multispectral Electrooptical Imaging Scanner (MEIS II), and the two dimensional arrays, including CCD cameras and imaging spectrometers such as the CASI, spectral configurations have focused on hyperspectral or narrow bands . Very little attention has been paid to bandwidth, with even less attention paid to band overlap. Vora and Trussel (1993)

prescribed a set of scanning filters for the accurate scanning of color images. They postulate that scanning filters need not be exact duplicates of CIE (Commission Internationale de L' Eclairage / International Commission on Illumination) color matching functions, but need only be a nonsingular transformation of them. The CIE tristimulus values (method adopted by the CIE for evaluating a color in terms of calibrated amounts of primary stimuli: X (red),Y (green),and Z (blue))[2] are measured with respect to one of a set of standard illuminants. The source illuminant is incorporated in the color matching functions, to define a subspace by a set of vectors. The defined subspace for a given illuminant is termed the human visual subspace (HVSS). Vora and Trussel (1993), note that the accurate calculation of CIE tristimulus values is possible only if the space spanned by the color scanning filters includes the HVSS for the illuminant. They also note that a set of three scanning filters that spans the HVSS is not realizable because of limitations of the filter fabrication process. Vora and Trussel (1993) recommend a four filter set (Kodak Wratten filters: Wr. 52, Wr. 49, Wr. 72B, and Wr. 57), which with the inclusion of the fourth filter, spans the HVSS.

In summary, narrow band sensors, are designed to optimize spectral resolution, achieving the greatest number of discrete lightness values possible for a given target. These sensors must be very sensitive in order to output a signal significantly stronger than the level of system noise, since noise can mask signal fluctuations that are weak in comparison to the level of noise. As noise levels increase even the strongest signal fluctuations can be masked. The quality of the output can be specified by a signal to noise ratio (S/N). The S/N ratio directly affects spectral resolution, as well as radiometric resolution, or the ability to detect slight radiance differences.

---

[2] The method consists of dividing the visible spectrum into a suitable number of equal wavelength intervals, determining the contribution to the tristimulus values made by the light within each interval, and summing the results (MacAdam, 1985) For a more comprehensive review see MacAdam, (1985).

Another factor affecting S/N performance is change in radiant energy flux. Narrow band sensors are extremely sensitive to changes in radiant energy flux as well as to abrupt surface signal fluctuations. In the worst scenario this can result in unusable imagery, even in less extreme cases scene irradiance from one image frame to another can change to the extent that the same target in two adjacent frames will not statistically classify as the same cover type. Broad band sensors are not as adversely affected by noise as are narrow band sensors and have, therefore, improved S/N ratios. Human color vision research has indicated that visual redundancy plays a significant role in chromatic adaptation and spectral pattern recognition (Cornsweet, 1970; Boynton, 1979; Shipley and Shore, 1990; Wang *et al.*, 1991). Redundancy between spectral bands may prove extremely useful in chromatic adaptive imaging where changes in radiant energy flux may not be adequately modelled.

Discounting the Illuminant

Methods akin to the CIE colorimetric specification and those reviewed under the section dealing with computational approaches to color constancy all have one thing in common. They involve the source illuminant, in color specification. As previously mentioned, for purposes of remote sensing, where natural color images are desired for purposes of interpretation or analysis, such methods, or variations on the theme, represent logical approaches. These methods are, however, only appropriate given the assumption that the source illuminant may be determined or in some way, can be approximated. Among the color constancy research community, criticism has centered around the limitations of 'unrealistic assumptions'. Those assumptions include the requirement of a white reflecting region, planar surfaces, no specularities, the constancy of illumination, and the constancy of surface reflectance (Finlayson, 1995; MacDonald, 1989). One might include in this list of criticisms the requirement of accounting for the source illuminant.

Land's (1977) retinex theory tends to be the one model that provides a means by which the illuminant can be discounted, although requiring the inclusion of a white region. Other computational approaches independent of ambient light flux have limited utility in remote sensing

applications because of other limitations, including knowing the average spectral reflectance functions of all objects within an image (Buschbaum, 1980). Variations on the approach postulated by Buschbaum (1980) have since then focused on estimating the chromatic component of the ambient light (Maloney and Wandell, 1986; Gershon *et al.*, 1987; Finlayson, 1995; Finlayson *et al.*, 1995).

Brightness and hue constancy (hue constancy being the analogue of color constancy (MacDonald, 1989)), are the underlying assumptions incorporated into integrated reflectance procedures by Land *et al.* (1971;1977). Both phenomena are contingent upon the relative reflectance of an object and its surround. While Land's (1977) method for calculating integrated reflectance of an object scene fails the color constancy test in some accounts (Maloney and Wandell, 1986), it remains, from a remote sensing perspective, the best departure point.

Particularly in the realm of multispectral digital video, remote sensing applications rarely employ band selections conforming to the filter specifications required for computing color constancy descriptors. Band configurations are normally determined by the application. Estimations for filter requirements for band configurations are made based upon the spectral response patterns of intended targets. Target areas are rarely homogenous, or restricted in homogeneity by scale and resolution. Surface reflectance varies almost continuously. Fluctuation in radiant energy varies as well, generally by unknown amounts. The need for a simplified approach to chromatic adaptive imaging has yet to be satisfied. The computational approaches to color constancy satisfy only a portion of the requirements of remote sensing applications. Most are computationally carking at best, given the amount of imagery associated with large remote sensing projects. As well, the dependency upon retrieving the source illuminant may be the reason many color constancy algorithms have not left the labs of their inventors to appear in image processing software packages. Any means of discounting the illuminant has ,therefore, a special appeal to the remote sensing and mapping sciences community.

Summary

The widely accepted view that color constant sensations result from the relative degree of excitation between three sets of photoreceptors with broadly overlapping wavebands whose range of sensitivities is under continuous adjustment, is the departure point for this experimental project. Assuming that Land's (1977), assertion that the final perceptual response of the visual system is lightness, and that each waveband set has its own characteristic response to the light stimulus of a scene with the final response being determined by the relative lightness between waveband sets, it is reasonable to assume that waveband overlap may contribute significantly to chromatic adaptation. While analytical procedures for color constancy corrections abound, and color constancy appears to be a product of chromatic adaptation, to the best of my knowledge, chromatic adaptive imaging procedures are not available.

An analogue approach to chromatic adaptive imaging, based upon the analogue conditions apparently exhibited by the human visual system's chromatic adaptive functions, was tested. A three waveband filter set which approximates the absorption spectra of the three photoreceptor (cones) sets, is not available. Three Kodak Wratten gelatin filters (Eastman Kodak, 1981), having transmittance peaks near the peak sensitivities of the three sets of cones were substituted. With the (short waveband), representing blue, (middle waveband), representing green, and (long waveband), representing red, the products of the three were combined in a color additive mixture, for color rendition. Peak transmissions of these filters do not exactly match cone sensitivity peaks, but they are close and perhaps more importantly have similar band overlap and extend reasonably close to the overlapping spectral ranges of the absorption spectra, as determined by Brown and Wald (1963;64) and used by Land (1977).

The degree of overlap afforded by the three waveband configuration permits overlap in band sensitivities. This overlap in sensitivities means that induced radiant energy shifts should produce overlapping effects between waveband sets. Overlapping effects can be used to

monitor overlapping sensor responses. By adjusting gain settings manually in a compensatory manor, some relative degree of sensor excitation should be maintained. The key element to reliably maintaining the relative degree of sensor excitation is contingent upon the availability of a white target region within the sensor field of view.

Considered a constraint to some degree, the inclusion of a white region may not be problematic in an applied setting. Consultation with video technical staff has revealed that such a demand may be accommodated by the superimposition of a white reference within a camera's angular field of view. A one millimeter thick chip of magnesium oxide has the properties of a perfect diffuse reflector and if illuminated by light reflected from the scene may be sufficient. Satisfying the requirement for an appropriate white reference in an airborne application demands testing a variety of possible techniques. For laboratory experimental purposes the inclusion of a white target region is satisfied by the color target used. The white target region acts as a benchmark to which each sensor is calibrated. The one hundred standard divisions, over which the 1V p-p video signal is maintained, uses the white target region for its 1 volt, peak setting.

By maintaining video responses to the benchmark setting the relative degree of sensor excitation can be maintained. An electronic device (waveform monitor) used to monitor video output, configured to be switchable between sensors, would permit overlapping band responses to be monitored and compensated for by manual gain adjustments. This technique provides the necessary feedback routine required for response compression. Success is contingent on the underlying assumption that sensor wavelength sensitivities and gain controls are sufficiently similar to produce like responses. A second assumption is that the relative lightness between target regions, within each individual waveband set, remains relatively unchanged with changes in radiant energy flux. It is not unrealistic to expect that, given sufficient band width, this condition can be maintained.

Each of the three spectral bands has its own characteristic response to the light reflected from the target. Target regions reflecting blue light have their highest reflectance or appear brightest in the blue waveband, their mid-range reflectance in the green waveband, and their

lowest reflectance in the red waveband. Similarly target regions reflecting red light have their highest reflectance in the red band, their mid-range and lowest reflectance, in the green and blue bands respectively. Given the assumption that these relative reflectances can be maintained by gain adjustments, an approximate analogue of response compression would result.

The series of adjustments described has been referred to herein as simulated response compression (SRC). While the series of adjustments is intended to result in a form of chromatic adaptation, the product of chromatic adaptation, color constancy, in its truest form, is not the expected outcome. The term color constancy infers a replication of true color as perceived by a human observer with normal color vision. The color rendering capability of the filter set used is not expected to reproduce a true color rendition of the target. The product of chromatic adaptive imaging, therefore, is not in this case color constancy, but rather a maintenance of the relative target reflectance / absorption characteristics between waveband sets, regardless of changes in illumination. One might expect that the color rendition produced by an additive mixture of the three waveband set, under the illumination condition of an equal energy spectrum (white light), would be maintained by applying SRC.

The intention of chromatic adaptive imaging is primarily to improve image classification results. By maintaining constancy of target reflectance / absorption characteristics under conditions of changing illumination, the repeatability of target identification should improve. This premise should hold true for both visual interpretation and statistical classification procedures.

III

Experimental Methods

Analogue Chromatic Adaptation

"If the illumination falling upon all scenes were constant the design of cameras and eyes could be greatly simplified" (Boynton, 1979). Boynton pointed out that the sensitivity range of the three sets of cone photoreceptors is under continuous adjustment over a range of luminance of approximately a million-to-one (1×10^6 :1), with each eye adjusting independently. He adds that cones are analogue devices, in the sense that they generate signals of graded amplitude. After photopigment bleaching and pupil size is accounted for, cones still handle light inputs over a three thousand-fold range and, if cone responses were linear and nonadapting, the problem of interpreting their signals by the horizontal and bipolar cells, would be similar to trying to meter voltage from one to three thousand volts without changing meter ranges (Boynton, 1979).

Photoreceptor adaptation is a complex process. Three mechanisms for adaptation are photopigment bleaching, pupillary constriction, and photoreceptor response compression. Response compression has been demonstrated by Boynton and Whitten (1970) to be the third retinal adaptive process after bleaching and pupil size are accounted for. Response compression is the nonlinear receptor adaptive process which permits the cones to handle a wide range of light inputs, providing in effect, a type of gain control (Boynton, 1979). It is not, however, just the sensitivity of a single photopic system under continuous adjustment, but that of a system with three inputs, capable of changing apparent color (Boynton, 1979). The most critical function of the first three cell layers of the retina (photoreceptors, horizontal and bipolar cells) is adaptation. Photoreceptors, horizontal, and bipolar cells adapt to widely varying amounts of incoming light and in doing so adapt their response to produce signals within a much narrower dynamic range (Mahowald and Mead, 1991).

The output from a panchromatic video camera can be viewed as analogous to the output from a photoreceptor cone set. Both the video sensing array (CCD) and the photoreceptors convert incoming light to electrical signals. As well, both produce nonlinear output. While the nature of adaptation transformations and their contribution to both brightness and color constancy are poorly understood, there is general agreement that the adaptive transformations involve multiplicative gain control mechanisms (feedback) as originally proposed by Barlow and Levick to accomplish a steady state sensitivity (Barlow, 1965; Barlow and Levick, 1969, 1976; Hayhoe and Wenderoth, 1991). The human visual system's overlapping range of sensitivities has important implications for chromatic adaptive video imaging, referred to herein as simulated response compression (SRC), which deserve investigation. This degree of overlap in spectral sensitivity could, in a video imaging system, provide the between-band feedback (SRC) necessary to compensate for spectral shifts which would otherwise result in poor color renditions in target reproduction.

Sensor Configuration

The experimental methods considered were intended to test the utility of chromatic adaptation imaging by between-band gain control (SRC). An analogue version of response compression was accomplished using three CCD (Charged Coupled Devices) video cameras, a waveform monitor to measure output voltage and controlled lighting. The three unfiltered panchromatic cameras, were first boresighted within a horizontally configured mount designed inhouse and built in the Simon Fraser University machine shop. This mount permitted removal of X and Y parallax by setscrew adjustment, permitting two to three pixel camera alignment. A standard tripod mounting thread was tapped into the base of the three camera mount.

Camera Registration

Boresighting was accomplished by first examining a two band, two color composite image of the MacBeth color checker test pattern of twenty-four scientifically prepared colored

squares (Edmund Scientific, 1994). When boresighted, the angular fields of view of the two cameras were coincident, and displayed target polygons were rendered as being without color when viewed as two color channels on a video monitor. Panchromatic input of the color target to a color video monitor produces a colorless scene when all three input angular fields of view are coincident. Where polygon edges exhibited a color within either edge rows or columns, misregistration existed and further adjustment was made to remove the parallax causing the color edge artifact. When each two-camera combination was aligned in both horizontal directions focus adjustments were required to fine tune the boresighting of all three cameras. Registration was achieved to between one to three pixels, and the camera lenses were taped to avoid accidental movement.

Filter selection

As no commercial filters have yet been produced to precisely replicate the absorption spectra of the three sets of cones, Kodak Wratten gelatin filters (Eastman Kodak, 1981), with bandwidth and transmission characteristics similar to those of the cones were used. Broadly overlapping band filtration (fig. 3.1) was accomplished using the Kodak filters Wr. 47B for the short waveband (blue), Wr. 61 for the middle waveband (green), and Wr. 59 for the long waveband (red),. These three filters have similar transmittance/diffuse density properties near the transmittance centers of 440, 535, and 565 nm. The color appearances of these filters are best described as deep blue (Wr. 47B), deep green (Wr. 61), and light green. The Wr. 47B is used for color separation and tricolor printing,

47B

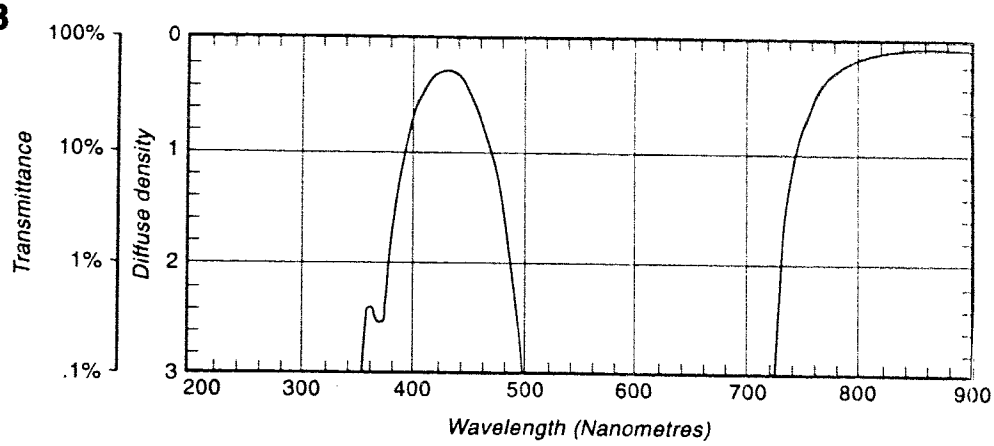

a

61

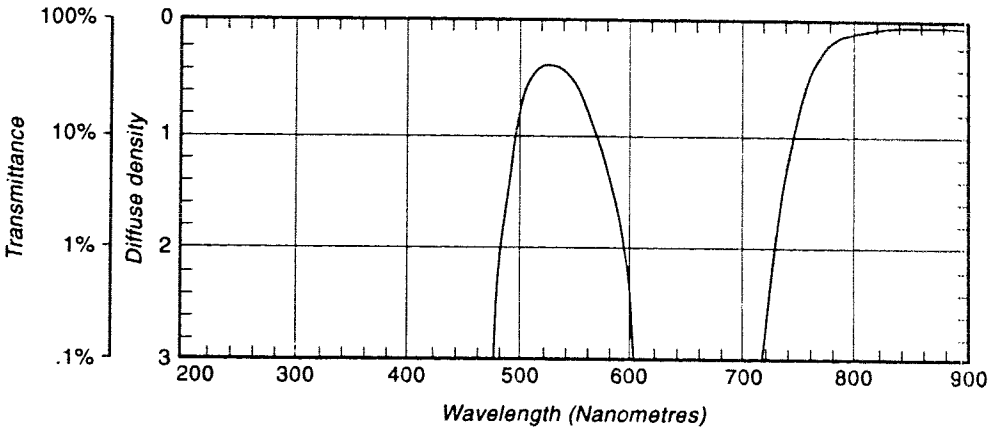

b

59

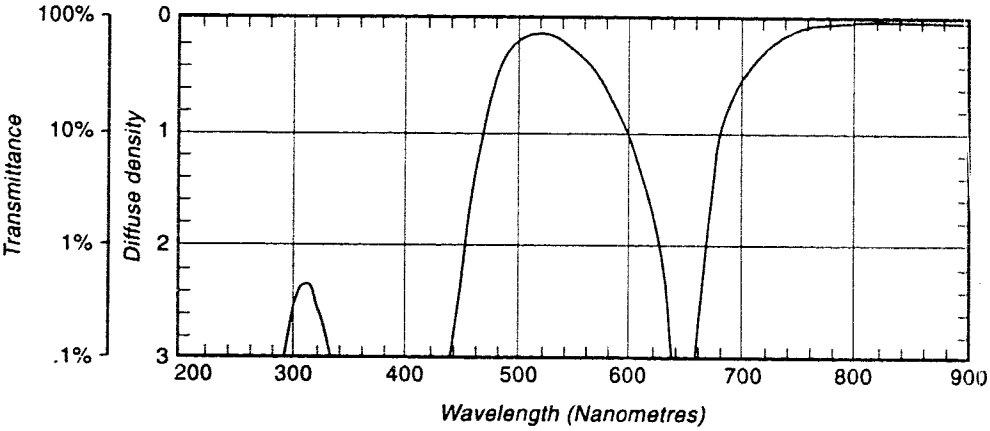

c

Combined

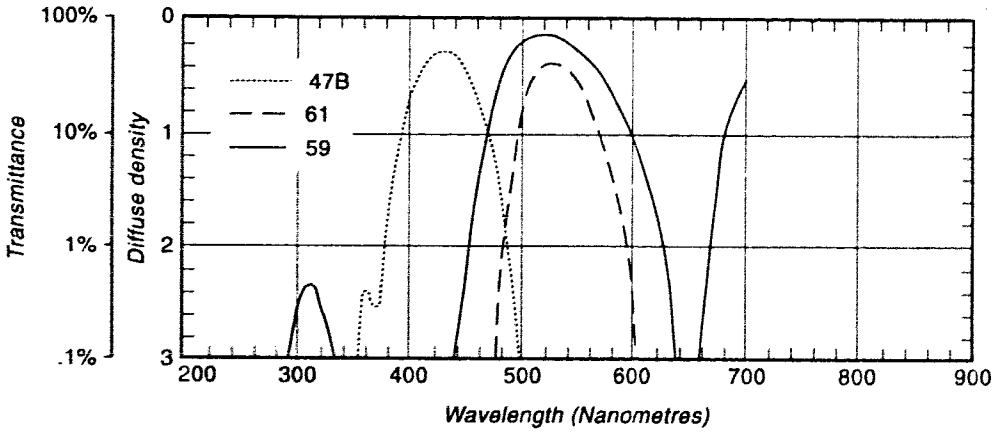

d

Fig 3.1

the Wr. 61 is used for tricolor projection and color separation, the Wr. 59 is a contrast filter, with good blue absorption with limited yellow, green and red absorption.

Filter mounts were adapted before boresighting to avoid disrupting boresighting adjustments. The filters were mounted to the video cameras prior to the system warm-up.

Camera Imaging System

The sensing system consisted of three Sony XC-75 Interline-transfer CCD panchromatic video cameras. Each camera imaging system consists of an effective picture element (pixel) array of 768 horizontal (columns) by 494 vertical (rows). External synchronization was provided by the a thirty-two bit image frame capture device. Video output was 1.0 volt peak to peak at 75 ohms. Camera outputs were patched by matched impedance cables through a switching device and input to a waveform monitor. The switching device permitted the monitoring of individual camera output signals. The waveform monitor permitted the monitoring of video output over a one hundred standard division range of the one volt peak to peak (1V p-p) camera output signal. Manual gain was used, permitting manual adjustment to gain of the video output signal.

Illumination Conditions

Target illumination conditions were controlled using six one thousand watt quartz halogen, General Electric lamps as a source illuminant and photo effect gels in oversized filter sheets (12 x 22 in.) The quartz halogen illuminant had a correlated color temperature of 3030 ^{o}K as measured by a color temperature meter. The superimposition of the photo effect gels over the source illuminant produced measured color temperatures of 3840 ^{o} K, for the blue gel, 3030 ^{o} K, for the green gel, and 2480 ^{o} K for the red gel. The dominant wavelength or wavelength at which a blackbody radiation curve reaches a maximum, is related to temperature by Wien's displacement law $\lambda_m = A/T$, where λ_m = wavelength of the maximum spectral radiant exitance,

μm, A = 2898 μm K, and T = temperature, K (Lillesand and Kiefer, 1994). The dominant wavelength for the broadspectrum illuminant and the three photo effect gels is by this equation equivalent to .956 μm, for the broadspectrum illuminant, .755 μm, for the blue gel, .956 μm, for the green gel, and 1.169 μm, for the red gel.

While the spectral distribution of the quartz halogen GE 1000 lamps was not available from the General Electric Corporation, communication with technical staff for the company, reported the source as providing an equal energy spectrum, relatively flat throughout the visible spectrum. Exact transmittance/absorption spectra for the three photo effect gels was also unavailable from the distributor upon request. RGB optical counts for the three filters has been included in Appendix A and their associated transmittance characteristics are discussed in context with the results.

The Static Target

The MacBeth color checker (Figure 4.8.3), a test pattern of twenty-four scientifically prepared colored squares designed to help determine true color balance or optical density of a color rendition system, was employed as a static target (Edmund Scientific, 1994). The target was mounted with a black matt background, held in place under a glass frame at a fixed focal distance from the three camera system. Illumination across the target was balanced by technical staff and considered to be even. The target was centered in the field of view of the cameras at a distance which provided sufficient resolution for analysis, while nearly filling the video image frame.

Image Capture

The experimental image set was captured under the following conditions. Analogue to digital conversion was provided in near real time by an Everex 32 bit video frame grab device. First the target was imaged under the broadspectrum condition provided by the source illuminant. Video output was set by manual gain control to one hundred standard divisions for the 1V p-p

video signal for each of the three cameras using the waveform monitor as a reference source. This image is referred to here as the broadspectrum illumination condition. Next the blue gels were superimposed over the source illuminant. The three camera responses to the shifted spectrum were recorded by the second captured image (bluegel illumination condition). After a successful image capture the waveform response to the induced spectral shift was recorded and adjustments to gain were made to bring all three cameras back to 1V p-p video output. The resulting captured image after gain adjustment is referred to as SRCBLUE.

The third illumination condition was induced by the superimposition of the green photo effect gel over the source illuminant. Individual camera waveform responses to the induced spectral shift were again recorded and the resulting image set greengel was captured. Next, adjustments to gain were made to bring all three cameras back to 1V p-p video output and the image set referred to as SRCGREEN, was captured. The fourth illumination condition was induced by superimposition of the red photo effect gel over the source illuminant. Individual camera waveform responses to the induced spectral shift were again recorded and the resulting image set redgel was captured. Next adjustments to gain were made to bring all three cameras back to 1 V p-p of video output, and the resulting image set referred to as SRCRED was captured.

The prefix SRC is intended to identify those image sets where gain settings associated with all three cameras were adjusted to produce a one volt peak to peak video output as indicated by the waveform monitor. The target polygon located at row 6, column 4, representing pure white, provided the reflectance source for the maximum of one volt or the equivalent one hundred standard divisions of the video output gain settings.

Preprocessing

Upon analogue to digital conversion the captured image sets were separated into their rgb, three band components and formatted for analysis on the image processing package Eidetic RSV1E. Image preprocessing involved applying a local average smoothing operation (3 x 3 pixel mask) to each of the three bands (rgb) for each image set. The local average filter mask of this kind is designed to deemphasize high spatial frequency detail associated with random noise produced by electronic devices. This type of filter evaluates an input pixel brightness value, BV_{in}, and the pixels surrounding the input pixel and outputs a new brightness value, BV_{out}, that is the mean of the nine pixels under examination. The spatial moving average then shifts to the next pixel, where the operation is repeated until all pixels have been evaluated (Jensen, 1986).

Training Stage

Upon completion of preprocessing each image set was prepared for classification. Supervised classification was conducted by first defining the representative sample sites, also called training sites. Training sites are used to compile a numerical interpretation key, which describes the spectral attributes for each class or category (Lillesand and Kiefer, 1994). The image processing package used permits the compilation of both calibration and test sites. Calibration and test sites are designed to permit the analyst to locate cover types (test sites) having like spectral properties to the sites of known cover type (calibration sites). Both calibration (C) and test (T) sites are incorporated when computing the descriptive statistics used in the classification stage.

Spatial complexity for a given target normally dictates the appropriate sampling scheme. The homogeneity of the target polygons was well suited to cluster sampling. When using a statistically based classifier, such as the maximum likelihood method used herein, the theoretical lower limit to the number of pixels that must be contained in a training set is n + 1, where n = the

number of spectral bands (Lillesand and Kiefer, 1994). In practice a minimum of 10n to 100n is used, since the estimates of the mean vectors and covariance matrices improve as the number of pixels in the training sets increases (Lillesand and Kiefer, 1994). Clustered samples for C and T data of approximately two hundred and eighty pixels each were selected well within target polygons (to avoid mixed pixels associated with polygon edges). The average target polygon consisted of approximately fifty-nine rows by forty-five columns, totalling two thousand six hundred and fifty-five pixels. Training site samples of approximately five hundred and sixty pixels (280 x 2), representing twenty-one percent of the total for each class, were used by the classifier. A total of fifteen classes, the maximum permitted by the software package, was identified by training sets. These classes are identified by a row and column coordinate of the MacBeth color checker. Class number, descriptions and coordinates for the target polygons are listed in Table1.

Table 1 Target Classes by Polygon

Class	Description	Row	Column
1	Bluish Green	1	1
2	Blue Flower	2	1
3	Foliage	3	1
4	Blue Sky	4	1
5	Orange Yellow	1	2
6	Yellow Green	2	2
7	Moderate Red	4	2
8	Purplish Blue	5	2
9	Orange	6	2
10	Cyan	1	3
11	Magenta	2	3
12	Yellow	3	3
13	Red	4	3
14	Green	5	3
15	Blue	6	3

Classification

The program set Eidetic RSV1SCL, employing the Maximum Likelihood Classifier was used. A full overview of the maximum likelihood procedure is beyond the scope of this thesis, and is therefore not included. Readers interested in a full description are referred to Lawley and Maxwell (1971), Jöreskog (1977), Morrison (1976) and (Davis, 1986). The program computes the mean, and covariance and correlation matrices for each of the classes defined by the training sets. The matrices are inverted and the determinant of each is computed. The Mahalanobis distance, or the measure of difference between the means of two multivariate groups is computed for each class and added to the determinant for each class to define the value of the descriminant function for each class (Davis, 1986; Peet, 1990). In determining the most likely class, a test is done checking that the unknown pixel lies 'close enough' to the training data of the class to which it has been assigned (Peet, 1990). The analyst defines a level of probability termed the alpha level, which in turn defines 'close enough'. This allows the frequency distribution of the sample to be compared to the hypothetical, measuring the degree of correspondence between the forms of the two distributions (Davis, 1986). The alpha level of .5% was selected. The alpha level defines the critical point for the Chi-squared distribution. If the Mahalanobis distance exceeds the critical distance, the unknown pixel is assigned to the null (unknown) class or otherwise left in the assigned class (Peet, 1990). At the alpha level of .5% those pixels with a Mahalanobis distance falling into the upper .5% of the chi-squared distribution are assigned to the null class (Peet, 1990).

Target polygons not included in the fifteen classes were expected to comprise the bulk of the pixels assigned to the null class. Target polygon edge pixels and border regions within the target were expected to contribute to the rest of the null class assignments. Classification errors of omission would also be assigned to the null class.

Evaluation

Classification accuracy assessment followed the most common means of expressing classification accuracy, that of the contingency table or error matrix (Lillesand and Kiefer, 1994; Fisher, 1994; Congalton, 1988; Story and Congalton, 1986; Rosenfeld and Fitzpatrik-Lins, 1986; Rosenfeld, 1986; Aroncff, 1985). This type of matrix expresses, on a category-by-category basis, the relationship between reference data (ground truth) and the results of the automated classification (Lillesand and Kiefer, 1994). In evaluating the completely random assignment of pixels to classes, the KHAT statistic was also computed for each error matrix. The KHAT statistic measures the difference between the actual agreement between reference data and the automated classifier used and the chance agreement between the reference data and a random classifier (Lillesand and Kiefer, 1994; Aronoff, 1982; Congalton *et al.*, 1981)

The equation used to compute KHAT is:

$$\hat{k} = \frac{N \sum_{i=1}^{r} x_{ii} - \sum_{i=1}^{r} (x_{i+} \cdot x_{+i})}{N^2 - \sum_{i=1}^{r} (x_{i+} \cdot x_{+i})}$$

where:

r = number of rows in error matrix

x_{ii} = the number of observations in row i and column i (on the major diagonal)

x_{i+} = total of observations in row i (marginal total to right of matrix)

x_{+i} = total of observations in column i (marginal total at bottom of matrix)

N = total number of observations included in matrix

The statistical procedure principal components analysis (pca) was also run on each of the image data sets. The covariance, correlation and eigenvalue matrices, provided as output from the principal components analysis, permitted the computation of other statistics intended to evaluate further the aspects of bandwidth, band overlap, redundancy and the outcome of the

induced spectral shifts. By computing the correlation of each image band with each principal component it is possible to determine how each band is associated with each component (Jensen, 1986).

The equation used to compute the factor loadings which expresses the association is:

$$R_{kp} = \frac{a_{kp} \times \sqrt{\lambda_p}}{\sqrt{Var_k}}$$

where: a_{kp} = eigenvector for band k and component p

λ_p = p th eigenvector (component)

Var_k = variance of band k in the covariance matrix

This computation results in an n x n matrix of factor loadings (Jensen, 1986).

Least Squares Analysis

In determining the relationship between the induced illumination conditions and the results of the application of the SRC function for the fifteen target polygons, least squares method was applied to the eighteen band/illumination condition combinations. The STAT program accompanying Davis, (1986) was used in producing this statistical output. This output provided a goodness-of-fit or coefficient of determination, expressing the degree of correlation between the band/illumination condition combinations. This procedure was intended to determine the degree of statistical similarity between conditions which produce dissimilar color renditions, which in turn inhibit accurate interpretation.

Qualitative evaluation of the color renditions produced by the induced spectral shifts and the results of the applied between-band gain control (SRC function) for the seven image sets, were included. Given the band configuration, degree of band overlap and incomplete coverage of the visual spectrum, an accurate color rendition of the static target would not be expected. The photographic product required for this purpose was produced by the color graphics recording device (Matrix Camera). This device provides a photographic product of the color additive digital images produced by the three band sensor output. Based on the assumption that the

photographic processing of this product was conducted under controlled conditions, one can expect that the photographic product provides an accurate reproduction of the digital display.

Summary

The sensor configuration employed was a prototype designed for laboratory use only. Design improvements, including vibration resistant sub-pixel camera registration would be required for field applications. As well, a variety of filter combinations, including various degrees of band overlap should ideally be tested. As for illumination conditions, a variety of natural daylight circumstances employing, at least at first, a static target, need also to be examined. The use of a static target eliminates the need for ground truth while incorporating a large number of target classes, as well as increasing accuracy at the training stage. Given the unpredictability of an applied test of the methods under examination, it was decided to conduct this pilot experiment under as controlled circumstances as possible.

IV

EXPERIMENTAL RESULTS

Introduction

The application of the simulated response compression (SRC) function as applied to the data sets herein did not always prove as successful as expected. The principal thesis, that the application of SRC would restore the relative degree of excitation between the three waveband set, proved successful in only one of the three applications, SRCRED. The order of examination of the experimental results is by short (blue), middle (green) and long (red) waveband sets. This order, while consistent with the order as addressed throughout, places the successful results last, after the failures. The reader is asked therefore, to bear with the examination as presented, while keeping in mind that there are successful results to come. Reference is made herein to the calibration and test data generated by the classification training stage. This actual data set, while too voluminous to be included in its original form has been summarized by the sample DN data included in Figures 4.8.1 and 4.8.2. Reference is also made to classes 1 through 15 by polygon color name.

The color names refer to the MacBeth Munsell color chart used as a target and were not assigned by the author. All figures referred to in this section have been included at the end of Chapter Four. Tables have been included in Appendix A. Many of these could only be printed in landscape format because of their size and therefore; are not well suited to immediately follow the page upon which they are referenced.

Classification Results

Tables 2 through 8, Appendix A, contain the error matrices resulting from classifying training set pixels, for the seven image data sets. These error matrices express the counts of agreement between classified categories and their associated training sets. The method

commonly used to express accuracy of classified or interpreted image or map data sets is by statement of percentage of pixels or area that have been correctly classified when compared to the reference data (Story and Congalton, 1986). Normally the number of rows and columns equals the number of categories whose classification results are to be assessed (Lillesand and Kiefer,1994). For the sake of a thorough evaluation of these experimental results an additional category, representing the null sets or pixels unassigned to a class, has been included.

Different measures of classification accuracy, if evaluated in isolation of each other, can be misleading in representing the degree of reliability of the classified data (Rosenfield, 1986). Several characteristics of classification performance can be evaluated using this type of matrix. One can examine the classification errors of omission (exclusion) and commission (inclusion) as well as overall accuracy. Errors of omission, which normally correspond to nondiagonal column elements (Lillesand and Kiefer,1994) have all been assigned to the null column. Commission errors are represented by nondiagonal row elements. Overall accuracy, as expressed by Tables 2 through 8, can be computed by dividing the total number of correctly classified pixels (the sum of the elements of the major diagonal) by the total number of pixels under consideration (the sum of the total column).

Given the outcome of the experimental data set classifications and the extremely low occurrence of errors of commission, accuracy assessment is primarily focused on individual class accuracy, based upon errors of omission. This was computed by dividing each major diagonal element by the row total for that class. Before proceeding, a point relating to interpreting the matrices must be considered. One will notice the absence of values, both row and column for class thirteen, with one exception, Table 8. This target polygon is represented by a fully saturated red. In all but the SRCRED image data set, pixels within this polygon were assigned to the null class. When computing accuracies, these null class values have been set to one to avoid spurious results.

The value representing the mean number of pixels per classified polygon has been included in each image data set to evaluate the degree of similarity to the expected polygon size (2655 pixels) as based upon selection criteria. Examination of the (rgb) image set "broadspectrum" before classification, revealed an average target polygon dimension of fifty-nine rows by forty-five columns (excluding edge errors resulting from image misregistration). Most of the pixels affected by misregistration were assigned to the null class but one must assume that some were included in the respective class assignments, particularly where the classified polygon dimension exceeded the expected 2655.

The image data set representing the broadspectrum condition of illumination has been used as a benchmark for comparisons of classification accuracy between image data sets. The underlying assumption is that the best results, including overall and individual class accuracies, would probably be associated with the broadspectrum condition of illumination. Error matrices included in Tables 2 through 8 were not based upon training data, or estimated, as is often the case, when determining classification accuracy (Rosenfield, 1986; Story and Congalton, 1986). The reason for not choosing this method was that accuracy assessments, incorporating training set data only, merely provide an assessment of the homogeneity of the training sets while giving little indication of overall classification accuracy (Lillesand and Kiefer,1994). To assure adequate accuracy assessment a "wall-to-wall" complete account, appropriate to a research situation, was used (Lillesand and Kiefer,1994). While not well suited to an applied remote sensing situation, this method provides a more reliable accuracy test than estimating procedures, by accounting for every classified image pixel (Congalton, 1988).

The error matrices referenced by the Tables 2 through 8 were not normalized (Aronoff, 1982) as the accuracy tests herein were conducted using the same method for all classification categories. Given the use of the "wall-to-wall" method for establishing reference data, one can expect a high reliability when computing accuracies. Establishing minimum accuracies for the purpose of evaluating classification results has for the most part been thoroughly covered where errors are estimated by sampling methods (Aronoff, 1985). Where "wall-to-wall" methods have

been applied, choices regarding acceptable minimum accuracy levels depend upon the application. Davis (1986) points out that setting a level of significance is the responsibility of the researcher. In avoiding the rejection of a true hypothesis, significance levels have, therefore, not been set for the results contained herein. This being the case each marked deviation from the accuracy of the image set broadspectrum will be examined. A, $\hat{K}$ "KHAT" statistic has also been computed for each error matrix. The "KHAT" statistic serves as an indicator of the extent to which the percentage correct values of an error matrix are due to "true" agreement versus "chance" agreement (Congalton *et al.*, 1981; Aronoff, 1982; Lillesand and Kiefer,1994).

Reference is also made to statistics computed in addition to those required for the image classification, (see Appendix A). These include principal components and their associated matrices indicating, covariance, correlation, eigenvalues and eigenvectors. The matrices output from principal components analysis have further been used to compute the correlation between each band and each component, or factor loadings (Jensen, 1986). From eigenvalues, the percentage of total variance explained by each principal component and the percentage of total variance contributed by each band, has been computed to aid in examining the aspects of redundancy (Jensen, 1986).

Image Set Broadspectrum

From Table 2, image set broadspectrum , the computed KHAT statistic equalled 0.96. In interpreting this statistic it is important to note, that as a true agreement approaches 1 and a chance agreement approaches 0, the "KHAT" value also approaches 1. Therefore, the observed classification is 96 percent better than a chance agreement (Lillesand and Kiefer,1994). Classes 1 (polygon color bluish green), at 93 percent and 12 (polygon color yellow), at 87 percent, are the only two classes which differ conspicuously from the general tendency of averages for this matrix. Where class 1 (polygon color bluish green) is concerned, the small gap between 440 and 480 nm, where no band overlap exists (see Figure 3.1), may be a contributing factor to its

somewhat reduced classification accuracy. Considering that this polygon color has a relatively high mean (short waveband (blue)) reflectance (70) associated with the calibration and test data and this DN value increased with the introduction of the bluegel illumination condition, one might also suspect a lack of shortwave energy emitted by the broadspectrum illuminant, as having contributed to this condition. The spectral distribution of power from thermal sources such as incandescent filament lamps, however, is normally smooth and continuous over the entire visible range (MacAdam, 1985). Conversations with General Electric technical support staff, confirmed this for the quartz-halogen illuminant used. The spectral bands represented by the blue (short) and green (middle) and red (long) wavebands, should adequately cover the reflectance from this target polygon.

Class 12 (polygon color yellow) exhibits the most conspicuous departure from the general tendency. It was observed while conducting the experiments, that an anomaly (possibly a surface contaminant from handling) on the sensing platen of the green (middle) waveband camera was associated spatially with this class polygon and is considered to be the main contributor to the large number of omission errors for this class. Or, considering that accuracies for this class are substantially improved under other illumination conditions, including the SRC... conditions, a discontinuity in the spectral continuum may also be a contributing factor.

With the possible exception of class 12, all other classes in Table 2 exhibit degrees of accuracy sufficient for most applied remote sensing applications, considering an overall accuracy (sum of the diagonal elements / sum of the row total) of 96 percent.

Image Set Bluegel

Table 3 contains the error matrix for the illumination condition, bluegel. The computed overall accuracy for this matrix shows a 1 percent increase over that of the broadspectrum condition, resulting in a 97 percent accuracy level. Calibration and test data for this image set indicate a marked increase in DN values in short waveband (blue) values for all classes,

accompanied by an associated decrease in DN values within the other two bands, as well. This tendency indicates a spectral shift toward the shorter wavelengths as expected.

Under these conditions, class 6, (polygon color yellow green), suffered the greatest decrease in accuracy, down from 98 (broadspectrum) to 88 percent. Considering that this target color roughly falls within the spectral range of 550 to 560 nm and both the middle (green) and long (red) wavebands adequately cover this spectral range, the reduced accuracy must have resulted from the induced spectral shift. The increased accuracy within class 1 (polygon color bluish green), over the broad spectrum condition, probably results from the increase in total variance contributed by the short (blue) waveband, under this illumination condition. As previously mentioned, this may be related to the quartz halogen illuminant. The KHAT statistic for this image set is 0.97, indicating a true agreement. The increase in the mean number of pixels per class polygon indicates the inclusion of edge pixels associated with misregistration.

Image Set Greengel

Table 4 contains the error matrix for the image set greengel. A similar performance in overall accuracy, 97 percent, is exhibited by the illumination condition. As in the case of the bluegel, this indicates that overall conditions associated with the spectral shift had little deleterious effects on spectral class separation. In examining the most marked departures in class accuracy for this image set, classes 1 (polygon color bluish green) and 10 (polygon color cyan) will be evaluated. Both classes in this case are polygon colors associated with a mixture of blue and green. A marked average drop in DN values for both of these classes is evident in the calibration and test data (class 1, -27; class 10, -23).

The spectral region of approximately 450 to 480 nm (blue green), is the only short wave spectral region within the three wavebands, with limited coverage. Figure 3.1.d, illustrates the percent transmittance by wavelength, of the three combined waveband sets. At approximately 460 nm, the percent transmittance, of the filters Wr. 47B and Wr. 59 drops to 10 percent. The

lack of coverage in this spectral region is consistent with the reduced accuracy of polygon colors with a high reflectance in the blue green.

Neither blue nor green colored polygons were similarly affected. The mean number of pixels per polygon rose only slightly over that of the broadspectrum, with this illumination condition. The KHAT statistic 0.97, again indicates a true agreement.

Image Set Redgel

Table 5 contains the error matrix for the image set redgel. Under this illumination condition overall accuracy fell to 93 percent, the lowest for all conditions. The individual class accuracies of classes 1 (polygon color bluish green), 2 (polygon color blue flower), 4 (polygon color blue sky), and 5 (polygon color orange yellow) represent the most marked decline, and therefore will be examined. Calibration and test data for all of the above classes exhibit elevated DN values for the short (blue) waveband, when compared to the broadspectrum data. This is accompanied by depressed DN values in the middle (green) and long (red) wavebands. As well the separation between DN values within the middle and long wavebands has been considerably compressed, leaving these DN values very similar. This is most likely due to the degree of redundancy between these two wavebands. It is assumed that the lack of variance between these two value sets led to their being spectrally less separable.

The anomalous increase in DN values for the short waveband, when compared to the broadspectrum illumination condition, deserves special attention. An explanation lies in the optical counts associated with the three gels. While the neutral densities of these three filters are very similar (0.31, 0.23, 0.27) for the red, green, and blue gels respectively, their associated RGB optical counts (Appendix A), are of course dissimilar. The red gel exhibits an optical count of 0.02 for the red, 1.48 for the green, and 0.79 for the blue. The red count is consistent with a low optical density where red light is concerned. The green count is consistent with a high optical density where green light is concerned, (as the red filter is a minus green filter). The blue count,

however, indicates that this filter passes a fair amount (15 to 16 %) of blue light[3] . This may account for the overall increase in short (blue) waveband DN values with this illumination condition.

The KHAT statistic for this image set 0.93 again indicates a true agreement.

Image Set SRCBLUE

Table 6 contains the error matrix for the image set SRCBLUE. The computed overall accuracy for this image set of 96 percent represents little change in accuracy from the bluegel or broadspectrum illumination conditions. Individual class accuracies fluctuate only slightly about those of the broadspectrum illumination condition, with the exceptions of classes 12 and 15. The accuracy of class 12 (polygon color yellow) increased by 13 percent with SRCBLUE. Within class 15 (polygon color blue) ,however, class accuracy dropped by 10 percent. It appears that the SRC effect (between band gain response) resulted in an increase in omission errors for this polygon color, represented by a fully saturated blue.

Calibration and training data for class 12 show an increase in the average short waveband (blue) DN values by 7 DN's, accompanied by a near match in DN value for the middle waveband (green), and a drop in DN's, down by 44, for the long waveband (red), when compared to the broadspectrum illumination condition. The increased DN's for the short waveband set for this class, are a result of the increased gain (return to 100 divisions) for the SRC condition. The accompanying gain increase for the long waveband camera (return to 100 divisions), failed to restore DN values for this class, (polygon color yellow).

Calibration and test data for class 15 (polygon color blue), indicate a similar increase in DN values for the short waveband (blue), resulting from the increased gain (return to 100

---

[3] Conversion according to the Density-Percent Transmittance Table, KODAK FILTERS FOR SCIENTIFIC AND TECHNICAL USES Eastman Kodak Company, 1981, Second Edition, pg. 88-89.

divisions) with SRC. Near matching middle waveband DN's resulted from SRC, when compared to the broadspectrum. Long waveband (red) DN values, while close to those of the broadspectrum condition, are too close to those of the middle waveband to be spectrally separable. Class 6, (polygon color yellow green), showed a marked improvement (+10 percent) in accuracy with SRC over the bluegel illumination condition, indicating some degree of success. Calibration and test data for the class indicate that only middle waveband DN values were restored to their broadspectrum condition, with SRC.

The computed KHAT statistic for the SRCBLUE image set of 0.96, indicates a true agreement.

Image Set SRCGREEN

Table 7 contains the error matrix for the image set SRCGREEN. The computed overall accuracy for this image set is 95 percent, down slightly from the broadspectrum and greengel illumination conditions. Individual class accuracies do not show a overall consistent improvement over the greengel illumination condition nor do they match the broadspectrum condition. The individual accuracies of classes 1 (polygon color bluish green) and 12 (polygon color yellow) show an improvement with SRC over both the broadspectrum and greengel accuracies. The improvement for class 1 is the most dramatic of the two. The accuracy for this class is up by 13 percent over that of the greengel illumination condition. Calibration and test data indicate very little spread in DN values for the image set SRCGREEN, when compared to the (rgb) DN spread for this class under the broadspectrum illumination condition. While the short waveband (blue) DN values, show an increase over those of the other associated conditions, middle waveband (green) DN values are for the most part unchanged and long waveband (red) values have dropped to those of the short waveband (blue). One might expect that under these circumstances of reduced variation between red and blue band values for this class, spectral separability would also be reduced. This, however, does not seem to be the case.

Class 12 (polygon color yellow) shows a considerable increase in accuracy over the broadspectrum illumination condition with only a modest increase over the green gel illumination condition. This is consistent with other illumination conditions when compared to the broadspectrum condition. Classes 2 (polygon color blue flower) and 4 (polygon color blue sky) indicate considerable decreases in accuracy over both the broadspectrum and greengel illumination conditions. DN values for the short waveband (blue), for SRCGREEN, were increased over those of the two associated conditions. Middle waveband (green) DN values are closely matched for all three conditions, while for the SRCGREEN image set the long waveband DN values fell below both of the counterparts. Again, middle (green) and long (red) waveband DN values show too little spread under the condition SRCGREEN to be spectrally separable.

The computed KHAT statistic for this image set is 0.95, indicating a true agreement.

Image Set SRCRED

Table 8 contains the error matrix for the illumination condition SRCRED. The computed overall accuracy for this image set is 94 percent, down slightly from the broadspectrum condition and up one percent, compared to the redgel condition. Individual class accuracies show an overall improvement when compared to the redgel illumination condition. Class 1 (polygon color bluish green) has improved in classification accuracy by 13 percent over the redgel condition, while matching the accuracy of the broadspectrum condition. Class 2 (polygon color blue flower) shows a small increased accuracy over the redgel condition but is still well below the accuracy achieved under the broadspectrum condition. Class 3 (polygon color foliage) has an improved accuracy over the redgel condition and is within 1 percentage point of that of the broadspectrum. Class 4 (polygon color blue sky) shows similar improvement, being up by 6 percent over the redgel condition and with a 1 percentage point improvement over the broadspectrum condition. Class 5 (polygon color orange yellow) has improved in accuracy by 10 percent over the redgel condition, again to within 1 percent of the broadspectrum.

Class 6 shows a marked decrease in class accuracy, down 14 percent over that of the redgel and 18 percent below the broadspectrum condition. This polygon color is yellowish green, and probably falls between 550 and 570 nm, well within the spectral area with the greatest redundancy. Calibration and test data for this class indicate good rgb spectral separation for the broadspectrum condition. Under the redgel condition the two redundant bands (middle and long), spectral separation was entirely lost, with DN values for these bands being nearly perfectly matched at 61 (middle) and 60 (long). SRCRED restored the separation between the two redundant bands, almost to within the exact proportions as those of the broadspectrum condition. This restored spectral separation, however, still resulted in greater than 4 times the number of errors of omission, accompanying the SRCRED condition. Polygon size and its associated misregistration errors does not seem to be a significant factor in the increased omission errors.

Class 8 (polygon color purple blue), shows decreased accuracy, slightly below both that of the redgel and broadspectrum conditions. Class 9 (polygon color orange), is also only slightly below that of the redgel and broadspectrum conditions. Class 10 (polygon color cyan), fell to 87 percent accuracy; below both of its other associated illumination conditions. Polygon size, which can affect the accuracy, having remained stable (Table 8) accounts only slightly for this decreased accuracy. Class 11 (polygon color magenta), shows a similar reduction in accuracy, down to 88 percent, 10 and 11 percentage points below the redgel and broadspectrum conditions respectively. Here again polygon size does not appear to be the major contributing factor to decreased accuracy. As well, associated DN values, from calibration and test data, do not reveal any obvious evidence, as the SRC function again restored the rgb separation associated with the broadspectrum.

Class 12 (polygon color yellow), showed similar improvement over the broadspectrum condition; as it did under other illumination conditions. Class 13 (polygon color red) deserves special attention. The SRCRED illumination condition was the only condition under which a reliable classification was achieved for this polygon. All other conditions of illumination resulted in complete assignment to the null class for this polygon. Class accuracy for this polygon is 99

percent. This is accompanied with a larger than average polygon size of 3107 pixels, incorporating a large number of edge pixels. Calibration and test data indicate an improved separation between middle (green) and long (red) wavebands for this polygon; over those of the redgel condition. There is also a slight increased separation between these bands over that exhibited by the broadspectrum condition. This may account for the overall improvement. Classes 14 and 15 (polygon colors green and blue respectively), round to 100 percent in class accuracy, with few errors of omission and do not represent substantial improvement over the other associated illumination conditions of the redgel and the broadspectrum.

The computed KHAT statistic of 0.93 indicates a true agreement.

Error Matrices Summarized

Figures 4.1 through 4.8 have been included to help summarize the results of the standardized accuracy assessment. Figure 4.1 indicates percent accurately classified by polygon color (class) for the broadspectrum and the three shifted spectral conditions represented by light source filters (bluegel greengel and redgel). With the exception of the yellow anomaly, under the broadspectrum condition all polygons have been classified to a degree of accuracy (>90 percent) sufficient for most remote sensing mapping applications. Classification accuracies associated with the bluegel condition indicate only one polygon color (yellow green) which fell markedly below this level of accuracy. Similarly with the greengel condition only one polygon color (bluish green) fell below the 90 percent accuracy level. The greatest degree of departure from the benchmark condition was associated with the redgel condition where three polygon colors (bluish green, blue flower, and orange yellow) fell below an accuracy level of 90 percent.

Figure 4.2 illustrates accuracies associated with the broadspectrum condition and associated SRC function conditions. Here it is evident that the SRC function generated mixed results, improving accuracies in some cases and reducing accuracies in other cases. This

somewhat "mixed bag" of results indicates a tendency for improved classification accuracy for some polygon colors at the inadvertent expense of others.

Under the three gel conditions four polygon colors (bluish green, blue flower, orange yellow, and yellow green) fell below the 90 percent level of classification accuracy, while under the SRC conditions six polygon colors (blue flower, blue sky, yellow green, cyan, magenta, and blue), fell below this level. Therefore, accuracy was improved only for the two polygon colors bluish green and orange yellow at the expense of the others mentioned. Both of these improvements were accompanied by twice as many inadvertent sacrifices within the same image set SRCRED.

Figures 4.3 through 4.5 illustrate the accuracies associated with each spectral shift and its associated SRC function plotted in conjunction with the benchmark set, broadspectrum. Figure 4.3 illustrates a "one improved over one sacrificed" account at the 90 percent accuracy level. Overall the performance of the SRC function is poor with only four SRC indicators (polygon colors foliage, blue sky, yellow and green) appearing above (improved accuracy) their bluegel counterparts. Figure 4.4 illustrates a "one improved over two sacrificed" account at the 90 percent accuracy level. Overall performance of the SRC function is indicated as poor with only four SRC indicators (polygon colors bluish green, cyan, yellow, and green) appearing above (improved accuracy) their greengel counterparts. Figure 4.5 illustrates a "two improved over three sacrificed" account at the 90 percent accuracy level. Overall performance of the SRC function is indicated as moderate with eight SRC indicators (polygon colors bluish green, blue flower, foliage, blue sky, orange yellow, yellow, red, and blue) appearing above (improved accuracy) their redgel counterparts.

Figures 4.6 through 4.8 illustrate the null class assignments representing the errors of omission for each spectral shift and its associated SRC function, plotted in conjunction with the bench mark set broadspectrum. As would be expected, increases in null class assignments accompany decreases in accuracy.

Performance of Simulated Response Compression

Bluegel Illumination Condition

Simulated response compression (SRC) or between band gain control was assessed for its performance in compensating for spectral shifts induced by the three gels. Mean rgb values were established for each class (polygon color) by sampling the individual classes, within each unclassified image set (see Figures 4.8.1 - 4.8.2). Means were extracted by cluster sampling. A total of seventy-five pixels, represented by three clusters, each blotch consisting of five by five pixels, were taken from within the polygons. Care was taken to avoid edge pixels. While the samples are much smaller than those used for training classifiers, the sampled means correspond very well with those from calibration and test data.

Figures 4.9 through 4.17 illustrate graphically the degree of correspondence between the broadspectrum and all associated conditions, for each band. Series one represents the broadspectrum, series two represents the spectrally shifted condition associated with the gels and series three represents the results after simulated response compression (SRC). Figure titles indicate which bands and conditions are represented by the plots.

The graphs were examined by the order, short (blue), middle (green), and long (red) wavebands. The short (Wr.47B) and middle (Wr.61) wavebands are approximately equal in bandwidth (approximately 100 nm) with the long (Wr.59) waveband, being about twice as wide (approximately 200 nm),(see Figure 3.1).

Figure 4.9 illustrates the short (blue) waveband, for the three conditions, broadspectrum, bluegel and SRCBLUE. The spectral shift toward short wavelengths induced by the bluegel in series 2, is indicated by an increase in DN values for polygon classes (1,2,4,8,10,11,15) reflecting in the blue region of the spectrum. Polygons represented by colors nonreflective in the blue (short wavelengths) were influenced far less, in terms of DN fluctuations. With the application of SRC, DN values of the classes most affected by the spectral shift were increased

even further. The SRC function also increased DN values slightly, and uniformly for all classes nonreflective in the blue. The result of the SRC function was to exacerbate the disproportional reflectances induced by the spectral shift for this waveband.

Figure 4.10 illustrates the middle (green) waveband responses for the three conditions. Here the spectral shift toward shorter wavelengths has resulted in an uneven but general decrease in DN values. Those polygon colors most affected (classes 1,6,12, and 14) all contain some combination of green or yellow. The polygon colors represented by classes reflecting beyond the spectral range of the middle (green) waveband, including blues (shorter) and oranges to reds (longer), are the least affected by the spectral shift. The yellow region of the spectrum (560nm to 590nm) is very near the edge of the spectral range of this waveband. The SRC function restored DN values in nearly all classes for this band. In doing so, all relative reflectances associated with the broadspectrum condition of illumination, were replicated.

Figure 4.11 illustrates the long (red) waveband responses for the three conditions. Here the spectral shift toward shorter wavelengths has resulted in an overall decrease in DN values, although not uniformly by class. This waveband being the widest of the three covers a broader spectral range which includes more of the target colors (classes). The classes least affected by the spectral shift for this waveband include red (class 13 (longer)) and blue (class 15 (shorter)), which fall at the edges of the spectral range of this band. Classes containing some combination of green or yellow were affected in a manner similar to that of the redundant middle band (Figure 4.10); but to a greater degree. The SRC function was unable to restore the affected DN values. As a result relative reflectances associated with the broadspectrum condition of illumination were not successfully restored.

In summary, under the shifted spectral condition induced by the bluegel, the application of SRC successfully restored DN values and hence, relative reflectances, within the middle (green) waveband only. Overall, this band was the least affected by the induced spectral shift, as well. In this case the narrower, middle waveband (green), was the least affected and provided the best SRC results, with the short wave spectral shift.

Greengel Illumination Condition

Figure 4.12 illustrates the short (blue) waveband response to the spectral shift induced by the green gel. In this instance the DN values represented by series 2 have been lowered. One would expect this to result with a spectral shift away from the shorter (blue) wavelengths. Those polygon colors most affected are represented by classes 1,2 4,8,10,11, and 15. Those polygon colors least affected fall outside the transmittance of this waveband, as was the case in the bluegel illumination condition. The application of SRC in this case resulted in increased DN values, with poor replication of the DN values associated with the broadspectrum illumination condition. Hence, relative reflectances were not restored.

Figure 4.13 illustrates the middle (green) waveband response to the induced spectral shift. All three series are for the most part collinear and coincident, indicating very little DN displacement for this band, under this illumination condition.

Figure 4.14 illustrates the long (red) waveband response to the induced spectral shift. The near collinearity and close agreement of series 1 and series 2 indicates that little DN displacement occurred under this illumination condition, within this waveband. One could probably infer that little spectral shift from the broadspectrum illumination condition occurred within the spectral region covered by this waveband. The application of the SRC function in this case resulted in an overall but uneven reduction in DN values, with some degree of collinearty. Classes represented by polygon colors containing some combination of yellow or green were the least well restored by the SRC function. The SRC function failed in this case to restore DN values associated with the broadspectrum illumination condition, hence relative reflectances were also not restored.

In summary the SRC function failed to restore DN values and hence, the relative reflectances of target polygons for this illumination condition, for any of the three wavebands.

Redgel Illumination Condition

Figure 4.15 illustrates the short (blue) waveband response to the redgel illumination condition. Under the spectrally shifted condition as indicated by series 2, DN values increased for polygon colors reflecting within the spectral range of this band. Again colors reflecting outside the spectral range of the band were the least affected. The collinearity and near coincidence of series 1 and series 3 indicates an almost exact restoration of DN values, and restoration of relative reflectances. It therefore, must be concluded that the SRC function was successful.

Figure 4.16 illustrates the middle (green) waveband response to the redgel illumination condition. As with series 2, DN values were decreased generally, but to a greater degree for polygon colors reflecting within the spectral range of this waveband. As indicated by the collinearty and near coincidence of series 1 and series 3, the SRC function successfully restored the DN values and the relative reflectances of the broadspectrum illumination condition.

Figure 4.17 illustrates the long (red) waveband response to the redgel illumination condition. As in series 2, DN values decreased markedly overall with the two exceptions of class 13 (polygon color red) and class 15 (polygon color blue). Again the collinearty and near coincidence of series 1 with series 3 indicates successful, although not exact restoration of DN values and hence, relative reflectances of the broadspectrum illumination condition by the SRC function.

In summary, under the illumination condition induced by the redgel the application of the SRC function could be considered successful in restoring DN values and the relative reflectances associated with the broadspectrum illumination condition. This result persisted for all three wavebands regardless of bandwidth.

Redundancy, Variance and SRC

To evaluate redundancy, it is necessary to consider covariance and correlation matrices, matrix traces and factor loadings for each image set. These matrices may be found in Appendix A. The percentage total variance contributed by each band, the percentage of variance explained by principal component, and the correlation of bands to components, ' factor loadings ', were also computed. These statistics are useful in examining the response of each band under varying spectral conditions.

Tables 9 through 15, in Appendix A, contain correlation matrices for the seven image sets. Band one is the short band, band two is the middle band, and band three is the long band. As indicated by the correlation matrix for each image set, the correlation between bands two and three is high (.99). A high correlation between bands indicates a substantial amount of redundancy (Jensen, 1986). The high degree of correlation between these bands is not surprising as band two lies completely within the spectral range covered by band three (see Figure 3.1).

Image Set Broadspectrum

Table 9 illustrates that the percentage of total variance contributed by each band is 22%, 25% and 53% for the short (blue), middle (green) and long (red) bands respectively. The relatively broader bandwidth of band three has resulted in this band contributing more than twice the variance of either accompanying band under the broadspectrum illumination condition. Factor loadings show the short waveband (blue) to be strongly correlated (.859) with the first principal component which accounts for 93 percent of the total variance of the rgb image set. This band contributes only 22 percent of the total variance, due to its relatively narrow bandwidth and the fact that it contains the least redundant spectral information for this target, under this illumination condition.

Image Set Bluegel

Table 10 illustrates that the percentage of total variance contributed by each band has changed from that of the broadspectrum illumination condition. The distribution of 57%, 22% and 21%, for the short, middle and long wavebands respectively, indicates that the spectral shift toward shorter wavelengths has resulted in an accompanying shift of variances contributed by each band. Most notably the shift has reduced the variance contributed by the long (red) waveband and added it (+35 percent) to the short waveband. Factor loadings for this image set indicate a strong correlation (.97) between the short waveband (blue) and the first principal component, which now accounts for 91 percent of the total variance.

Image Set Greengel

Table 11 illustrates that the percentage of total variance contributed by each band has also changed from that of the broadspectrum illumination condition. The distribution of 8%, 32% and 60%, for the short, middle and long wavebands respectively, indicates that the spectral shift toward longer wavelengths has resulted in an accompanying shift of variances contributed by each band. Here again an increased variance has accompanied the spectral shift but less pronounced than with the bluegel. The broadest, long (red) waveband has increased (+7%) only slightly in total variance contributed, up to 60%. Similarly the middle (Green) waveband shows an increase (+7%), over its contribution under the broadspectrum condition of illumination. Factor loadings indicate a relatively strong correlation (.827) between the short (blue) waveband and the first principal component, with the total variance contributed by this band, reduced 14% from its contribution under the broadspectrum condition, to a low 8 percent.

Image Set Redgel

Table 12 illustrates that the percentage of total variance contributed by each band in the redgel set has also changed from that of the broadspectrum illumination condition. The distribution of 71%, 13% and 16%, for the short, middle and long wavebands respectively, indicates that the spectral shift toward longer wavelenghths has resulted in an opposed shift of variances contributed by each band. The total variance contributed by the short (blue) waveband has increased by 49% over that of the broadspectrum condition, with the middle (green) and long (red) bands reduced by 12% and 37%, respectively, from their broadspectrum illumination condition. Factor loadings computed for this image set indicate a high degree of correlation (.983) between principal component one and the short (blue) waveband.

Image Set SRCBLUE

Table 13 illustrates that the percentage of total variance contributed by each band has also changed from that of the broadspectrum illumination condition. The distribution of 48%, 27% and 25%, for the short, middle and long wavebands respectively, indicates that the changed variances induced by the spectral shift associated with the bluegel have changed only slightly over that condition. This indicates that the SRC function did not successfully restore the variance distribution accompanying the broadspectrum illumination condition. Factor loadings for the illumination condition SRCBLUE indicate a relatively high correlation (.949) between the short waveband (blue) and the first principal component. This result matches the bluegel condition more than the broadspectrum condition.

Image Set SRCGREEN

Table 14 illustrates that the percentage of total variance contributed by each band has also changed from that of the broadspectrum illumination condition. The distribution of 48%, 26% and 26%, for the short, middle and long wavebands respectively, indicates that a good deal change has occurred with the SRC function over the greengel condition but the application of SRC has again failed to restore the variances accompanying the broadspectrum condition. The SRCGREEN distribution, in fact closely corresponds to the distribution of the SRCBLUE image set, indicating that a similar outcome resulted under both conditions with the application of SRC. Factor loadings indicate a stronger correlation (.945) between the short waveband (blue) of SRCGREEN and the first principal component, than for both of the compared conditions, broadspectrum (.859) and greengel (.827).

Image Set SRCRED

Table 15 illustrates that the percentage of total variance contributed by each band has also changed from that of the broadspectrum illumination condition. The distribution of 23%, 25% and 52%, for the short, middle and long wavebands respectively, indicates that a good deal of change has occurred with the SRC function over the redgel condition. The percentage of total variance contributed by each band now closely corresponds to what is found under the broadspectrum condition. Factor loadings for the image SRCRED correspond well with those for the broadspectrum condition.

Summary

The most notable relationship between bandwidth, the induced spectral shifts, SRC functions, and percent total variance contributed by each band, is that the variance contributed by the broadest of the three bands appears to have been relatively stable under the experimental conditions. Table 16, factor loadings, Appendix A, illustrates that the mean percentage of the total contributed variance for the short (narrow) waveband is 40 percent with an accompanying variance of 502.2857. The mean percentage of the total contributed variance for the middle (most redundant/narrow) waveband is 24 percent with an accompanying variance of 33.90476. The mean percentage of the total contributed variance for the long (broadest) waveband is 36 percent with an accompanying variance of 327.8095.

This condition is also evident when the SRC function results are eliminated and only the broadspectrum and three gels are considered. Again, the mean percentage of total variance contributed is similar for the narrow (%var_S) and broad (%var_L) bands, with less variation exhibited for the broader of the two bands. While contributing less of the percent total variance, the redundant band (%var_M) varies the least of the three under the experimental conditions. Caution should be exercised in interpreting these results as they relate very specifically to the target and illumination conditions used herein and are not representative of all possible illumination/target conditions for this type of sensor and band configuration.

fig.4.1

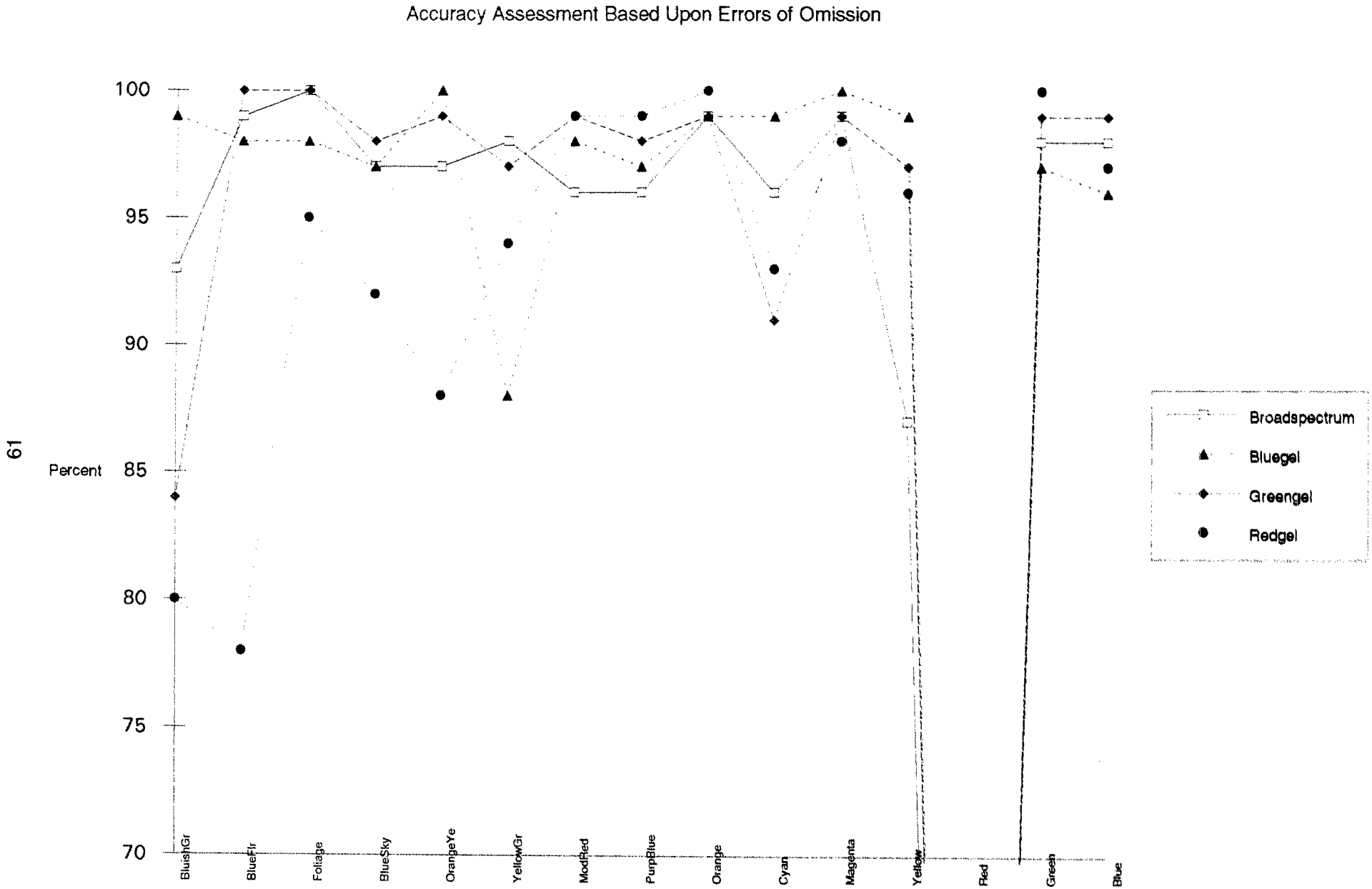
Accuracy Assessment Based Upon Errors of Omission
100
95
90
85
80
75
70
Percent
61
BluishGr
BlueFir
Foliage
BlueSky
OrangeYe
YellowGr
ModRed
PurpBlue
Orange
Cyan
Magenta
Yellow
Red
Green
Blue
Broadspectrum
Bluegel
Greengel
Redgel

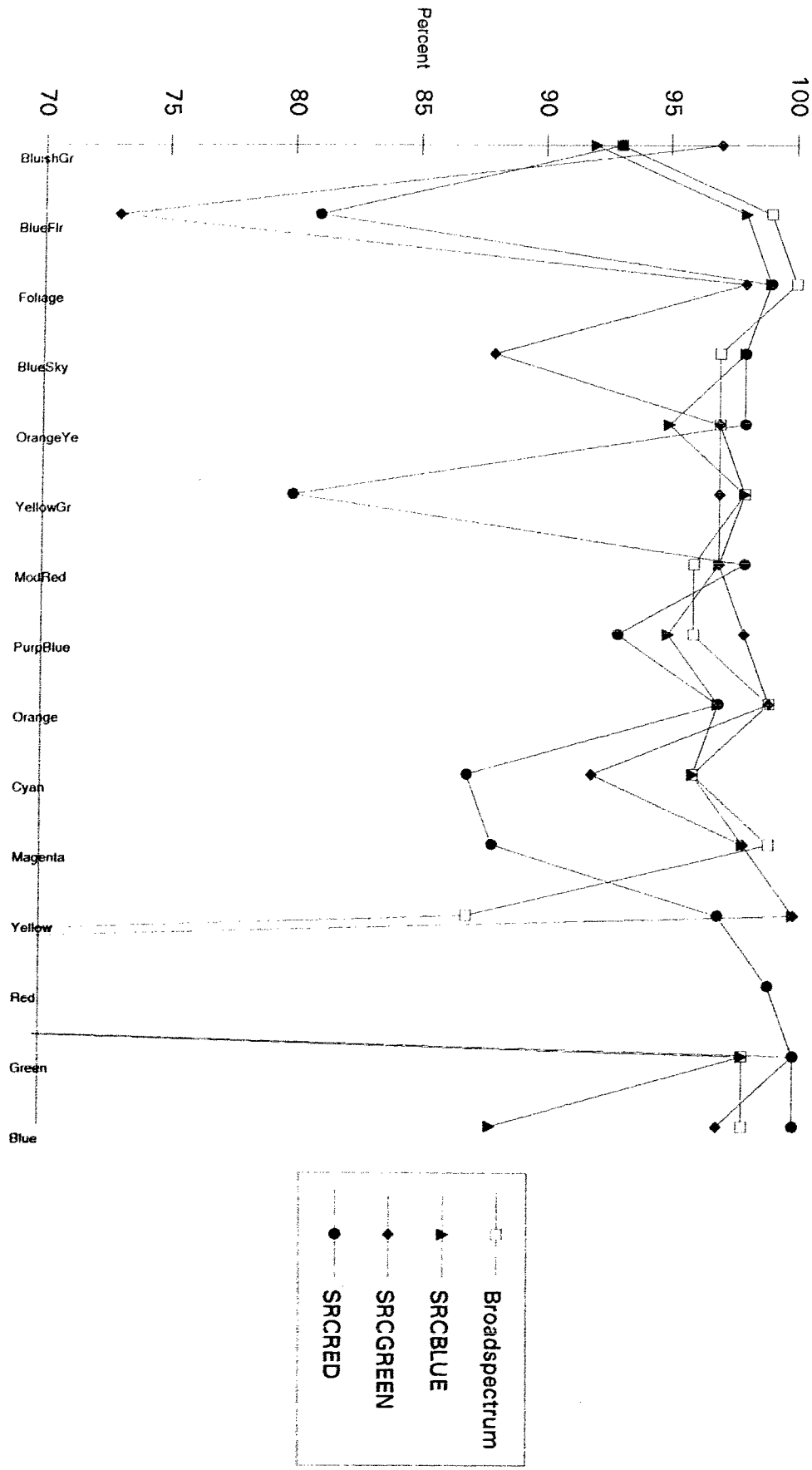
Accuracy Assessment Based Upon Errors of Omission
Percent
70
75
80
85
90
95
100
BluishGr
BlueFlr
Foliage
BlueSky
OrangeYe
YellowGr
ModRed
PurpBlue
Orange
Cyan
Magenta
Yellow
Red
Green
Blue
Broadspectrum
SRCBLUE
SRCGREEN
SRCRED

fig. 4.2

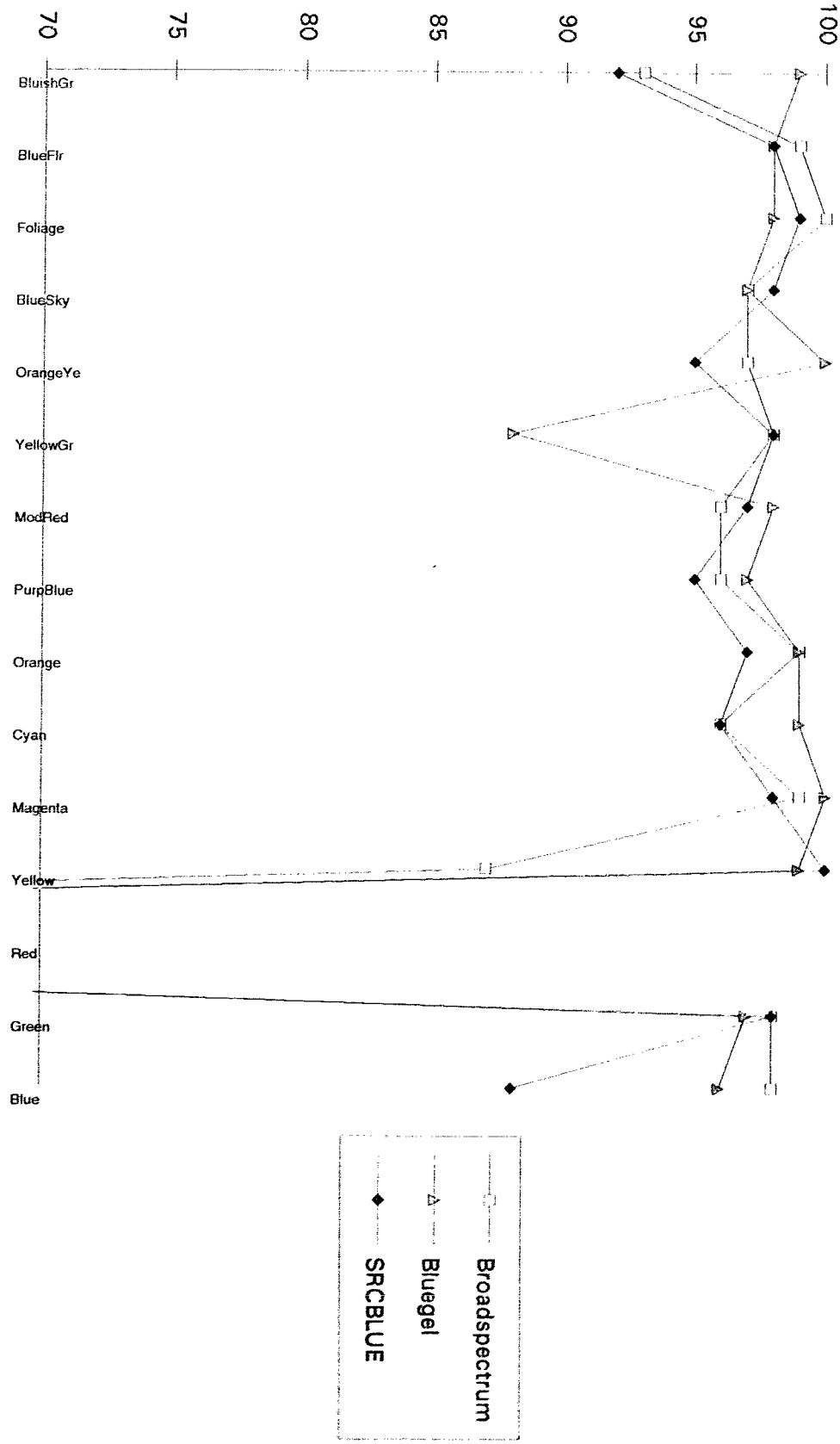
Accuracy Assessment Based Upon Errors of Omission
Percent
70
75
80
85
90
95
100
BluishGr
BlueFlr
Foliage
BlueSky
OrangeYe
YellowGr
ModRed
PurpBlue
Orange
Cyan
Magenta
Yellow
Red
Green
Blue
Broadspectrum
Bluegel
SRCBLUE

fig. 4.3

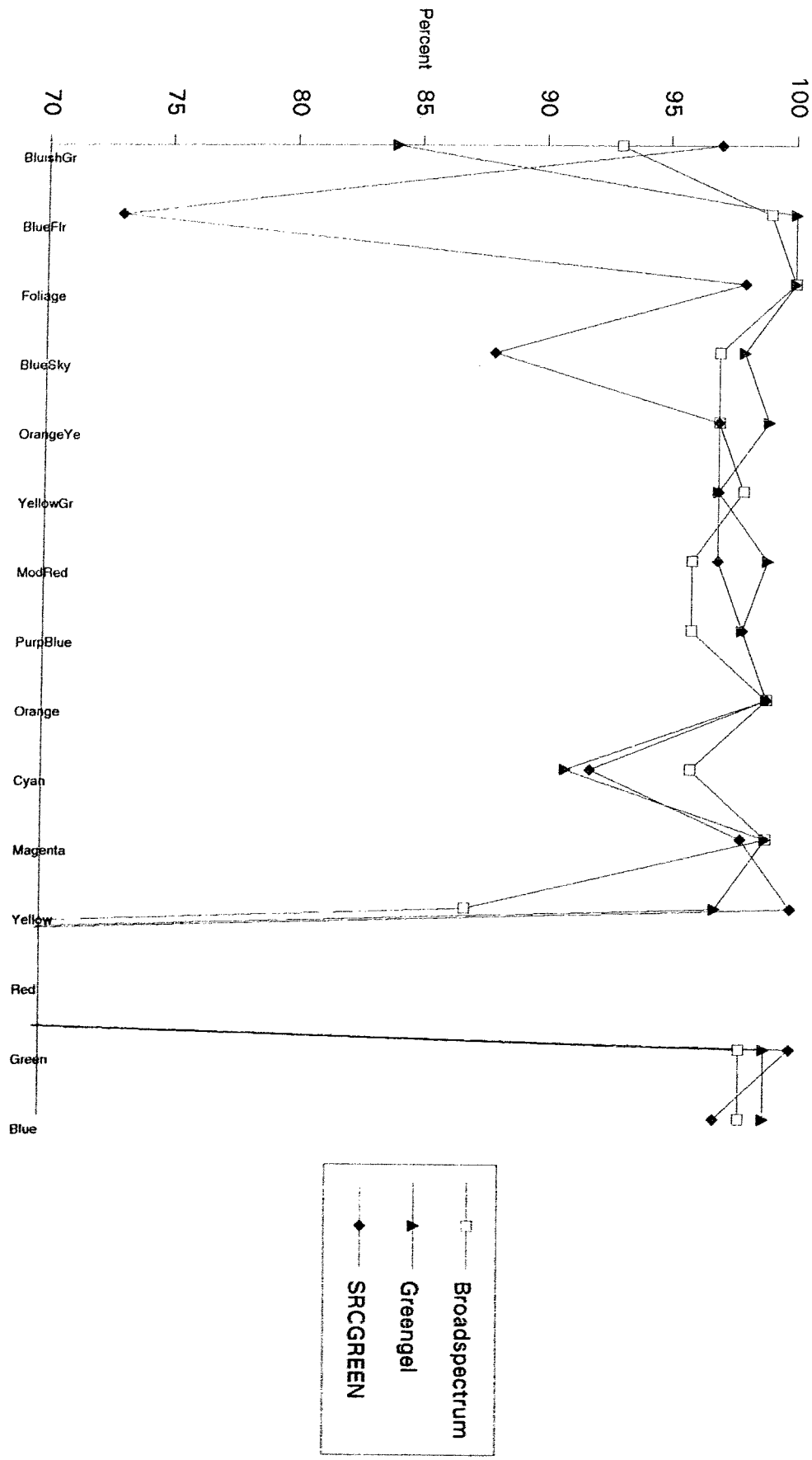
Accuracy Assessment Based Upon Errors of Omission
Percent
70
75
80
85
90
95
100
BluishGr
BlueFlr
Foliage
BlueSky
OrangeYe
YellowGr
ModRed
PurpBlue
Orange
Cyan
Magenta
Yellow
Red
Green
Blue
Broadspectrum
Greengel
SRCGREEN

fig. 4.4

fig. 4.5

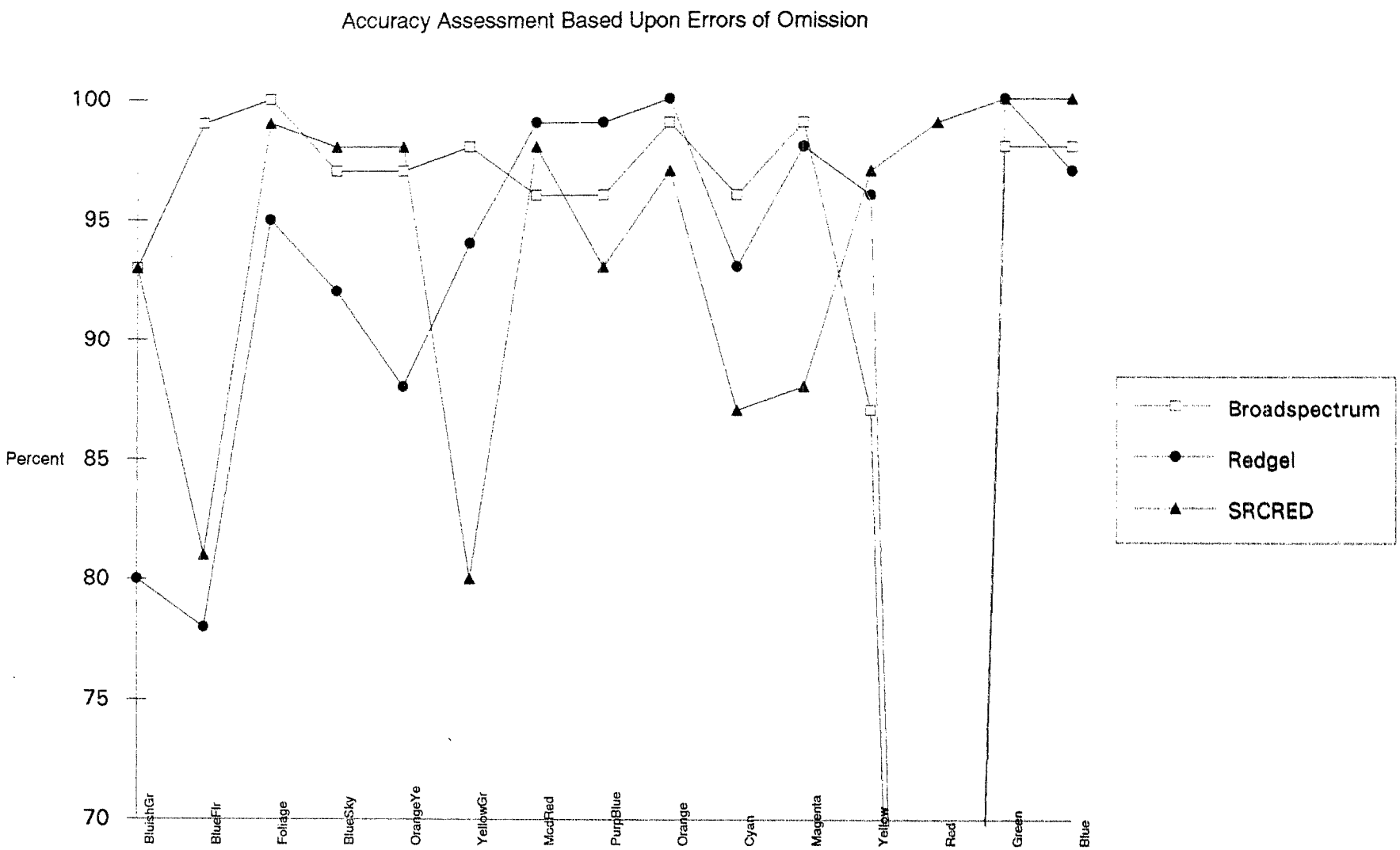
Accuracy Assessment Based Upon Errors of Omission
Percent
100
95
90
85
80
75
70
BluishGr
BlueFlr
Foliage
BlueSky
OrangeYe
YellowGr
ModRed
PurpBlue
Orange
Cyan
Magenta
Yellow
Red
Green
Blue
Broadspectrum
Redgel
SRCRED

fig. 4.6

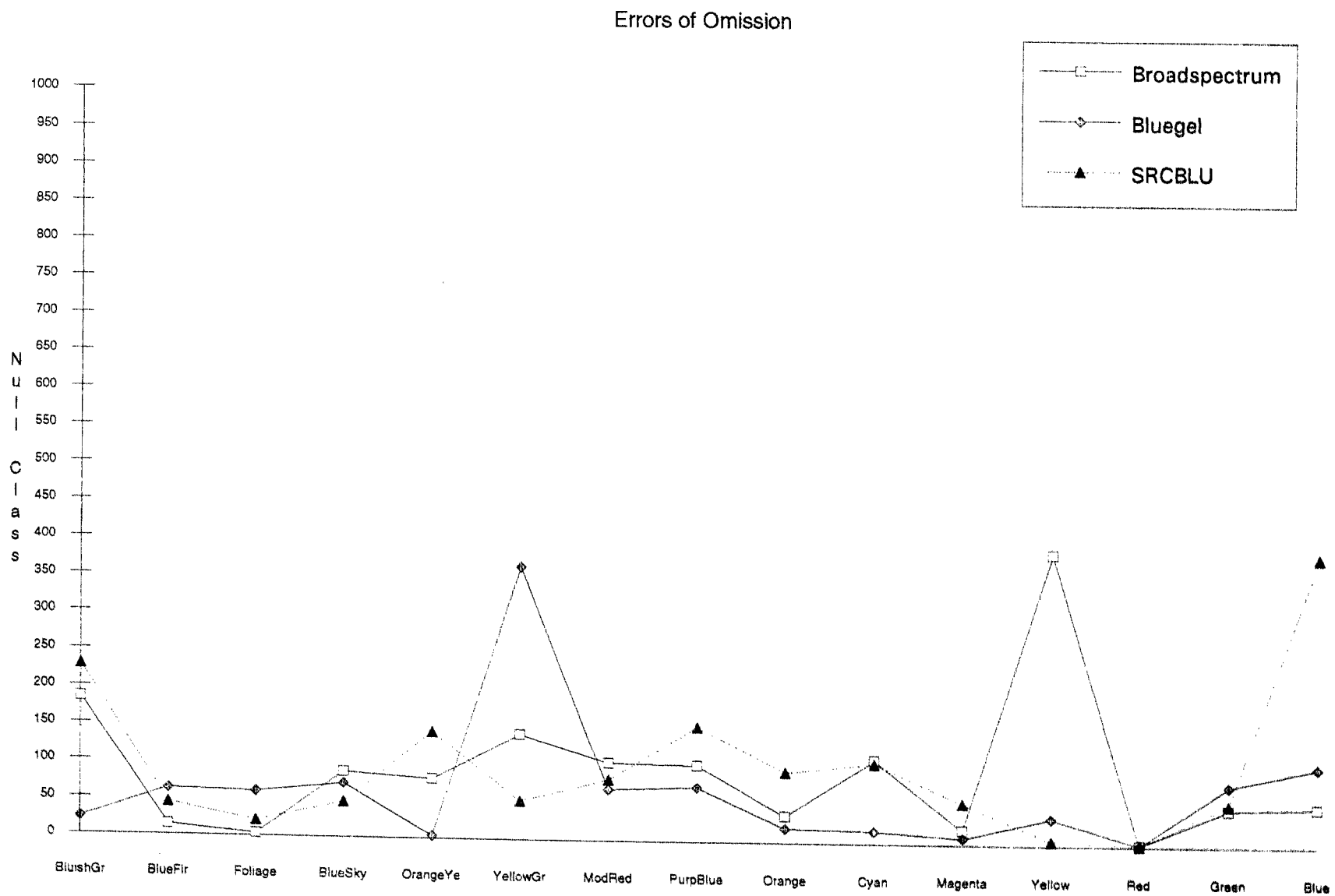
Errors of Omission
Broadspectrum
Bluegel
SRCBLU
Null Class
1000
950
900
850
800
750
700
650
600
550
500
450
400
350
300
250
200
150
100
50
0
BluishGr
BlueFir
Foliage
BlueSky
OrangeYe
YellowGr
ModRed
PurpBlue
Orange
Cyan
Magenta
Yellow
Red
Green
Blue

fig. 4.7

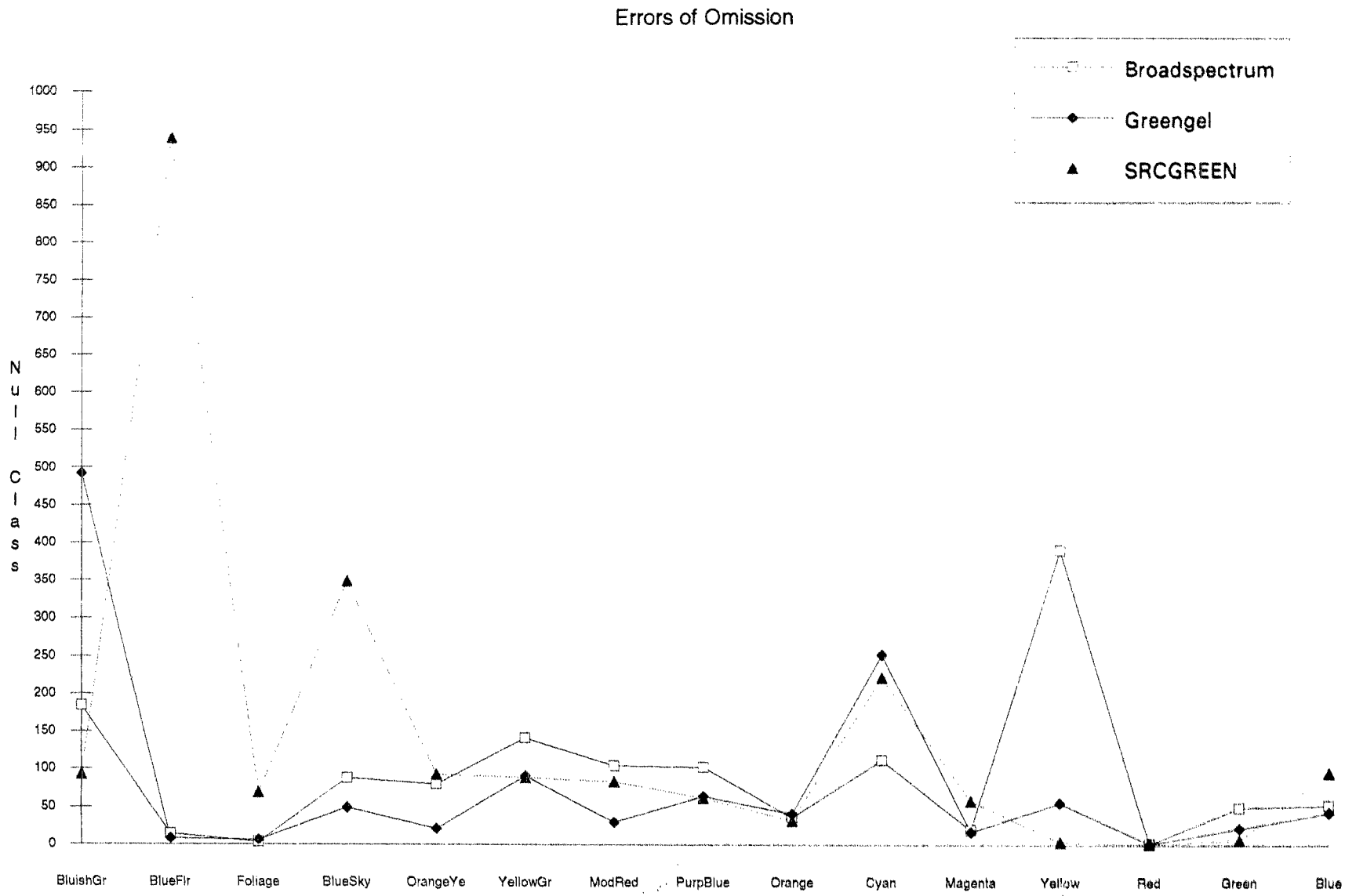
Errors of Omission
Broadspectrum
Greengel
SRCGREEN
Null Class
1000
950
900
850
800
750
700
650
600
550
500
450
400
350
300
250
200
150
100
50
0
BluishGr
BlueFlr
Foliage
BlueSky
OrangeYe
YellowGr
ModRed
PurpBlue
Orange
Cyan
Magenta
Yellow
Red
Green
Blue

fig. 4.8

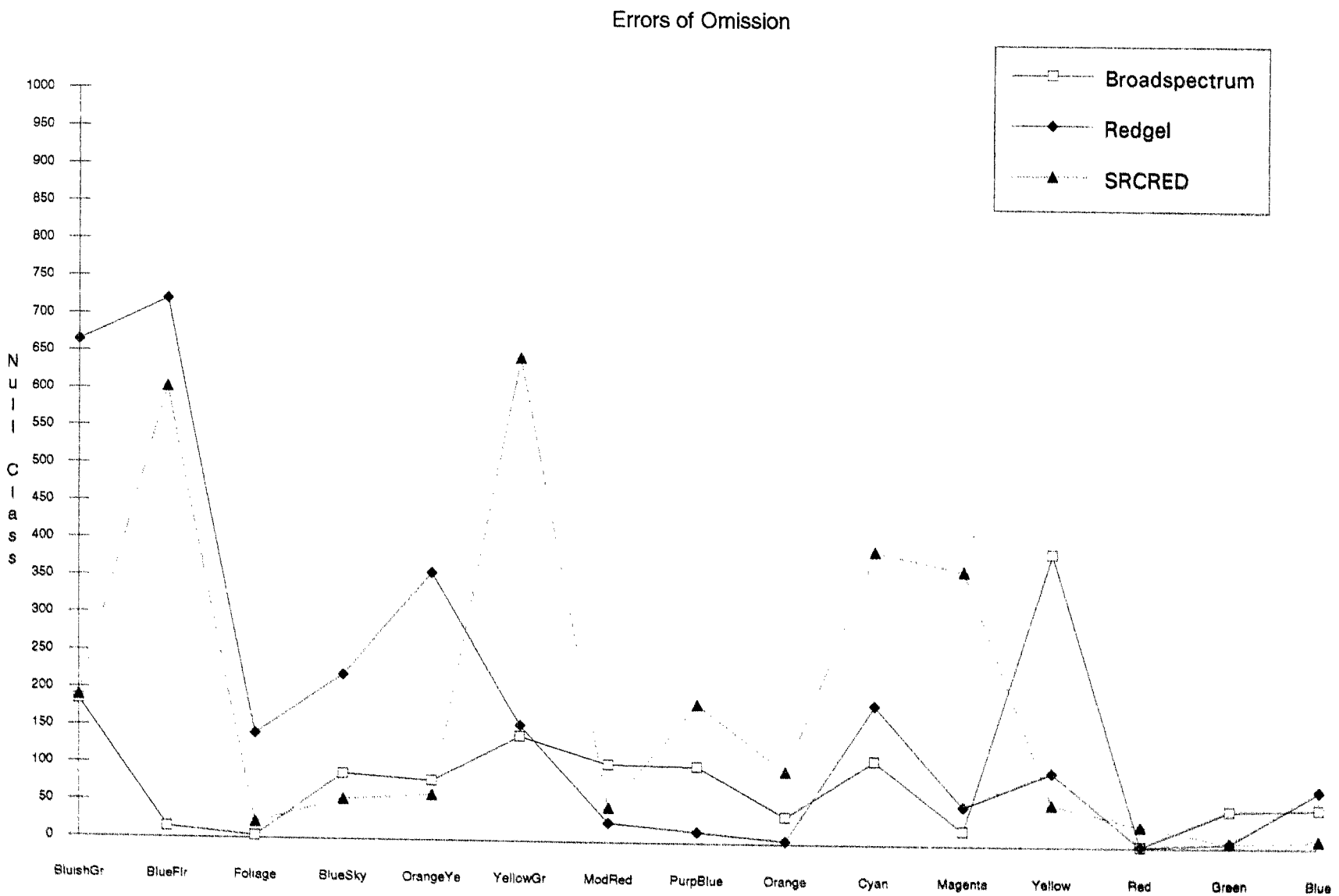
Errors of Omission
Broadspectrum
Redgel
SRCRED
Null Class
1000
950
900
850
800
750
700
650
600
550
500
450
400
350
300
250
200
150
100
50
0
BluishGr
BlueFlr
Foliage
BlueSky
OrangeYe
YellowGr
ModRed
PurpBlue
Orange
Cyan
Magenta
Yellow
Red
Green
Blue

BROADSPECTRUM

R 128 G 97 B 71	R 89 G 63 B 29	R 72 G 57 B 66	R 27 G 25 B 23
R 74 G 56 B 80	R 115 G 91 B 29	R 51 G 38 B 64	R 36 G 31 B 29
R 50 G 42 B 28		R 134 G 98 B 30	R 58 G 46 B 44
R 64 G 50 B 63	R 45 G 34 B 38	R 32 G 26 B 27	R 95 G 73 B 70
	R 48 G 38 B 72	R 76 G 64 B 29	R 146 G 108 B 105
	R 60 G 41 B 28	R 34 G 28 B 62	R 217 G 156 B 155

BLUEGEL

R 69 G 75 B 84	R 44 G 47 B 34	R 44 G 48 B 79	R 20 G 23 B 27
R 44 G 46 B 94	R 59 G 69 B 34	R 32 G 33 B 75	R 25 G 29 B 35
R 31 G 35 B 33		R 67 G 73 B 34	R 34 G 38 B 53
R 38 G 41 B 75	R 28 G 29 B 44	R 22 G 25 B 32	R 52 G 57 B 83
	R 31 G 33 B 85	R 44 G 52 B 35	R 77 G 83 B 126
	R 34 G 35 B 33	R 25 G 26 B 75	R 112 G 118 B 186

GREENGEL

R 120 G 96 B 44	R 80 G 60 B 24	R 69 G 57 B 41	R 26 G 25 B 20
R 69 G 55 B 49	R 109 G 90 B 24	R 46 G 37 B 41	R 35 G 30 B 25
R 49 G 43 B 24		R 124 G 97 B 25	R 56 G 46 B 31
R 61 G 50 B 41	R 42 G 33 B 29	R 31 G 26 B 24	R 90 G 73 B 45
	R 46 G 37 B 47	R 75 G 65 B 24	R 138 G 108 B 64
	R 55 G 40 B 24	R 33 G 28 B 43	R 207 G 157 B 92

REDGEL

R 64 G 64 B 98	R 51 G 45 B 42	R 39 G 41 B 90	R 20 G 22 B 29
R 42 G 41 B 116	R 60 G 62 B 41	R 33 G 31 B 94	R 25 G 27 B 40
R 32 G 34 B 40		R 72 G 68 B 45	R 37 G 37 B 64
R 39 G 39 B 93	R 31 G 29 B 57	R 24 G 24 B 40	R 54 G 53 B 105
	R 31 G 32 B 110	R 45 G 49 B 42	R 79 G 76 B 161
	R 40 G 35 B 41	R 25 G 26 B 93	R 117 G 110 B 234

Fig 4.8.1

SRCBLUE

R 94 G 101 B 98	R 57 G 59 B 36	R 57 G 61 B 91	R 22 G 25 B 28
R 56 G 58 B 111	R 80 G 91 B 37	R 38 G 39 B 87	R 28 G 31 B 37
R 38 G 43 B 36		R 89 G 98 B 37	R 44 G 48 B 61
R 49 G 52 B 87	R 33 G 34 B 50	R 25 G 27 B 34	R 69 G 75 B 97
	R 38 G 40 B 100	R 56 G 67 B 38	R 105 G 111 B 149
	R 41 G 40 B 34	R 28 G 29 B 87	R 156 G 163 B 222

SRCGREEN

R 91 G 96 B 92	R 61 G 61 B 38	R 53 G 57 B 86	R 22 G 24 B 28
R 54 G 55 B 108	R 84 G 91 B 39	R 37 G 38 B 87	R 28 G 32 B 38
R 39 G 43 B 38		R 95 G 96 B 41	R 44 G 47 B 60
R 47 G 49 B 88	R 33 G 33 B 53	R 24 G 26 B 37	R 70 G 74 B 99
	R 36 G 38 B 103	R 57 G 65 B 40	R 105 G 109 B 151
	R 44 G 41 B 38	R 27 G 29 B 88	R 155 G 159 B 219

SRCRED

R 116 G 90 B 69	R 87 G 60 B 32	R 65 G 53 B 63	R 26 G 24 B 23
R 71 G 53 B 81	R 109 G 87 B 32	R 51 G 37 B 66	R 35 G 30 B 30
R 50 G 42 B 31		R 133 G 96 B 34	R 57 G 46 B 46
R 63 G 50 B 66	R 48 G 34 B 42	R 36 G 27 B 31	R 95 G 73 B 73
	R 48 G 38 B 77	R 76 G 65 B 32	R 149 G 110 B 111
	R 67 G 43 B 32	R 35 G 29 B 66	R 224 G 161 B 159

Fig 4.8.2

Diagram of Macbeth Color Checker Chart

Bluish Green Class 1	Orange Yellow Class 5	Cyan Class 10	Black (1.50)*
Blue Flower Class 2	Yellow Green Class 6	Magenta Class 11	Neutral 3.5 (1.05)*
Foliage Class 3	Purple Not Used	Yellow Class 12	Neutral 5 (.70)*
Blue Sky Class 4	Moderate Red Class 7	Red Class 13	Neutral 6.5 (.44)*
Light Skin Not Used	Purplish Blue Class 8	Green Class 14	Neutral 8 (.23)*
Dark Skin Not Used	Orange Class 9	Blue Class 15	White (.05)*

**Optical Density*

Fig 4.8.3

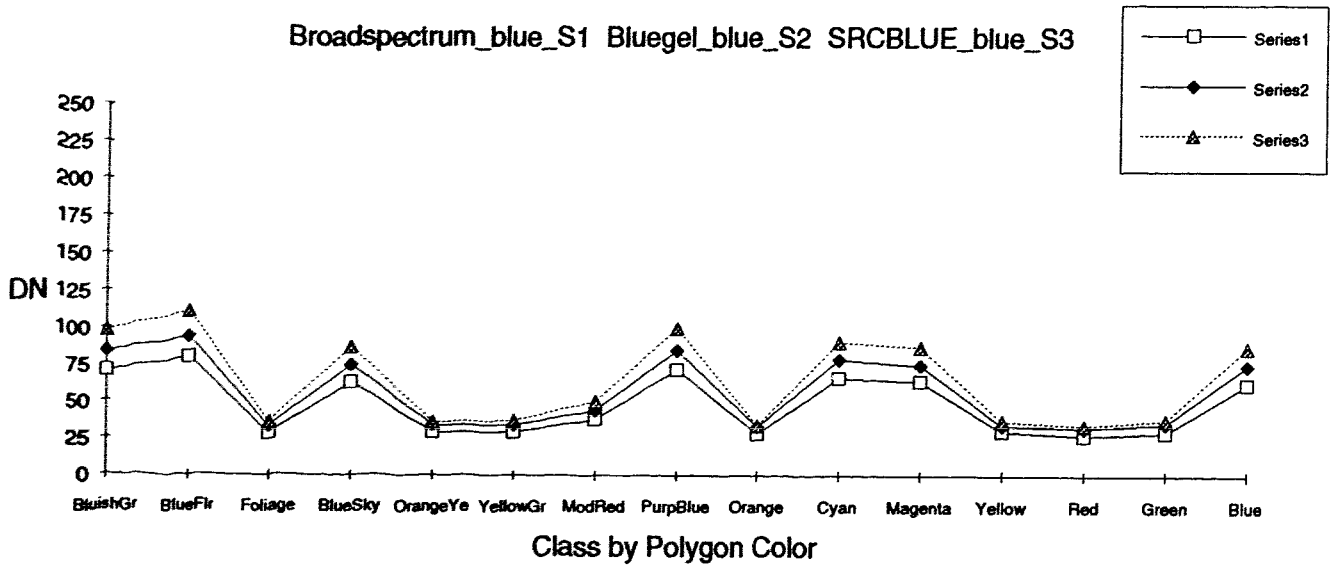
Broadspectrum_blue_S1 Bluegel_blue_S2 SRCBLUE_blue_S3
Series1
Series2
Series3
DN
250
225
200
175
150
125
100
75
50
25
0
BluishGr
BlueFir
Foliage
BlueSky
OrangeYe
YellowGr
ModRed
PurpBlue
Orange
Cyan
Magenta
Yellow
Red
Green
Blue
Class by Polygon Color

Fig.4.9

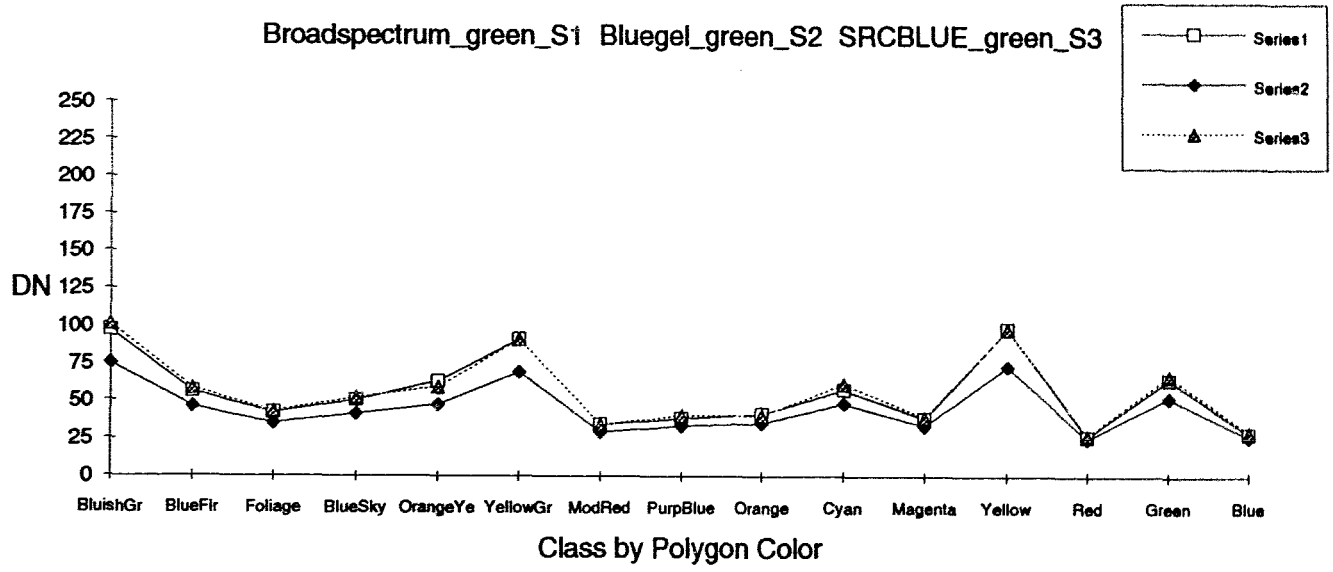
Broadspectrum_green_S1 Bluegel_green_S2 SRCBLUE_green_S3
Series1
Series2
Series3
250
225
200
175
150
DN 125
100
75
50
25
0
BluishGr
BlueFir
Foliage
BlueSky
OrangeYe
YellowGr
ModRed
PurpBlue
Orange
Cyan
Magenta
Yellow
Red
Green
Blue
Class by Polygon Color

Fig.4.10

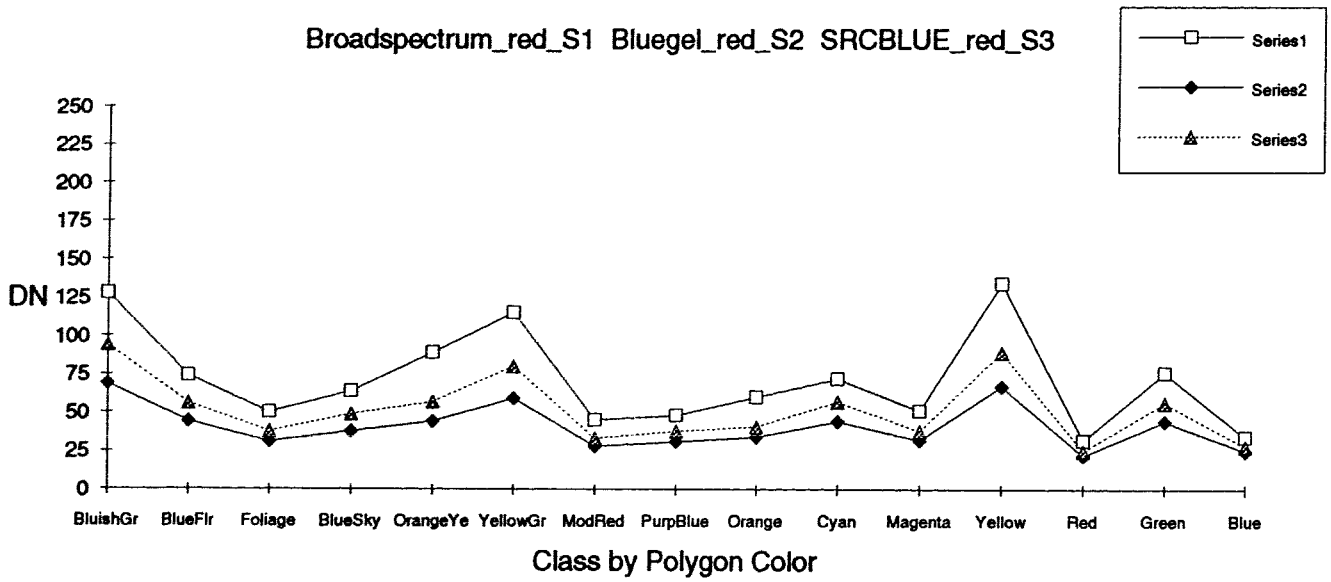
Broadspectrum_red_S1 Bluegel_red_S2 SRCBLUE_red_S3
Series1
Series2
Series3
DN
250
225
200
175
150
125
100
75
50
25
0
BluishGr
BlueFlr
Foliage
BlueSky
OrangeYe
YellowGr
ModRed
PurpBlue
Orange
Cyan
Magenta
Yellow
Red
Green
Blue
Class by Polygon Color

Fig. 4.11

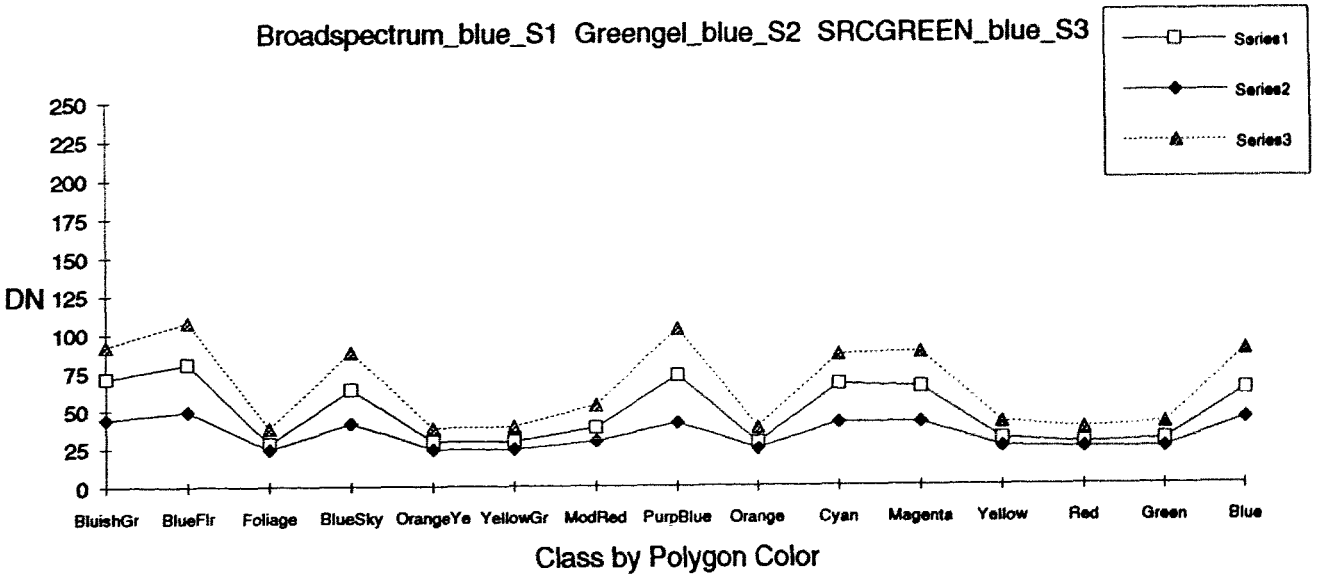
Broadspectrum_blue_S1 Greengel_blue_S2 SRCGREEN_blue_S3
Series1
Series2
Series3
DN
250
225
200
175
150
125
100
75
50
25
0
BluishGr
BlueFlr
Foliage
BlueSky
OrangeYe
YellowGr
ModRed
PurpBlue
Orange
Cyan
Magenta
Yellow
Red
Green
Blue
Class by Polygon Color

Fig. 4.12

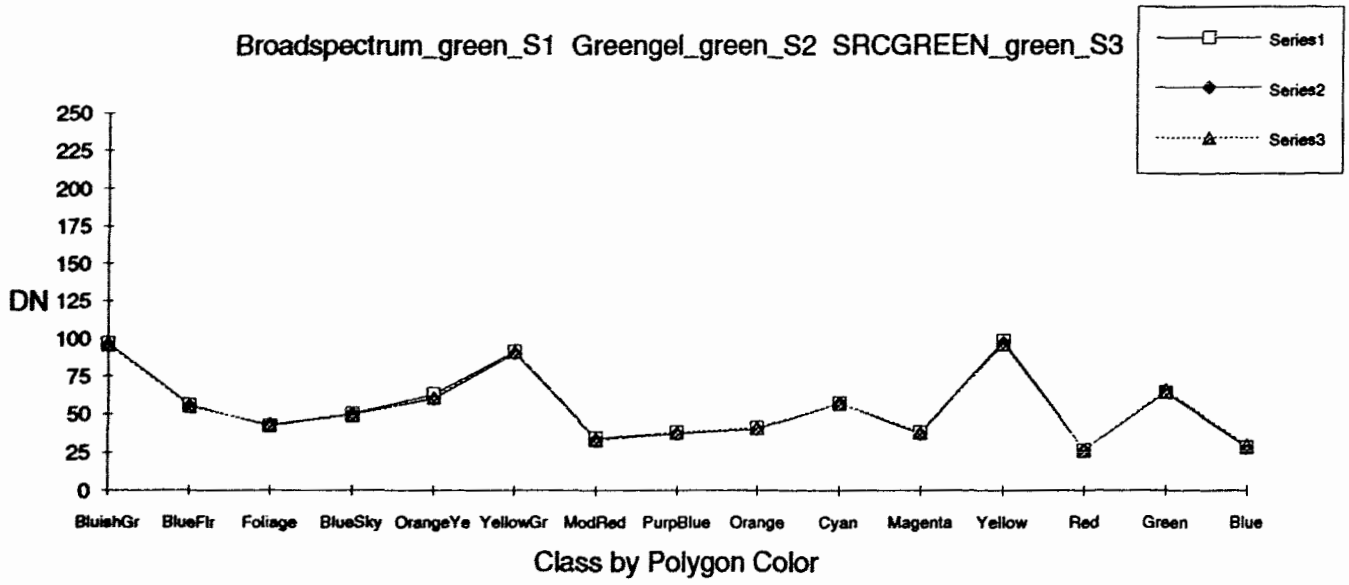
Broadspectrum_green_S1 Greengel_green_S2 SRCGREEN_green_S3
Series1
Series2
Series3
DN
250
225
200
175
150
125
100
75
50
25
0
BluishGr
BlueFlr
Foliage
BlueSky
OrangeYe
YellowGr
ModRed
PurpBlue
Orange
Cyan
Magenta
Yellow
Red
Green
Blue
Class by Polygon Color

Fig. 4.13

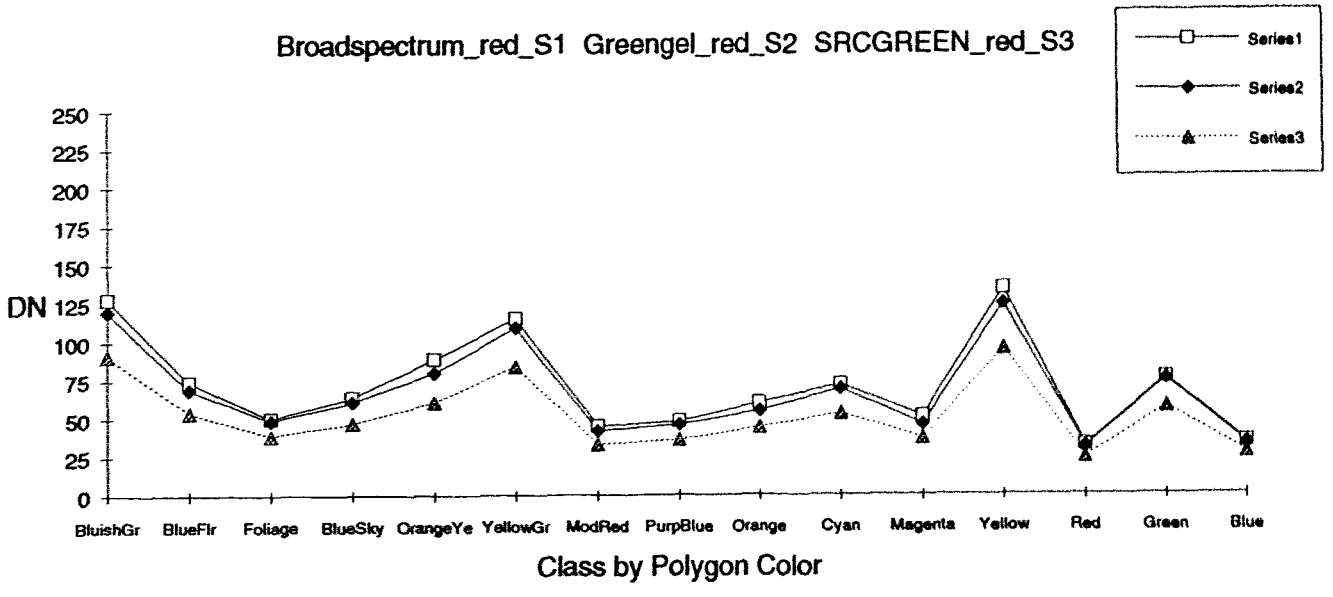
Broadspectrum_red_S1 Greengel_red_S2 SRCGREEN_red_S3
Series1
Series2
Series3
DN
250
225
200
175
150
125
100
75
50
25
0
BluishGr
BlueFlr
Foliage
BlueSky
OrangeYe
YellowGr
ModRed
PurpBlue
Orange
Cyan
Magenta
Yellow
Red
Green
Blue
Class by Polygon Color

Fig. 4.14

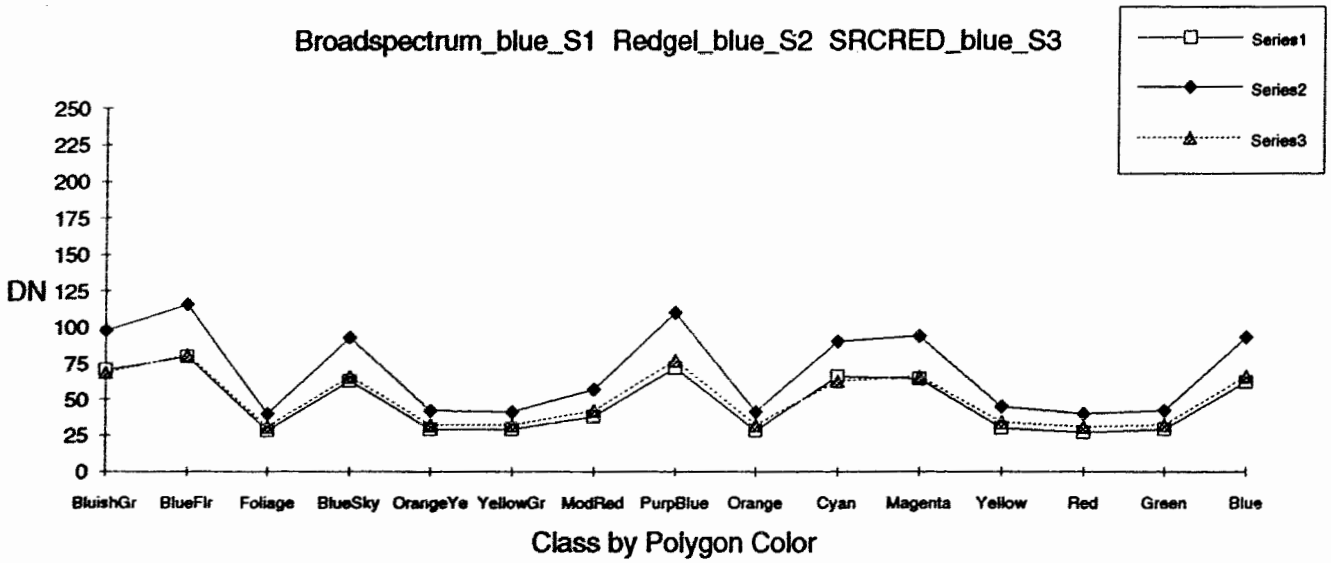
Broadspectrum_blue_S1 Redgel_blue_S2 SRCRED_blue_S3
Series1
Series2
Series3
250
225
200
175
150
DN 125
100
75
50
25
0
BluishGr
BlueFlr
Foliage
BlueSky
OrangeYe
YellowGr
ModRed
PurpBlue
Orange
Cyan
Magenta
Yellow
Red
Green
Blue
Class by Polygon Color

Fig. 4.15

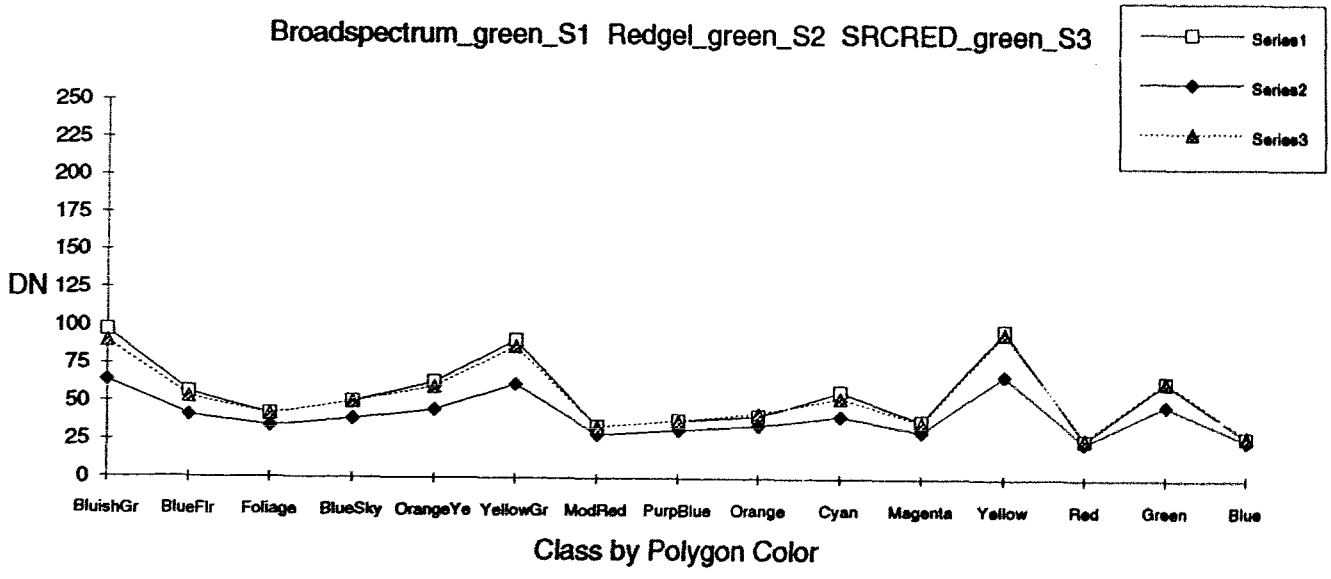
Broadspectrum_green_S1 Redgel_green_S2 SRCRED_green_S3
Series1
Series2
Series3
DN
250
225
200
175
150
125
100
75
50
25
0
BluishGr
BlueFlr
Foliage
BlueSky
OrangeYe
YellowGr
ModRed
PurpBlue
Orange
Cyan
Magenta
Yellow
Red
Green
Blue
Class by Polygon Color

Fig. 4.16

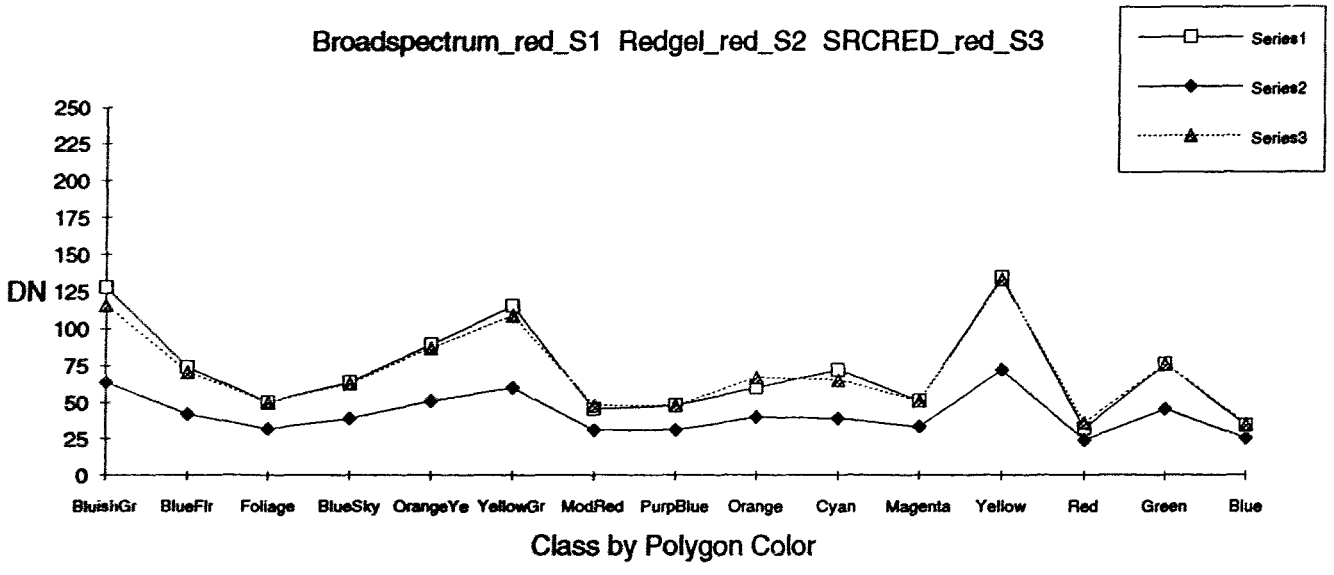
Broadspectrum_red_S1 Redgel_red_S2 SRCRED_red_S3
Series1
Series2
Series3
DN
250
225
200
175
150
125
100
75
50
25
0
BluishGr
BlueFlr
Foliage
BlueSky
OrangeYe
YellowGr
ModRed
PurpBlue
Orange
Cyan
Magenta
Yellow
Red
Green
Blue
Class by Polygon Color

Fig. 4.17

V

Discussion

Examination of the error matrices in Tables 1.1 through 1.7, has revealed that overall and individual class accuracies for the classification results are, with few exceptions, good. The spectral shifts induced by the use of the three gels, while affecting the raw DN values substantially, did not result in an unacceptable classification performance. A least squares analysis (Charts 1 through 18) Appendix B, of the three bands, where each band, illumination condition and resulting SRC function was compared to its broadspectrum bench mark condition, indicated that a high degree of correlation (Goodness of Fit) exists between illumination conditions for each waveband. The high degree of correlation exhibited, combined with the robustness of the maximum likelihood classifier, resulted in overall good classification results.

The charts indicate two important aspects of the data set regarding bandwidth and the SRC (between-band gain control) function. The broader of the three bands (red) exhibited a broader dynamic range of DN values for the target than either of the narrower, short (blue) or middle (green), wavebands. Induced spectral shifts affected the dynamic range mostly by compressing it. The application of the SRC function resulted in a stretch of the compressed ranges, inducing a broader separation by DN values for the fifteen target polygons.

The scatter plots of Charts 1 through 18, also indicate effects upon gain induced by the gels and SRC function. Channel (rgb) gain is represented by the slope of a line defined by the scatter plot. Changes in slope represent changes in gain. As expected, increased slopes resulted, in nearly all instances where the SRC function was applied, as a response to increased gain. One exception to this trend was for the broadest (red) band, where superimposition of the green gel induced an increase in dynamic range and channel gain. This is probably due to the fact that the broadspectrum and green gel illumination conditions are spectrally very similar, as indicated by the dominant wavelength of the two conditions. Here also, the application of the SRC function resulted in reducing the overall channel gain. Another exception was for the

narrowest (blue) band, where superimposition of the red gel resulted in a higher channel gain than produced by the application of the SRC function. As mentioned, this result probably relates to the diffuse density of the red gel and its degree of transmittance of shortwave (blue) energy.

The application of between-band gain control, or simulated response compression (SRC) had mixed results. The slight differences between the red and green bands evident under the broadspectrum illumination condition were not restored with the application of SRC. While failing to restore relative reflectances when applied to the illumination conditions of the blue and green gels, the SRC function produced similar results in these cases both digitally by DN and in the resulting visual images. The overwhelming success of the SRC function in restoring the relative reflectances, both digitally and visually, of the broadspectrum condition, when applied to the redgel condition is important. The explanation lies in the nature of the three band filter configuration and the dual transmittance properties or bi-modal spectral distribution of the long waveband. The long waveband represented by Wr. 59 has predominantly green transmittance with a narrow far red transmittance of approximately 680 to 700 nm. Under the illumination conditions induced by the blue and green gels, transmittance associated with the long waveband was predominantly within the green, central portion of the transmittance curve. Sensor excitation, being dominated by the greatest (peak) area under the transmittance curve, in conjunction with the spectral quality of the illumination, resulted in a three band combination of short waveband (blue), middle waveband (green), and long waveband (green) of a largely two color system.

With the induced spectral shift generated by the superimposition of the red gel, sensor excitation shifted, to be dominated by the far red transmittance component of the Wr. 59 filter. This condition resulted in changing the largely two color system imposed by the blue and green gels back into a three color system. The induced spectral shift resulted in an increased excitation for the long waveband, with the narrow 680 to 700 nm transmittance range dominating, or at least contributing equally to the long waveband sensor excitation. This effect produced a more balanced three color (blue, green, red) sensing system, with increased red sensitivity, similar to

that of the broadspectrum illumination condition. The application of SRC to the image set redgel, successfully restored the relative reflectances of the broadspectrum illumination condition, largely because of this restoration to a three color sensing system.

The three waveband, two color system explanation is further supported by the fact that the application of the SRC function to the bluegel and greengel image sets produced extremely similar color renditions for the two resulting image sets (see color transparencies, SRCBLUE and SRCGREEN). Induced spectral shifts associated with these two gels would have limited the long waveband contribution to the between-band gain control, of the SRC function. Hence, the between-band gain control would have been largely a three band, two color, function. Under this condition the relative reflectances associated with a three band, three color system would be lacking the third band, third color contribution. This would explain the failure to restore the relative reflectances associated with the broadspectrum illumination condition for the SRCBLUE and SRCGREEN image sets. This conclusion is supported by the resulting near matches in DN values for classes 15 and 6 (SRCBLUE) with the application of the SRC function. As well, with the application of the SRC function represented by SRCGREEN for classes 1,2,4, and 12, a drop in long waveband (red) DN values, resulting in near matches in DN values to those of the short waveband (blue) image set, further supports this conclusion. For these reasons the one-in-three success rate of the SRC function is very promising. The bi-modal spectral distribution of the Wr. 59 filter was clearly the "weak link" in the performance of the SRC function. Further experimentation involving broader spectral representation with no spectral sensitivity gaps, as was the case with the Wr. 59 (approx. 630 to 670 nm.) would no doubt produce more consistently successful results, where between band gain control is applied.

The color renditions produced by the three band combinations under the experimental illuminations provide an interesting insight when interpreting the results. As the spectral bands for this experiment were chosen to only approximate the peak absorption spectra of human photoreceptors, with peak transmittances near 440, 535, and 565 nm, this researcher did not

expect a typical rgb color rendition. As expected the color rendition of the MacBeth color checker produced by additive mixture of the three spectral bands, is indeed, not true.

A lack of complete longwave (red) spectral coverage produced a color rendition with poor red representation. This condition is defined by the lack of classification accuracy for the polygon target or class normally described as fully saturated red, class thirteen. It is clearly evident that from an interpretation perspective, the color rendition produced under the condition of the three gels would seriously inhibit interpretive accuracy. The inadequate color rendering capacity of the illumination conditions generated by the superimposition of the gels, resulted in false color representation in nearly all instances.

The spectral shifts induced by the three gels were recorded very reliably by the gray tone step array, represented by column four of the MacBeth color checker. Here, the lack of chromatic adaptation, is evidenced by the hues taken on by the gray tone array. The polygon target located at row six, column four, represents a pure white. This polygon represents the white region within the target that provided the benchmark for the one hundred standard divisions, for video gain settings. As recorded by the color additive image for the blue gel, the white target region has taken on a bluish hue, induced by the spectral shift. As recorded by the color additive image for the image set greengel, this same polygon has taken on a yellowish hue. In the color additive image for the image set redgel, this same polygon has taken on a bluish hue, similar to that induced by the blue gel. The resulting adopted hues clearly indicate a lack of chromatic adaptation by the sensors.

The additive color images representing the application of the SRC function also provide evidence supportive of the experimental results. Without examining each polygon target individually, evidence as to the performance of the SRC function is clearly supported by the target polygon, white (row 6, col 4). After the application of the SRC function to the bluegel condition, the white polygon retained a bluish hue. Similarly, the color additive image for the image set SRCGREEN, resulted in a similar bluish hue for the white polygon. For the color additive image representing the SRCRED image set, however, the target polygon at row six,

column four, appears white as it did under the broadspectrum illumination condition. Again this provides evidence for the success of the SRC function in restoring the relative reflectances as recorded under the broadspectrum illumination condition. As well, the similarity between the SRCBLUE and SRCGREEN additive images, both having a bluish hue attached to the white polygon, further supports the possibility that the between-band gain control, when applied to these two image sets, was dominated by a two color gain balance.

The departure point for this experimental project has embraced the widely accepted view that color constant sensations result from the relative degree of excitation between three sets of broadly overlapping wavebands whose range of sensitivities is under continuous adjustment. In terms of a multiband video imaging system, the premise has been adopted that brightness constancy gain control alone, would provide chromatic adaptive imaging capabilities, given sufficient overlap in band range sensitivities.

Land's (1977), assertion that the final perceptual response of the visual system is lightness with the final response being determined by the relative lightness between waveband sets, has been successfully replicated by analogy herein. While this has been demonstrated under only one in three conditions, the photographic recordings of the digital images have provided convincing evidence of the promise of this technique.

Conclusions

A simulation of chromatic adaptation has been tested by means of analogue between-band gain control, herein referred to as SRC (simulated response compression). While the test parameters were not intended to fully replicate the consequence of human chromatic adaptation known as color constancy, a similarity in utility is no doubt evident. The primary intention of this experiment was to improve classification accuracy by monitoring gain responses to chromatic shifts within a three band system and compensate for those chromatic shifts by between band gain adjustments.

The band composition selected for this experiment was based upon the following criteria. The peak transmittance centers roughly approximated those of the absorption spectra for the three classes of cones found in the human retina (Cornsweet, 1970). The extent of between-band overlap roughly approximated the overlap between the above-mentioned absorption spectra. Broadly overlapping bands were further chosen for this experiment for two additional reasons. First, overlapping band sensitivities were expected to produce overlapping effects indicating the extent of the between band effect and overall relative degree of sensor excitation and required gain adjustment. Second, very little experimentation has been conducted using overlapping bands for airborne imaging systems.

The induced spectral shifts generated by the superimposition of photographic effect gels over the source illuminant, produced the desired variations of illumination quality. Color additive images produced by the three wavebands, indicated that color shifts generated were sufficiently disruptive to inhibit reliable target interpretative identification from the photographic and digital display products. The robustness of the maximum-likelihood classifier used, combined with the careful selection of training set pixels, produced very reliable classification accuracies, in spite of the lack of chromatic adaptation to induced spectral shifts. Classification accuracies were not significantly improved by the application of SRC for the following reasons. First, the three band filter combination used failed under two illumination conditions to produce a three band, three color, spectral composition. The interrupted red band coverage of the Wr. 59 gelatin filter used for the long waveband, produced bi-modal gain effects. The interruption in spectral coverage within the mid red portion of the spectrum for this waveband produced results similar in effect to having two filters for the one waveband. Induced short and middle wavelength spectral shifts left the far red sensitivity of the long waveband sensor without sufficient energy to produce a three color image. This condition resulted in the SRC function being unable to restore the three color relative reflectances produced by the broadspectrum illuminant. This condition could easily be avoided by using a long waveband filter with uninterrupted red spectral coverage, which would provide the degree of band overlap desired, with more complete spectral coverage in the red

region of the spectrum. Multispectral video systems without broad overlapping bands and between band gain control would not permit the same relative degree of excitation to be recorded by each waveband. Because of this the resulting brightness values are not readily comparable by relative degree.

The between band gain control as applied herein, requires a white target region within each sensor's angular field of view, for accurate gain adjustment. The static target used in this experiment included a white target region to which all gain adjustments and settings were calibrated to one hundred standard divisions. Field applications of this imaging technique may require sensor modification to include a white region in the angular field of view.

While no commercial filters have been created to precisely replicate the absorption spectra of the three sets of human cones, filters providing sufficient band overlap to control for between band gain responses are available. The degree of overlap required has not been determined herein and should be determined by experimentation. The degree of transmittance within the overlapping range must be sufficient to permit CCD signal responses of sufficient amplitude to identify a spectral shift. The degree of overlap required should be determined for the specific sensor and filter combination. Camera gain sensitivities should also be matched. During the course of the experiment it was determined that under the fixed gain settings the three cameras did not have the same offset, differing by as many as fifteen standard divisions (ie:15 percent of 1 volt), when imaging, unfiltered, the same (boresighted) target, illuminated by the broadspectrum. Channel offset, also called intercept (the distance from the origin to a point where a graph crosses a coordinate axis), represents the difference in terms of a voltage constant, of the baseline signal, between 0 and 1 volt. Bandwidths as determined by filter combinations should also be nearly equal to assure similar output dynamic ranges. Sensor offset tended not to be a problem, however, when manual gain settings were used. The same condition would have to be true for any automatic between band gain control.

Shadows incident in most terrain imaging, would provide the pedestal for the black clipping, lower end output, while an inset, white target would provide the benchmark for the

maximum one hundred standard divisions. Under these conditions no sensor offset should be present. Further experiments should be conducted using a static target and imaging under varying daylight conditions. Under such conditions, one may find it desirable to vary sensor bandwidths to compensate for skylight and atmospheric constituents.

The logical direction in which to proceed regarding further experimentation, would be to design and build an electronic controller to monitor, record and control between-band gain responses. Such a device would provide some degree of chromatic adaptation for multispectral video imaging systems. The utility of this type of between-band gain control is uncertain when used with discrete non-overlapping waveband, multispectral sensors.

Table 2 **Error Matrix Resulting From Classifying Training Set Pixels Image Set Broadspectrum**

Training Set Data — Classes 1 through 15 and Null Class

	1	2	3	4	5	6	7	8	9	10	11	12	13	14	15	Null	Total
Classification Data																	
1.	2430	0	0	0	0	0	0	0	0	0	0	0	0	0	0	184	2614
2.	0	2591	0	0	0	0	0	0	0	0	0	0	0	0	0	14	2605
3.	0	0	2815	0	0	0	0	0	0	0	0	0	0	0	0	3	2818
4.	0	0	0	2642	0	0	0	0	0	0	0	0	0	0	0	88	2730
5.	0	0	0	0	2672	0	0	0	0	0	0	0	0	0	0	80	2752
6.	0	0	0	0	0	2506	0	0	0	0	0	0	0	0	0	141	2647
7.	0	0	0	0	0	0	2720	0	0	0	0	0	0	0	0	104	2824
8.	0	0	0	0	0	0	0	2679	0	0	0	0	0	0	0	102	2781
9.	0	0	0	0	0	0	0	0	2804	0	0	0	0	0	0	36	2840
10.	0	0	0	0	0	0	0	0	0	2606	0	0	0	0	0	112	2718
11.	0	0	0	0	0	0	0	0	0	0	2688	0	0	0	0	20	2708
12.	0	0	0	0	0	0	0	0	0	0	0	2658	0	0	0	389	3047
13.	0	0	0	0	0	0	0	0	0	0	0	0	0	0	0	0	0
14.	0	0	0	0	0	0	0	0	0	0	0	0	0	2715	0	49	2764
15.	0	0	0	0	0	0	0	0	0	0	0	0	0	0	2826	52	2878
Column Total	2430	2591	2815	2642	2672	2506	2720	2679	2804	2606	2688	2658	0	2715	2826	1374	38726

Accuracy Assessment based upon omission error (diagonal element / row total)

(1-15)	93%	99%	100%	97%	97%	98%	96%	96%	99%	96%	99%	87%	0%	98%	98%	

Mean number of pixels per polygon (class) = 2668

Number of pixels per average polygon based upon selection criteria = 2655

Σ diagonal elements = 37352

Table 3 **Error Matrix Resulting From Classifying Training Set Pixels Image Set Bluegel**

	Training Set Data — Classes 1 through 15 and Null Class																
	1	2	3	4	5	6	7	8	9	10	11	12	13	14	15	Null	Total
Classification Data																	
1.	2698	0	0	0	0	0	0	0	0	0	0	0	0	0	0	23	2721
2.	0	2641	0	0	0	0	0	0	0	0	0	0	0	0	0	63	2704
3.	0	0	2846	0	0	0	0	0	0	0	0	0	0	0	0	60	2903
4.	0	0	0	2713	0	0	0	0	0	0	0	0	0	0	0	72	2785
5.	0	0	0	0	2767	0	0	0	0	0	0	0	0	0	0	3	2770
6.	0	0	0	0	0	2675	0	0	0	0	0	0	0	0	0	366	3041
7.	0	0	0	0	0	0	2849	0	0	0	0	0	0	0	0	69	2918
8.	0	0	0	0	0	0	0	2709	0	0	0	0	0	0	0	73	2782
9.	0	0	0	0	0	0	0	0	2908	0	0	0	0	0	0	20	2928
10.	0	0	0	0	0	0	0	0	0	2665	0	0	0	0	0	17	2682
11.	0	0	0	0	0	0	0	0	0	0	2751	0	0	0	0	9	2760
12.	0	0	0	0	0	0	0	0	0	0	0	2685	0	0	0	36	2721
13.	0	0	0	0	0	0	0	0	0	0	0	0	0	0	0	0	0
14.	0	0	0	0	0	0	0	0	0	0	0	0	0	2756	0	80	2836
15.	0	0	0	0	0	0	0	0	0	0	0	0	0	0	2821	105	2926
Column Total	2698	2641	2846	2713	2767	2675	2849	2709	2908	2665	2751	2685	0	2756	2821	996	39480

Accuracy Assessment based upon omission error (diagonal element / row total)

(1-15)	99%	98%	98%	97%	100%	88%	98%	97%	99%	99%	100%	99%	0%	97%	96%		

Mean number of pixels per polygon (class) = 2749

Number of pixels per average polygon based upon selection criteria = 2655

Σ diagonal elements = 38484

Table 4 **Error Matrix Resulting From Classifying Training Set Pixels Image Set Greengel**

Training Set Data — Classes 1 through 15 and Null Class

	1	2	3	4	5	6	7	8	9	10	11	12	13	14	15	Null	Total
Classification Data																	
1.	2616	0	0	0	0	0	0	0	0	0	0	0	0	0	0	492	3108
2.	0	2665	0	0	0	0	0	0	0	0	0	0	0	0	0	8	2673
3.	0	0	2809	0	0	0	0	0	0	0	0	0	0	0	0	6	2815
4.	0	0	0	2696	0	0	0	0	0	0	0	0	0	0	0	49	2745
5.	0	0	0	0	2676	0	0	0	0	0	0	0	0	0	0	21	2697
6.	0	0	0	0	0	2519	0	0	0	0	0	0	0	0	0	91	2610
7.	0	0	0	0	0	0	2849	0	0	0	0	0	0	0	0	30	2879
8.	0	0	0	0	0	0	0	2719	0	0	0	0	0	0	0	64	2783
9.	0	0	0	0	0	0	0	0	2754	0	0	0	0	0	0	41	2795
10.	0	0	0	0	0	0	0	0	0	2627	0	0	0	0	0	252	2879
11.	0	0	0	0	0	0	0	0	0	0	2755	0	0	0	0	17	2772
12.	0	0	0	0	0	0	0	0	0	0	0	2098	0	0	0	55	2153
13.	0	0	0	0	0	0	0	0	0	0	0	0	0	0	0	0	0
14.	0	0	0	0	0	0	0	0	0	0	0	0	0	2756	0	22	2778
15.	0	0	0	0	0	0	0	0	0	0	0	0	0	0	2864	42	2906
Column Total	2616	2665	2809	2696	2676	2519	2849	2719	2754	2627	2755	2098	0	2756	2864	1190	38593

Accuracy Assessment based upon omission error (diagonal element / row total)

(1-15)	84%	100%	100%	98%	99%	97%	99%	98%	99%	91%	99%	97%	0%	99%	99%	

Mean number of pixels per polygon (class) = 2672

Number of pixels per average polygon based upon selection criteria = 2655

Σ diagonal elements = 37403

Table 5 **Error Matrix Resulting From Classifying Training Set Pixels Image Set Redgel**

	Training Set Data — Classes 1 through 15 and Null Class																
	1	2	3	4	5	6	7	8	9	10	11	12	13	14	15	Null	Total
Classification Data																	
1.	2644	0	0	0	0	0	0	0	0	0	0	0	0	0	0	664	3308
2.	0	2570	0	0	0	0	0	0	0	0	0	0	0	0	0	720	3290
3.	0	0	2900	0	0	0	0	0	0	0	0	0	0	0	0	141	3041
4.	0	0	0	2689	0	0	0	0	0	9	0	0	0	0	0	221	2919
5.	0	0	0	0	2737	0	0	0	0	0	0	0	0	0	0	358	3095
6.	0	0	0	0	0	2653	0	0	0	0	0	0	0	0	0	156	2809
7.	0	0	0	0	0	0	2805	0	0	0	0	0	0	0	0	26	2831
8.	0	0	0	0	0	0	0	2619	0	0	0	0	0	0	0	15	2634
9.	0	0	0	0	0	0	0	0	2842	0	0	0	0	0	0	4	2846
10.	0	0	0	0	0	0	0	0	0	2644	0	0	0	0	0	186	2830
11.	0	0	0	0	0	0	0	0	0	0	2671	0	0	0	0	52	2723
12.	0	0	0	0	0	0	0	0	0	0	0	2295	0	0	0	98	2393
13.	0	0	0	0	0	0	0	0	0	0	0	0	0	0	0	0	0
14.	0	0	0	0	0	0	0	0	0	0	0	0	0	2825	0	6	2831
15.	0	0	0	0	0	0	0	0	0	0	0	0	0	0	2820	76	2896
Column Total	2644	2570	2900	2689	2737	2653	2805	2619	2842	2653	2671	2295	0	2825	2820	2723	40437
Accuracy Assessment based upon omission error (diagonal element / row total)																	
(1-15)	80%	78%	95%	92%	88%	94%	99%	99%	100%	93%	98%	96%	0%	100%	97%		

Mean number of pixels per polygon (class) = 2693

Number of pixels per average polygon based upon selection criteria = 2655

Σ diagonal elements = 37714

Table 6 **Error Matrix Resulting From Classifying Training Set Pixels Image Set SRCBLUE**

	Training Set Data — Classes 1 through 15 and Null Class																
	1	2	3	4	5	6	7	8	9	10	11	12	13	14	15	Null	Total
Classification Data																	
1.	2671	0	0	0	0	0	0	0	0	0	0	0	0	0	0	229	2900
2.	0	2588	0	0	0	0	0	0	0	0	0	0	0	0	0	44	2632
3.	0	0	2825	0	0	0	0	0	0	0	0	0	0	0	0	21	2846
4.	0	0	0	2657	0	0	0	0	0	9	0	0	0	0	0	48	2705
5.	0	0	0	0	2684	0	0	0	0	0	0	0	0	0	0	143	2827
6.	0	0	0	0	0	2630	0	0	0	0	0	0	0	0	0	52	2682
7.	0	0	0	0	0	0	2824	0	0	0	0	0	0	0	0	82	2906
8.	0	0	0	0	0	0	0	2658	0	0	0	0	0	0	0	154	2812
9.	0	0	0	0	0	0	0	0	2780	0	0	0	0	0	0	95	2875
10.	0	0	0	0	0	0	0	0	0	2647	0	0	0	0	0	107	2754
11.	0	0	0	0	0	0	0	0	0	0	2694	0	0	0	0	55	2749
12.	0	0	0	0	0	0	0	0	0	0	0	2279	0	0	0	6	2285
13.	0	0	0	0	0	0	0	0	0	0	0	0	0	0	0	0	0
14.	0	0	0	0	0	0	0	0	0	0	0	0	0	2784	0	55	2839
15.	0	0	0	0	0	0	0	0	0	0	0	0	0	0	2788	385	3173
Column Total	2671	2588	2825	2657	2684	2630	2824	2658	2780	2647	2694	2279	0	2784	2788	1476	38985

Accuracy Assessment based upon omission error (diagonal element / row total)

(1-15)	92%	98%	99%	98%	95%	98%	97%	95%	97%	96%	98%	100%	0%	98%	88%

Mean number of pixels per polygon (class) = 2679

Number of pixels per average polygon based upon selection criteria = 2655

Σ diagonal elements = 37509

Table 7 **Error Matrix Resulting From Classifying Training Set Pixels Image Set SRCGREEN**

Training Set Data — Classes 1 through 15 and Null Class

	1	2	3	4	5	6	7	8	9	10	11	12	13	14	15	Null	Total
Classification Data																	
1.	2630	0	0	0	0	0	0	0	0	0	0	0	0	0	0	93	2723
2.	0	2573	0	0	0	0	0	0	0	0	0	0	0	0	0	939	3512
3.	0	0	2736	0	0	0	0	0	0	0	0	0	0	0	0	69	2805
4.	0	0	0	2632	0	0	0	0	0	0	0	0	0	0	0	348	2980
5.	0	0	0	0	2691	0	0	0	0	0	0	0	0	0	0	93	2784
6.	0	0	0	0	0	2625	0	0	0	0	0	0	0	0	0	89	2714
7.	0	0	0	0	0	0	2767	0	0	0	0	0	0	0	0	83	2850
8.	0	0	0	0	0	0	0	2640	0	0	0	0	0	0	0	62	2702
9.	0	0	0	0	0	0	0	0	2839	0	0	0	0	0	0	32	2871
10.	0	0	0	0	0	0	0	0	0	2593	0	0	0	0	0	222	2815
11.	0	0	0	0	0	0	0	0	0	0	2672	0	0	0	0	58	2730
12.	0	0	0	0	0	0	0	0	0	0	0	2278	0	0	0	4	2282
13.	0	0	0	0	0	0	0	0	0	0	0	0	0	0	0	0	0
14.	0	0	0	0	0	0	0	0	0	0	0	0	0	2770	0	7	2777
15.	0	0	0	0	0	0	0	0	0	0	0	0	0	0	2807	95	2902
Column Total	2630	2573	2736	2632	2691	2625	2767	2640	2839	2593	2672	2278	0	2770	2807	1880	39133

Accuracy Assessment based upon omission error (diagonal element / row total)

(1-15)	97%	73%	98%	88%	97%	97%	97%	98%	99%	92%	98%	100%	0%	100%	97%	

Mean number of pixels per polygon (class) = 2661

Number of pixels per average polygon based upon selection criteria = 2655

Σ diagonal elements = 37253

Table 8 **Error Matrix Resulting From Classifying Training Set Pixels Image Set SRCRED**

Training Set Data — Classes 1 through 15 and Null Class

	1	2	3	4	5	6	7	8	9	10	11	12	13	14	15	Null	Total
Classification Data																	
1.	2523	0	0	0	0	0	0	0	0	0	0	0	0	0	0	190	2713
2.	0	2575	0	0	0	0	0	0	0	0	0	0	0	0	0	603	3178
3.	0	0	2780	0	0	0	0	0	0	0	0	0	0	0	0	22	2802
4.	0	0	0	2640	0	0	0	0	0	0	0	0	0	0	0	54	2694
5.	0	0	0	0	2699	0	0	0	0	0	0	0	0	0	0	61	2760
6.	0	0	0	0	0	2568	0	0	0	0	0	0	0	0	0	645	3213
7.	0	0	0	0	0	0	2741	0	0	0	0	0	0	0	0	46	2787
8.	0	0	0	0	0	0	0	2579	0	0	0	0	0	0	0	186	2765
9.	0	0	0	0	0	0	0	0	2744	0	0	0	0	0	0	97	2841
10.	0	0	0	0	0	0	0	0	0	2569	0	0	0	0	0	391	2960
11.	0	0	0	0	0	0	0	0	0	0	2652	0	0	0	0	365	3017
12.	0	0	0	0	0	0	0	0	0	0	0	2130	0	0	0	56	2186
13.	0	0	0	0	0	0	0	0	0	0	0	0	3107	0	0	28	3135
14.	0	0	0	0	0	0	0	0	0	0	0	0	0	2788	0	7	2795
15.	0	0	0	0	0	0	0	0	0	0	0	0	0	0	2783	10	2793
Column Total	2523	2575	2780	2640	2699	2568	2741	2579	2744	2569	2652	2130	3107	2788	2783	2761	42639

Accuracy Assessment based upon omission error (diagonal element / row total)

(1-15)	93%	81%	99%	98%	98%	80%	98%	93%	97%	87%	88%	97%	99%	100%	100%	

Mean number of pixels per polygon (class) = 2627 *(where n=14), = 2659 *(where n=15)

Number of pixels per average polygon based upon selection criteria = 2655

Σ diagonal elements = 39878

* For tables 2 through 8, n=14 (zero values for class 13 were omitted to avoid skewed results)

Appendix A

Table 9

COVARIANCE MATRIX FOR IMAGE: broadspe
COMPONENT PICTURES: 4 5 6 (SHORT, MIDDLE, LONG)

434.42	366.25	534.92
366.25	487.77	703.73
534.92	703.73	1030.83

CORRELATION MATRIX IS:

1.00	0.80	0.80
0.80	1.00	0.99
0.80	0.99	1.00

EIGENVALUES ARE:

1817.47	0.00	0.00
0.00	130.55	0.00
0.00	0.00	5.00

EIGENVECTORS ARE:

0.42	0.91	0.00
0.51	-0.24	0.82
0.75	-0.35	-0.57

PERCENT OF TOTAL VARIANCE CONTRIBUTED BY EACH BAND

SHORT	22%
MIDDLE	25%
LONG	53%

PERCENT OF VARIANCE EXPLAINED BY PRINCIPAL COMPONENT

PC1	93%
PC2	6.7%
PC3	.3%

FACTOR LOADINGS (CORRELATION OF BANDS TO COMPONENT)

SHORT	.859
MIDDLE	-0.124
LONG	-0.039

Appendix A

Table 10

COVARIANCE MATRIX FOR IMAGE: bluegel
COMPONENT PICTURES: 4 5 6 (SHORT, MIDDLE, LONG)

624.66	315.39	308.42
315.39	243.69	232.83
308.42	232.83	225.88

CORRELATION MATRIX IS:

1.00	0.81	0.82
0.81	1.00	0.99
0.82	0.99	1.00

EIGENVALUES ARE:

994.27	0.00	0.00
0.00	98.24	0.00
0.00	0.00	1.73

EIGENVECTORS ARE:

0.77	-0.64	-0.02
0.46	0.57	-0.68
0.45	0.51	0.73

PERCENT OF TOTAL VARIANCE CONTRIBUTED BY EACH BAND

SHORT	57%
MIDDLE	22%
LONG	21%

PERCENT OF VARIANCE EXPLAINED BY PRINCIPAL COMPONENT

PC1	91%
PC2	8.9%
PC3	.1%

FACTOR LOADINGS (CORRELATION OF BANDS TO COMPONENTS)

SHORT	.971
MIDDLE	.361
LONG	.063

Appendix A

Table 11

COVARIANCE MATRIX FOR IMAGE: greengel
COMPONENT PICTURES: 4 5 6 (SHORT, MIDDLE, LONG)

123.95	197.06	271.27
197.06	485.99	660.51
271.27	660.51	910.17

CORRELATION MATRIX IS:

1.00	0.80	0.81
0.80	1.00	0.99
0.81	0.99	1.00

EIGENVALUES ARE:

1475.01	0.00	0.00
0.00	40.75	0.00
0.00	0.00	4.35

EIGENVECTORS ARE:

0.24	0.97	0.02
0.57	-0.15	0.81
0.78	-0.19	-0.59

PERCENT OF TOTAL VARIANCE CONTRIBUTED BY EACH BAND

SHORT	8%
MIDDLE	32%
LONG	60%

PERCENT OF VARIANCE EXPLAINED BY PRINCIPAL COMPONENT

PC1	97%
PC2	2.7%
PC3	.3%

FACTOR LOADINGS (CORRELATION OF BANDS TO COMPONENTS)

SHORT	.827
MIDDLE	-0.043
LONG	-0.040

Appendix

Table 12

COVARIANCE MATRIX FOR IMAGE: redgel
COMPONENT PICTURES: 4 5 6 (SHORT, MIDDLE, LONG)

1054.47	366.89	414.27
366.89	193.39	216.18
414.27	216.18	246.57

CORRELATION MATRIX IS:

1.00	0.81	0.81
0.81	1.00	0.99
0.81	0.99	1.00

EIGENVALUES ARE:

1379.61	0.00	0.00
0.00	112.64	0.00
0.00	0.00	2.17

EIGENVECTORS ARE:

0.86	-0.51	0.00
0.34	0.57	-0.75
0.38	0.65	0.66

PERCENT OF TOTAL VARIANCE CONTRIBUTED BY EACH BAND

SHORT	71%
MIDDLE	13%
LONG	16%

PERCENT OF VARIANCE EXPLAINED BY PRINCIPAL COMPONENT

PC1	92.3%
PC2	7.5%
PC3	.2%

FACTOR LOADINGS (CORRELATION OF BANDS TO COMPONENTS)

SHORT	.983
MIDDLE	.435
LONG	.061

Appendix A

Table 13

COVARIANCE MATRIX FOR IMAGE: srcblue
COMPONENT PICTURES: 4 5 6 (SHORT, MIDDLE, LONG)

934.57	565.18	559.09
565.18	522.21	504.69
559.09	504.69	494.47

CORRELATION MATRIX IS:

1.00	0.81	0.82
0.81	1.00	0.99
0.82	0.99	1.00

EIGENVALUES ARE:

1769.84	0.00	0.00
0.00	178.09	0.00
0.00	0.00	3.32

EIGENVECTORS ARE:

0.69	-0.72	-0.02
0.52	0.51	-0.68
0.51	0.46	0.73

PERCENT OF TOTAL VARIANCE CONTRIBUTED BY EACH BAND

SHORT 48%

MIDDLE 27%

LONG 25%

PERCENT OF VARIANCE EXPLAINED BY PRINCIPAL COMPONENT

PC1 90.7%

PC2 9.1%

PC3 .2%

FACTOR LOADINGS (CORRELATION OF BANDS TO COMPONENTS)

SHORT .949

MIDDLE .297

LONG .059

Appendix A

Table 14

COVARIANCE MATRIX FOR IMAGE: srcgreen
COMPONENT PICTURES: 4 5 6 (SHORT, MIDDLE, LONG)

908.30	534.54	539.86
534.54	490.87	489.93
539.86	489.93	495.58

CORRELATION MATRIX IS:

1.00	0.80	0.80
0.80	1.00	0.99
0.80	0.99	1.00

EIGENVALUES ARE:

1706.37	0.00	0.00
0.00	185.09	0.00
0.00	0.00	3.28

EIGENVECTORS ARE:

0.69	-0.72	-0.01
0.51	0.49	-0.71
0.51	0.48	0.71

PERCENT OF TOTAL VARIANCE CONTRIBUTED BY EACH BAND

SHORT	48%
MIDDLE	26%
LONG	26%

PERCENT OF VARIANCE EXPLAINED BY PRINCIPAL COMPONENT

PC1	90%
PC2	9.8%
PC3	.2%

FACTOR LOADINGS (CORRELATION OF BANDS TO COMPONENTS)

SHORT	.945
MIDDLE	.300
LONG	.057

Appendix A

Table 15

COVARIANCE MATRIX FOR IMAGE: srcred
COMPONENT PICTURES: 4 5 6 (SHORT, MIDDLE, LONG)

464.60	386.88	562.27
386.88	486.41	700.16
562.27	700.16	1026.53

CORRELATION MATRIX IS:

1.00	0.81	0.81
0.81	1.00	0.99
0.81	0.99	1.00

EIGENVALUES ARE:

1844.49	0.00	0.00
0.00	127.03	0.00
0.00	0.00	6.03

EIGENVECTORS ARE:

0.44	0.90	-0.01
0.51	-0.25	0.83
0.74	-0.37	-0.56

PERCENT OF TOTAL VARIANCE CONTRIBUTED BY EACH BAND

SHORT 23%

MIDDLE 25%

LONG 52%

PERCENT OF VARIANCE EXPLAINED BY PRINCIPAL COMPONENT

PC1 93.3%

PC2 6.4%

PC3 .3%

FACTOR LOADINGS (CORRELATION OF BANDS TO COMPONENTS)

SHORT .876

MIDDLE -0.127

LONG -0.042

Image_Set	%var_S	%var_M	%var_L	F_loads_S	F_loads_M	F_loads_L
broadspe	22	25	53	0.859	-0.124	-0.039
bluegel	57	22	21	0.971	0.361	0.063
greengel	8	32	60	0.827	-0.043	-0.04
redgel	71	13	16	0.983	0.435	0.061
SRCBLUE	48	27	25	0.949	0.297	0.059
SRCGREEN	48	26	26	0.945	0.3	0.057
SRCRED	23	25	52	0.876	-0.127	-0.042
mean	39.57143	24.28571	36.14286			
var	502.2857	33.90476	327.8095			
stand_dev	22.412	5.823	18.106			
Stats for Sub-set Broadspectrum and Gels (Row 2 through 5, Col. B through D)						
mean	39.5	23	37.5			
var	865.6667	62	493.6667			
stand_dev	25.23886	7.874008	22.21861			

Appendix A Table 16 Factor Loadings

Appendix A

Table 17

Transmission Densitometry Optical Counts For Gels

Percent Transmittance

	Bluegel	Greengel	Redgel
Blue	0.05 (88.1%)	1.12 (7.6%)	0.79 (16.1%)
Green	0.22 (59.6%)	0.17 (66.8%)	1.48 (3.3%)
Red	1.45 (3.6%)	2.02 (.9%)	0.02 (94.4%)
Neutral	0.27 (53.2%)	0.23 (58.3%)	0.31 (48.5%)

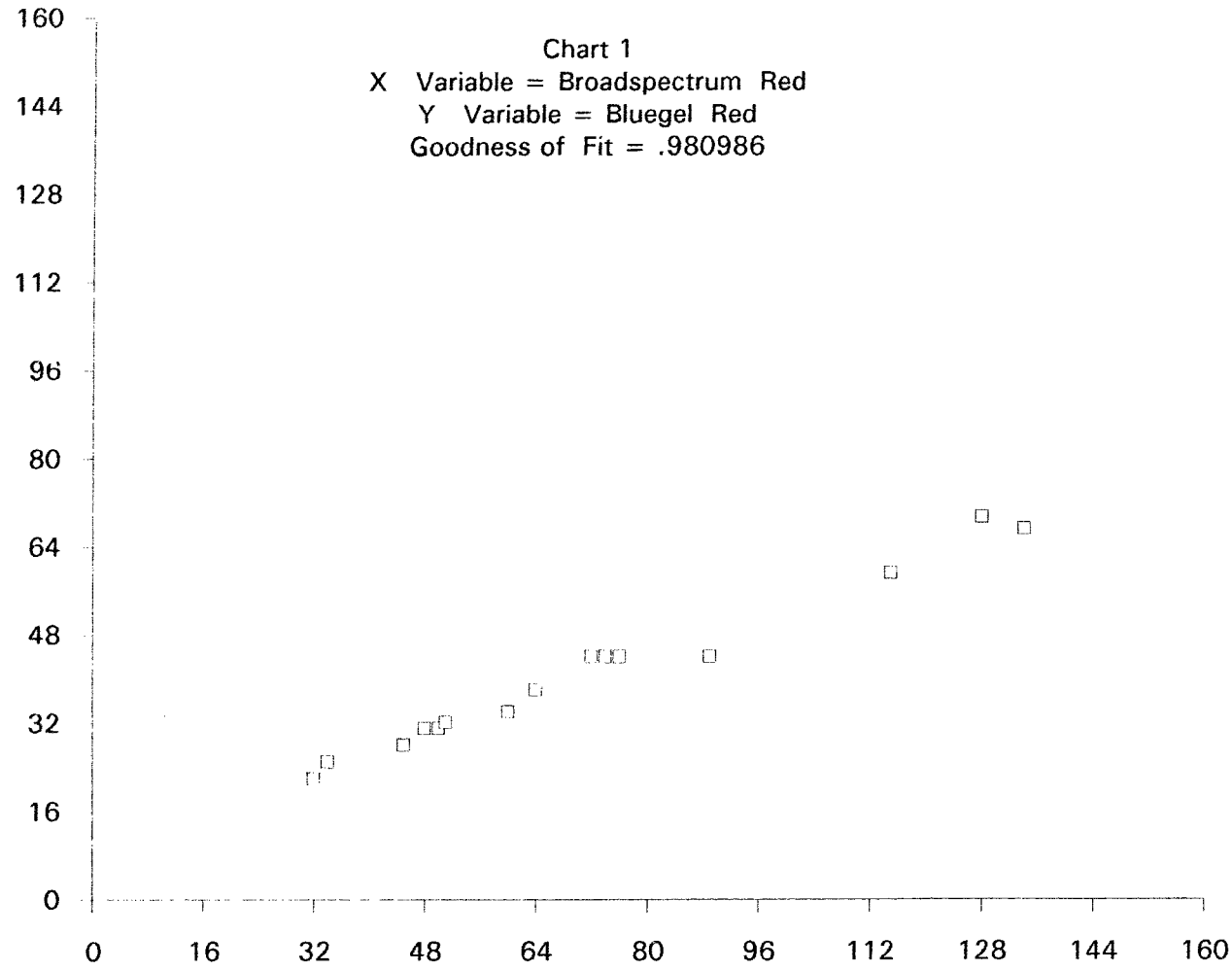
Chart 1
X Variable = Broadspectrum Red
Y Variable = Bluegel Red
Goodness of Fit = .980986
160
144
128
112
96
80
64
48
32
16
0
0
16
32
48
64
80
96
112
128
144
160

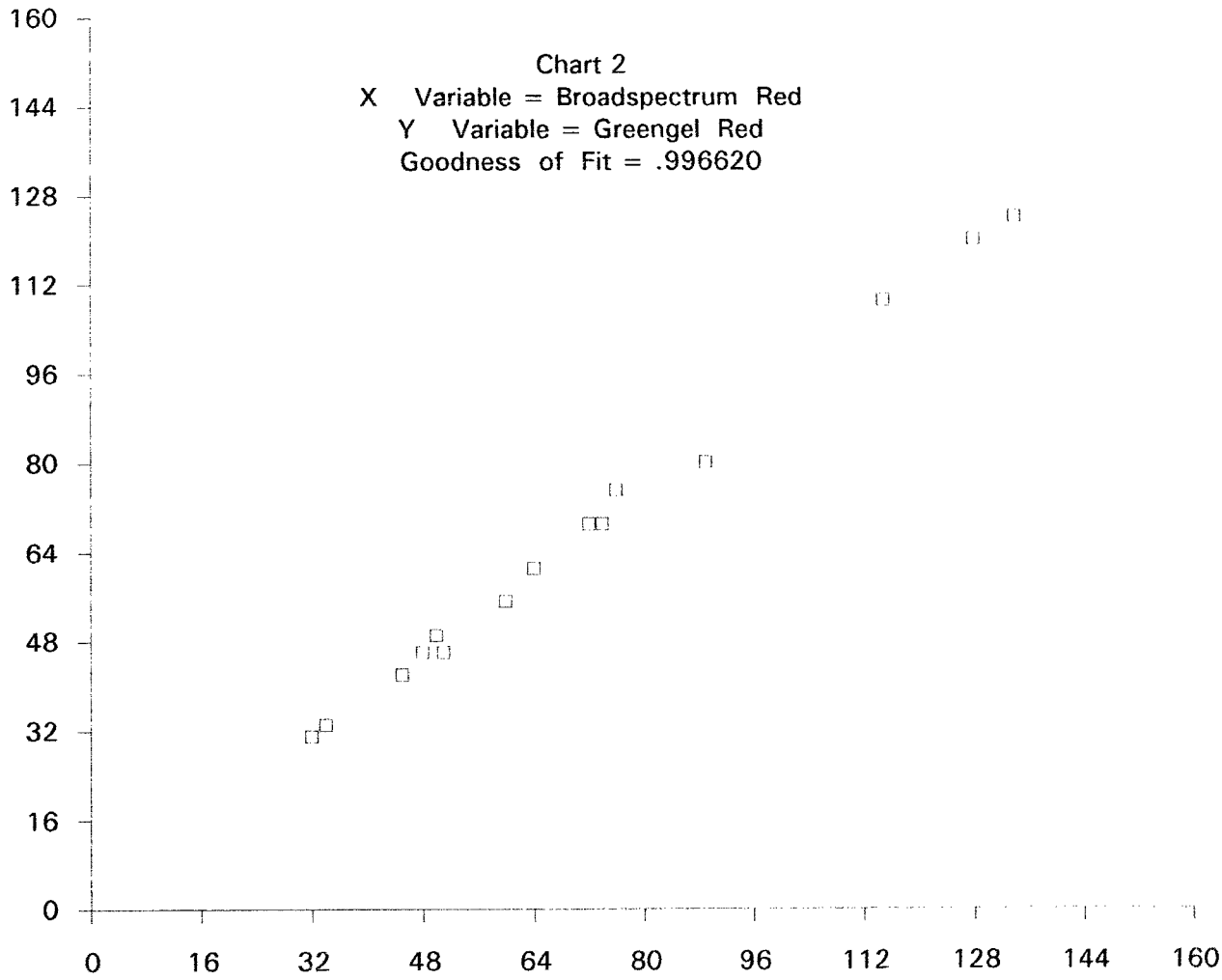
Chart 2
X Variable = Broadspectrum Red
Y Variable = Greengel Red
Goodness of Fit = .996620
160
144
128
112
96
80
64
48
32
16
0
0
16
32
48
64
80
96
112
128
144
160

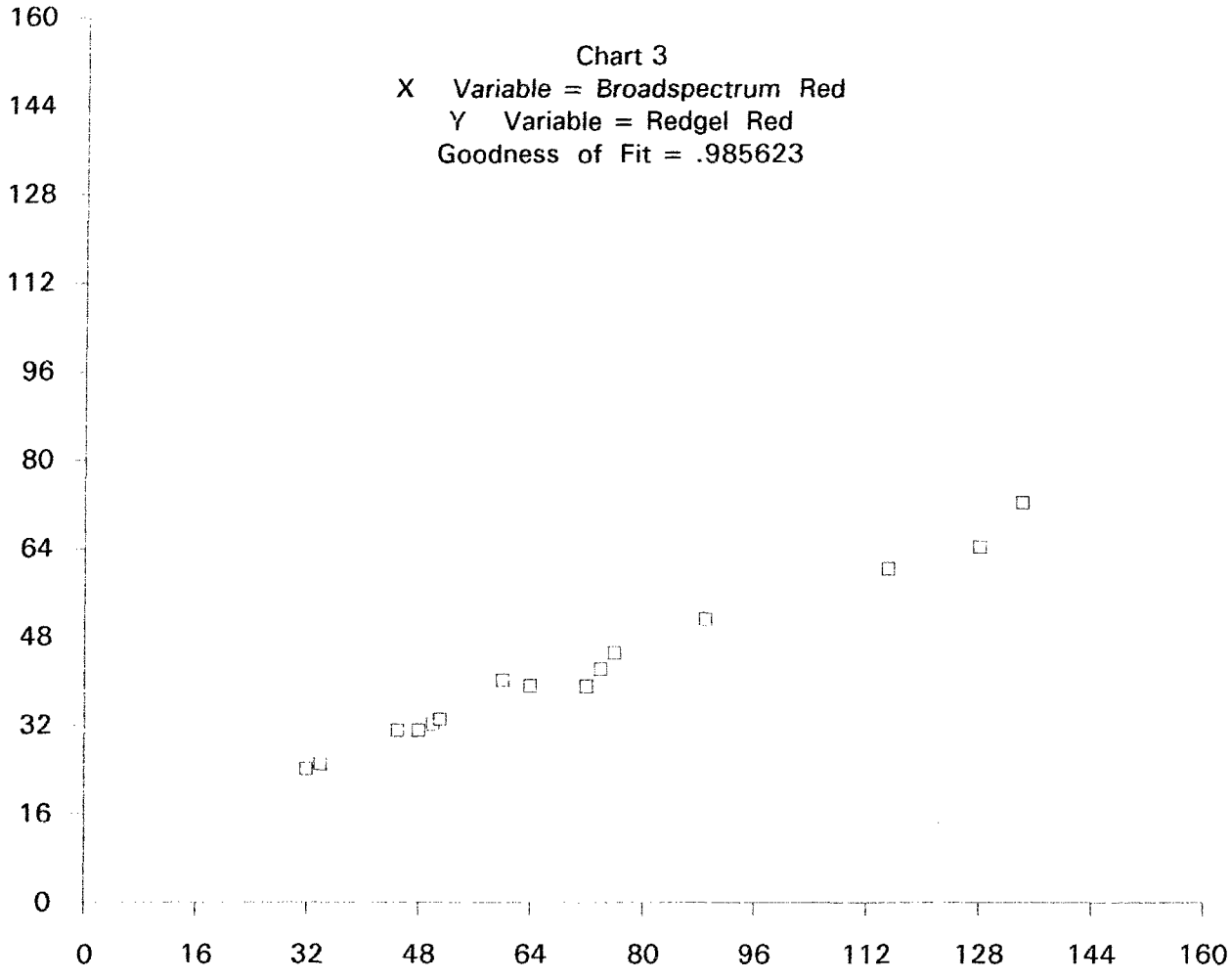
Chart 3
X Variable = Broadspectrum Red
Y Variable = Redgel Red
Goodness of Fit = .985623
160
144
128
112
96
80
64
48
32
16
0
0
16
32
48
64
80
96
112
128
144
160

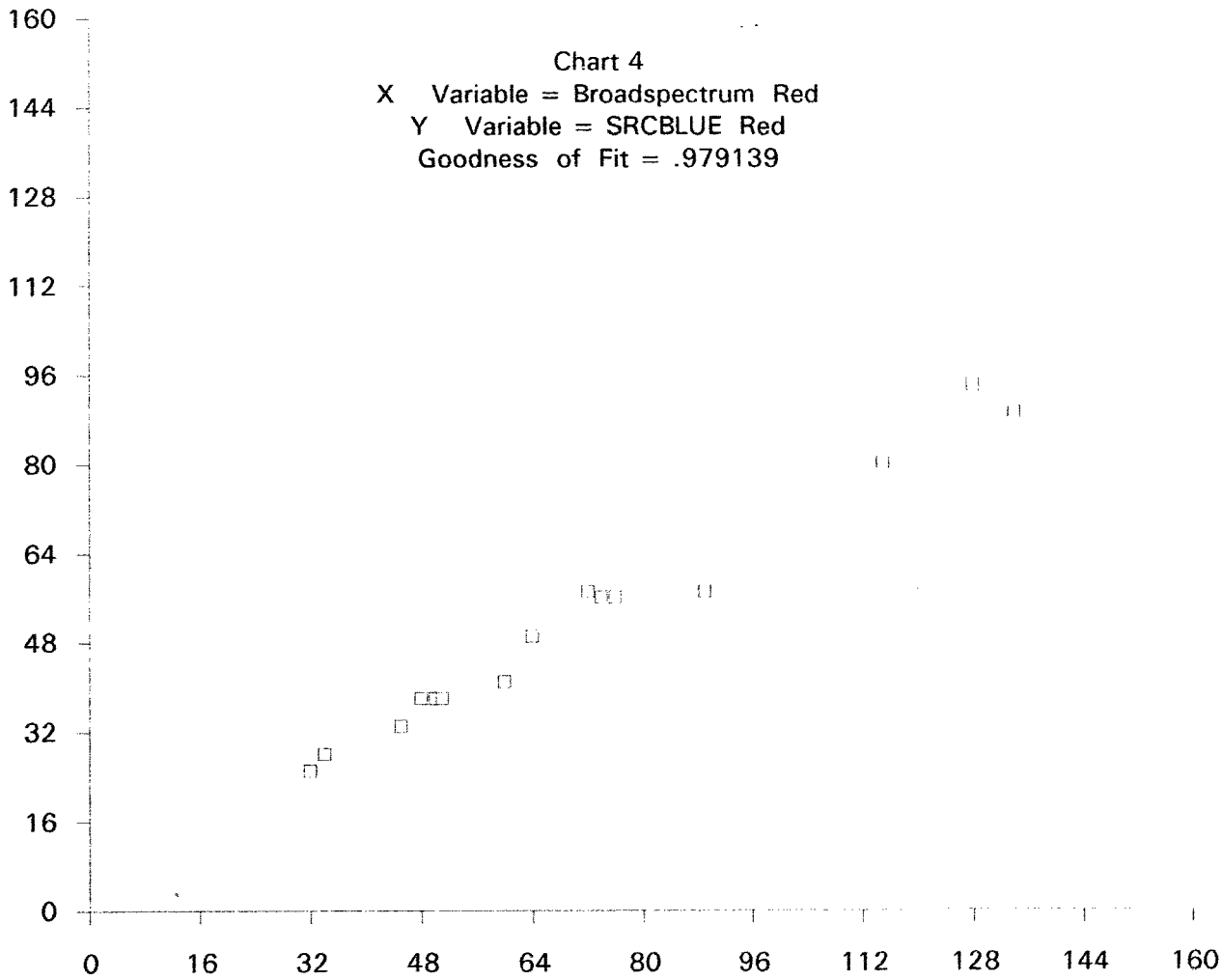
Chart 4
X Variable = Broadspectrum Red
Y Variable = SRCBLUE Red
Goodness of Fit = .979139
160
144
128
112
96
80
64
48
32
16
0
0
16
32
48
64
80
96
112
128
144
160

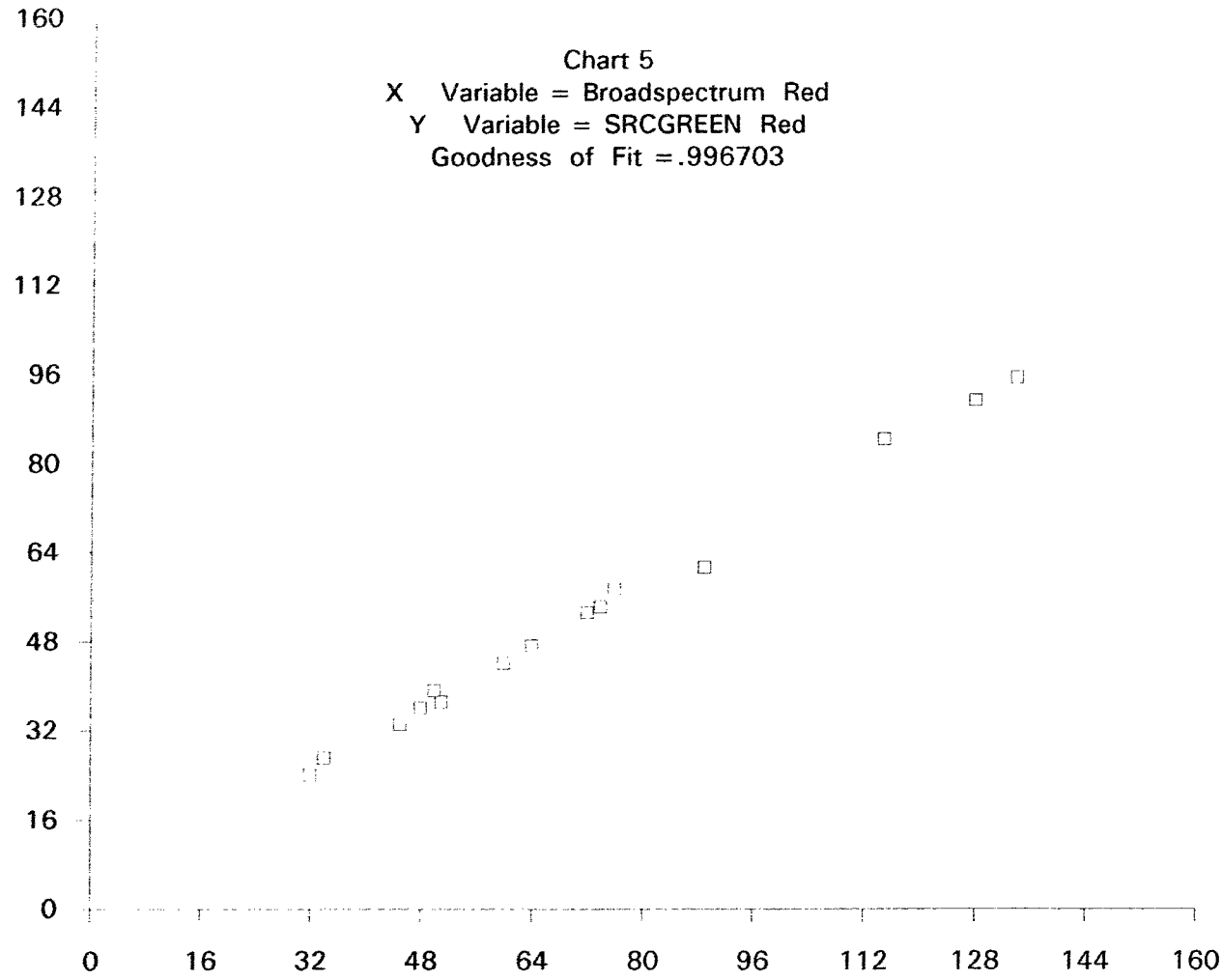
Chart 5
X Variable = Broadspectrum Red
Y Variable = SRCGREEN Red
Goodness of Fit =.996703
160
144
128
112
96
80
64
48
32
16
0
0
16
32
48
64
80
96
112
128
144
160

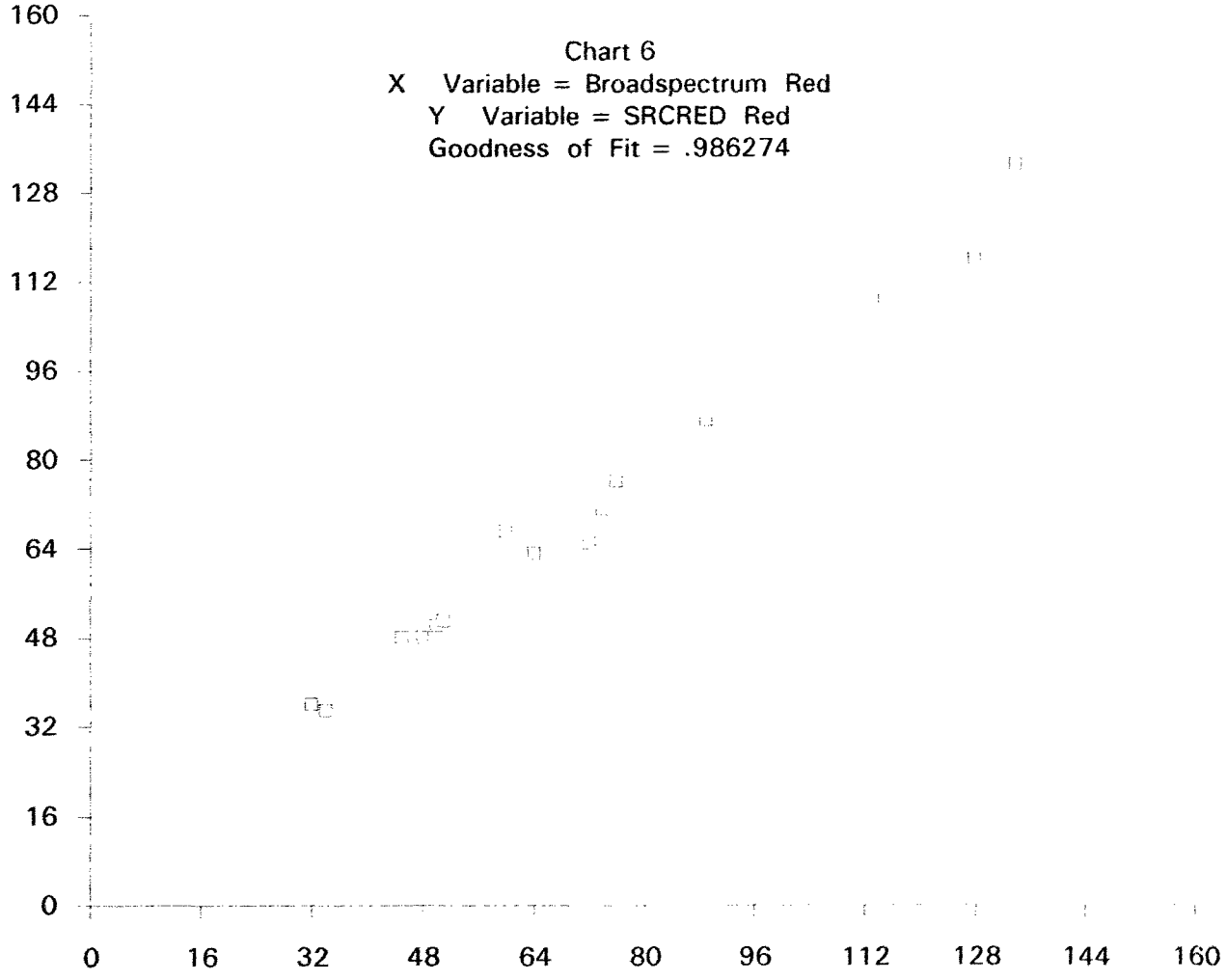
Chart 6
X Variable = Broadspectrum Red
Y Variable = SRCRED Red
Goodness of Fit = .986274
160
144
128
112
96
80
64
48
32
16
0
0
16
32
48
64
80
96
112
128
144
160

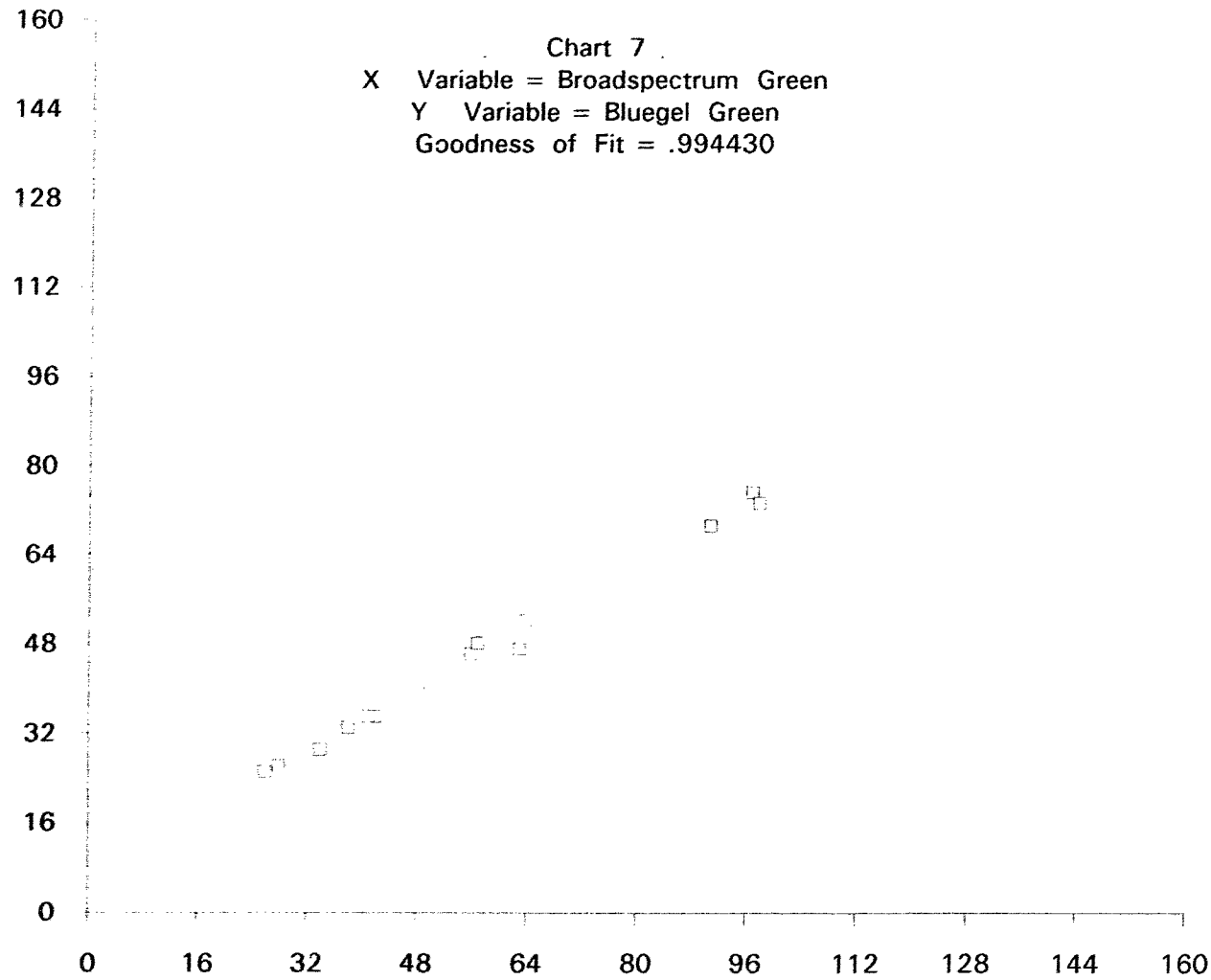
Chart 7
X Variable = Broadspectrum Green
Y Variable = Bluegel Green
Goodness of Fit = .994430
160
144
128
112
96
80
64
48
32
16
0
0
16
32
48
64
80
96
112
128
144
160

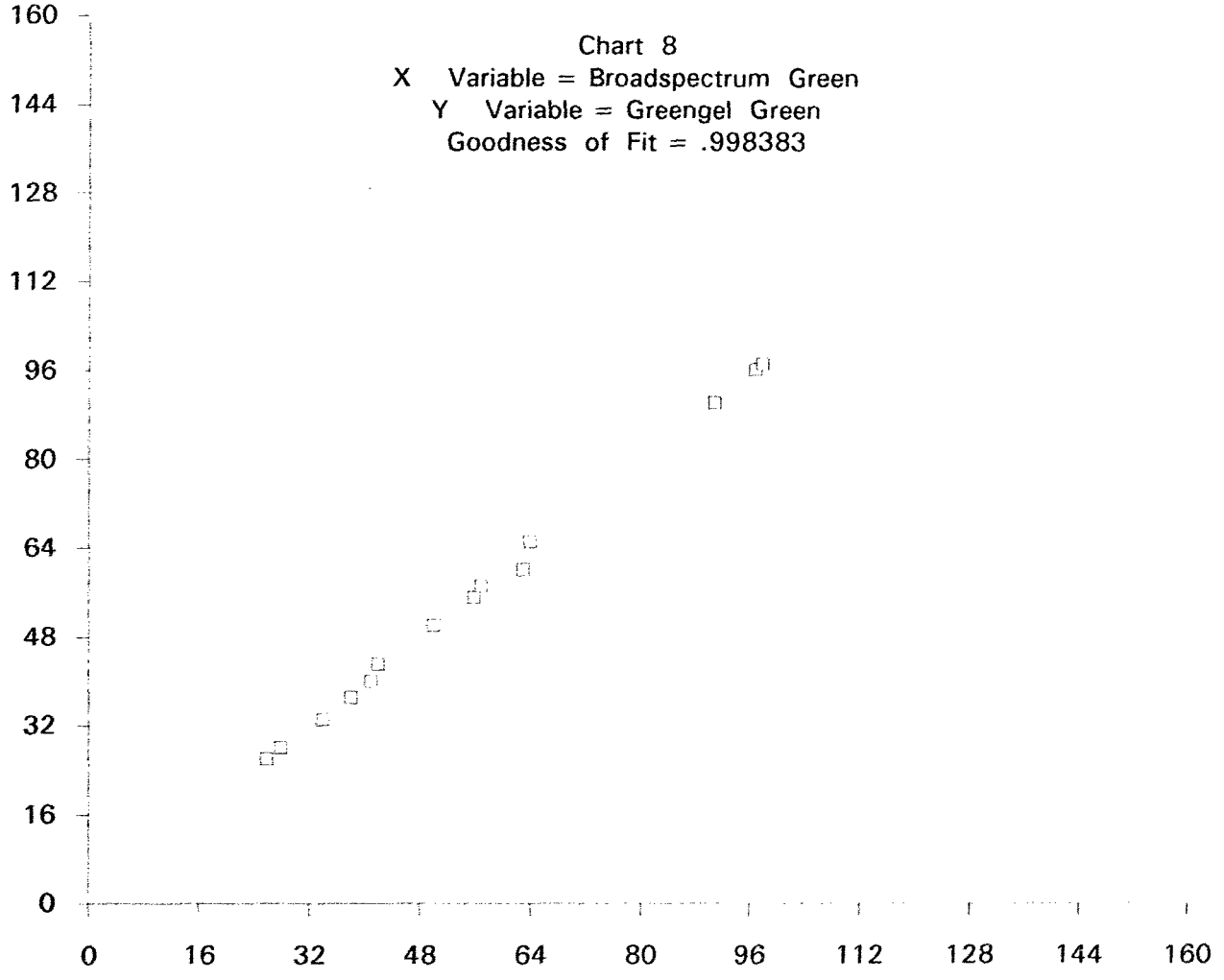
Chart 8
X Variable = Broadspectrum Green
Y Variable = Greengel Green
Goodness of Fit = .998383
160
144
128
112
96
80
64
48
32
16
0
0
16
32
48
64
80
96
112
128
144
160

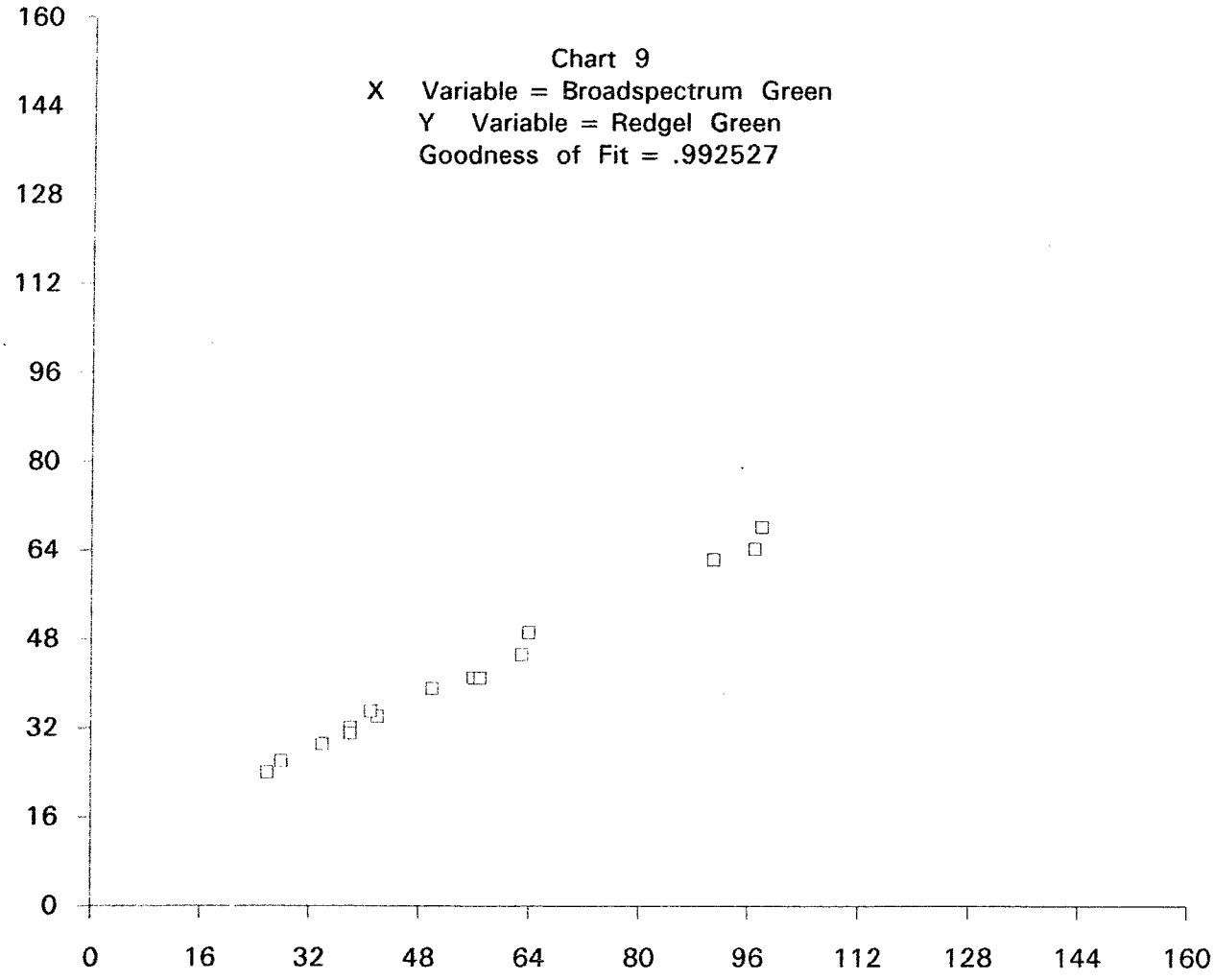
Chart 9
X Variable = Broadspectrum Green
Y Variable = Redgel Green
Goodness of Fit = .992527
160
144
128
112
96
80
64
48
32
16
0
0
16
32
48
64
80
96
112
128
144
160

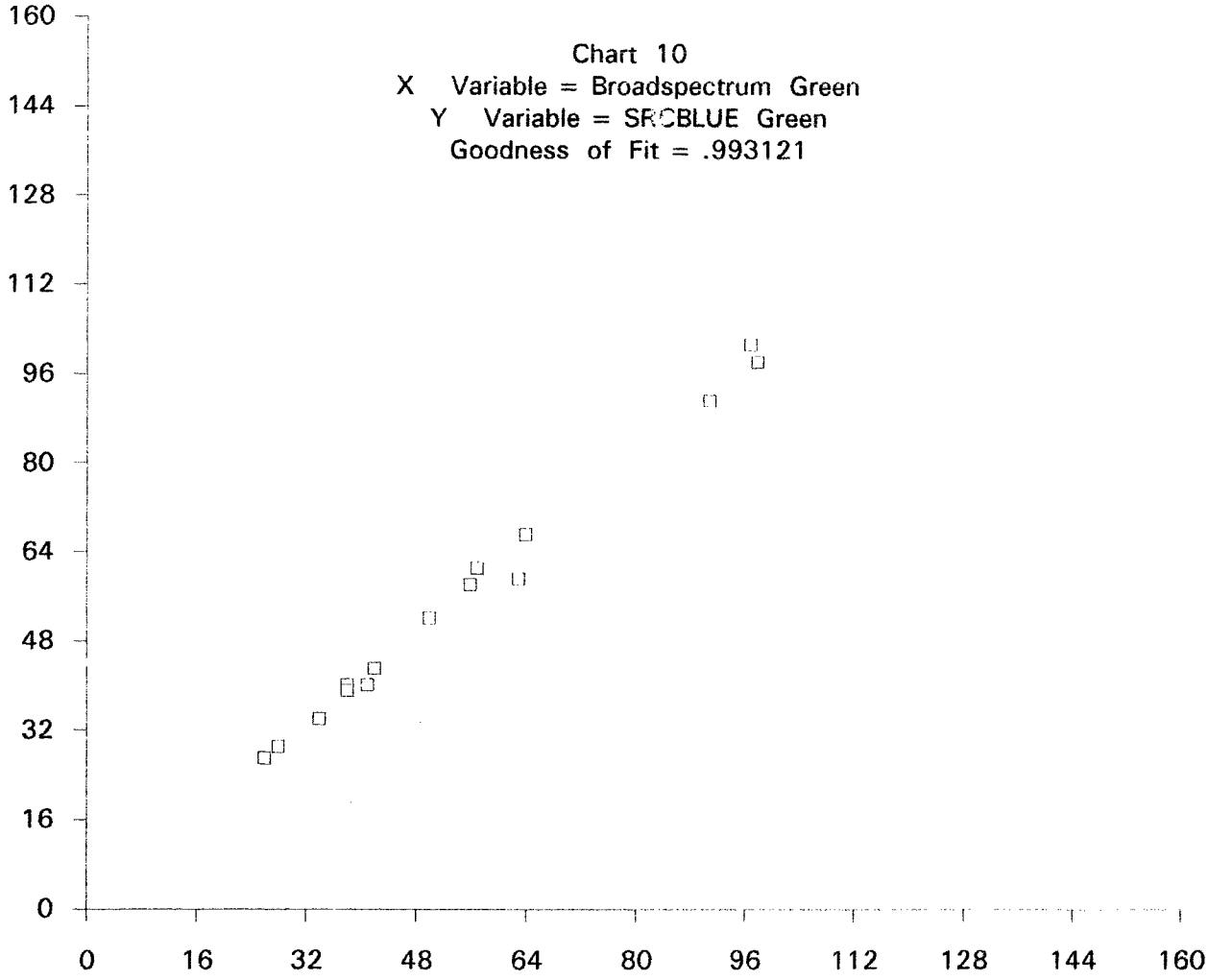
Chart 10
X Variable = Broadspectrum Green
Y Variable = SRCBLUE Green
Goodness of Fit = .993121
160
144
128
112
96
80
64
48
32
16
0
0
16
32
48
64
80
96
112
128
144
160

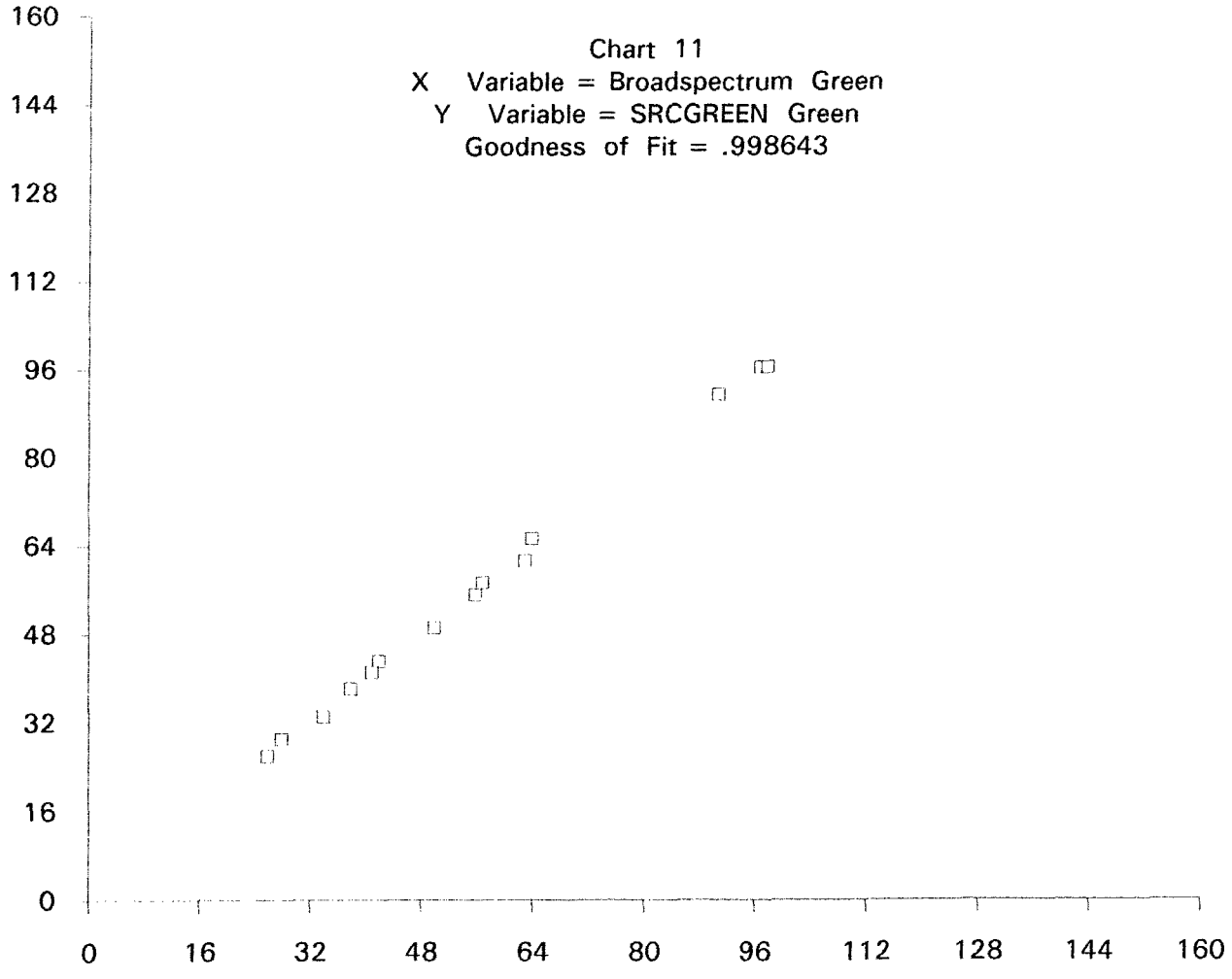
Chart 11
X Variable = Broadspectrum Green
Y Variable = SRCGREEN Green
Goodness of Fit = .998643
160
144
128
112
96
80
64
48
32
16
0
0
16
32
48
64
80
96
112
128
144
160

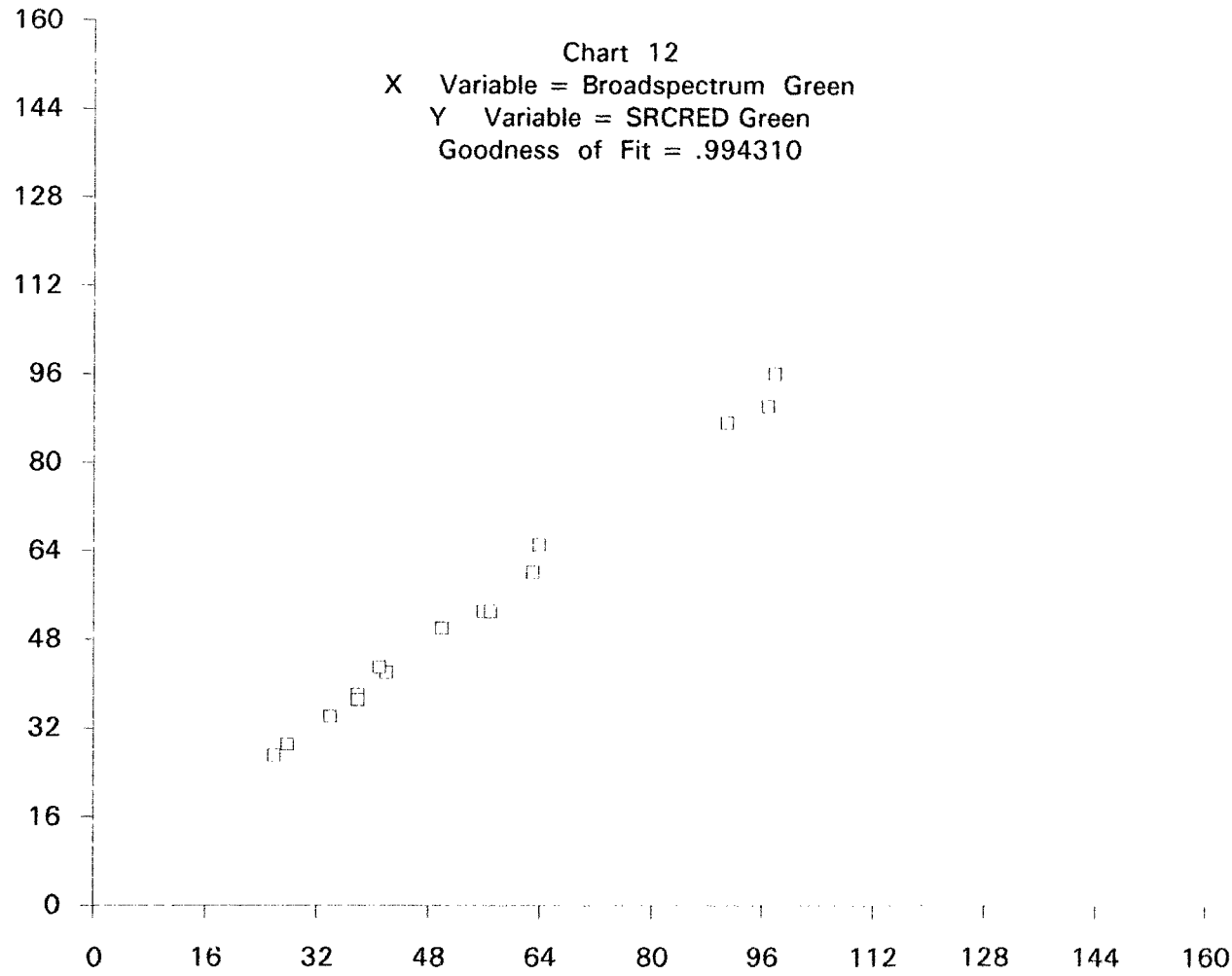
Chart 12
X Variable = Broadspectrum Green
Y Variable = SRCRED Green
Goodness of Fit = .994310
160
144
128
112
96
80
64
48
32
16
0
0
16
32
48
64
80
96
112
128
144
160

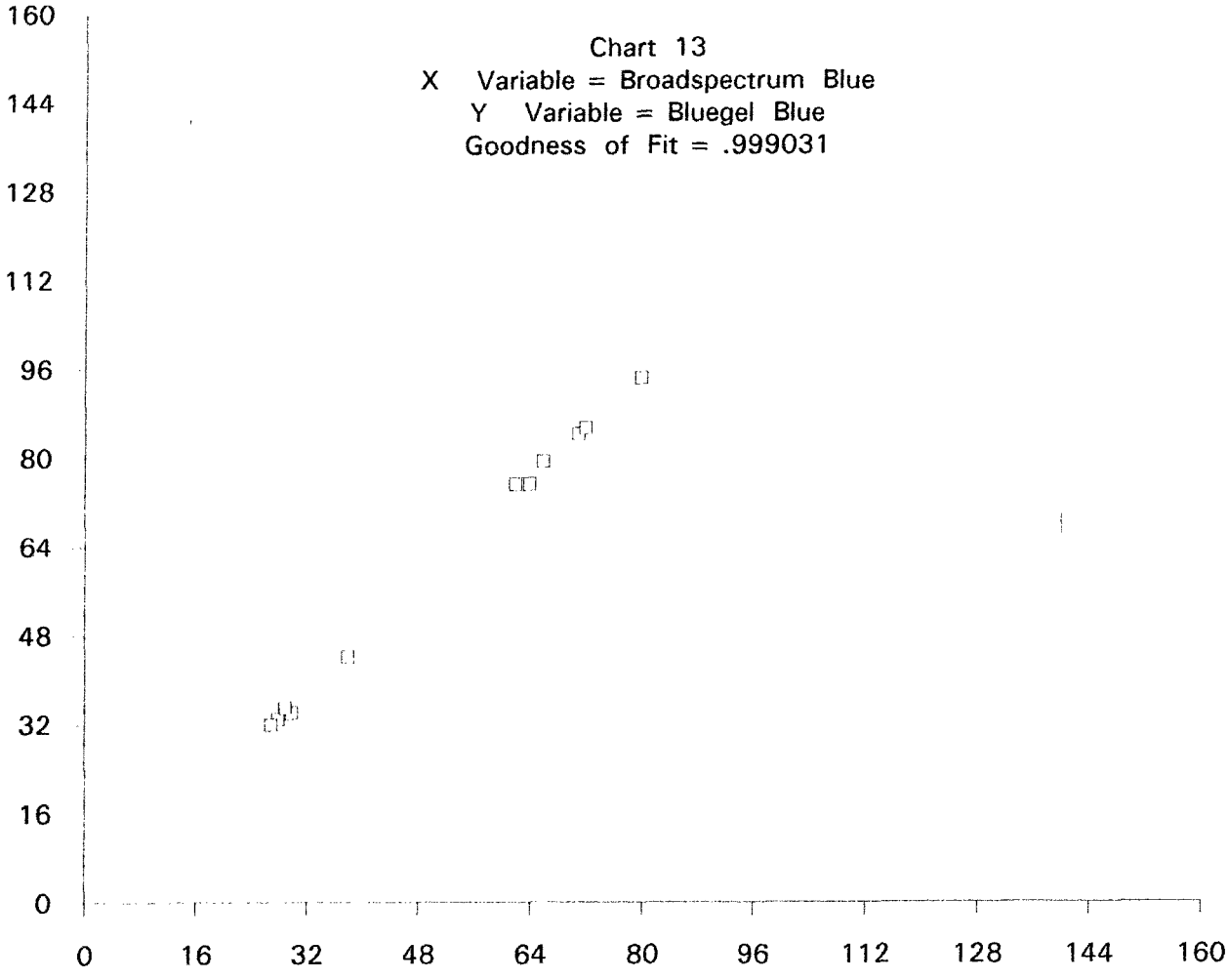
Chart 13
X Variable = Broadspectrum Blue
Y Variable = Bluegel Blue
Goodness of Fit = .999031
160
144
128
112
96
80
64
48
32
16
0
0
16
32
48
64
80
96
112
128
144
160

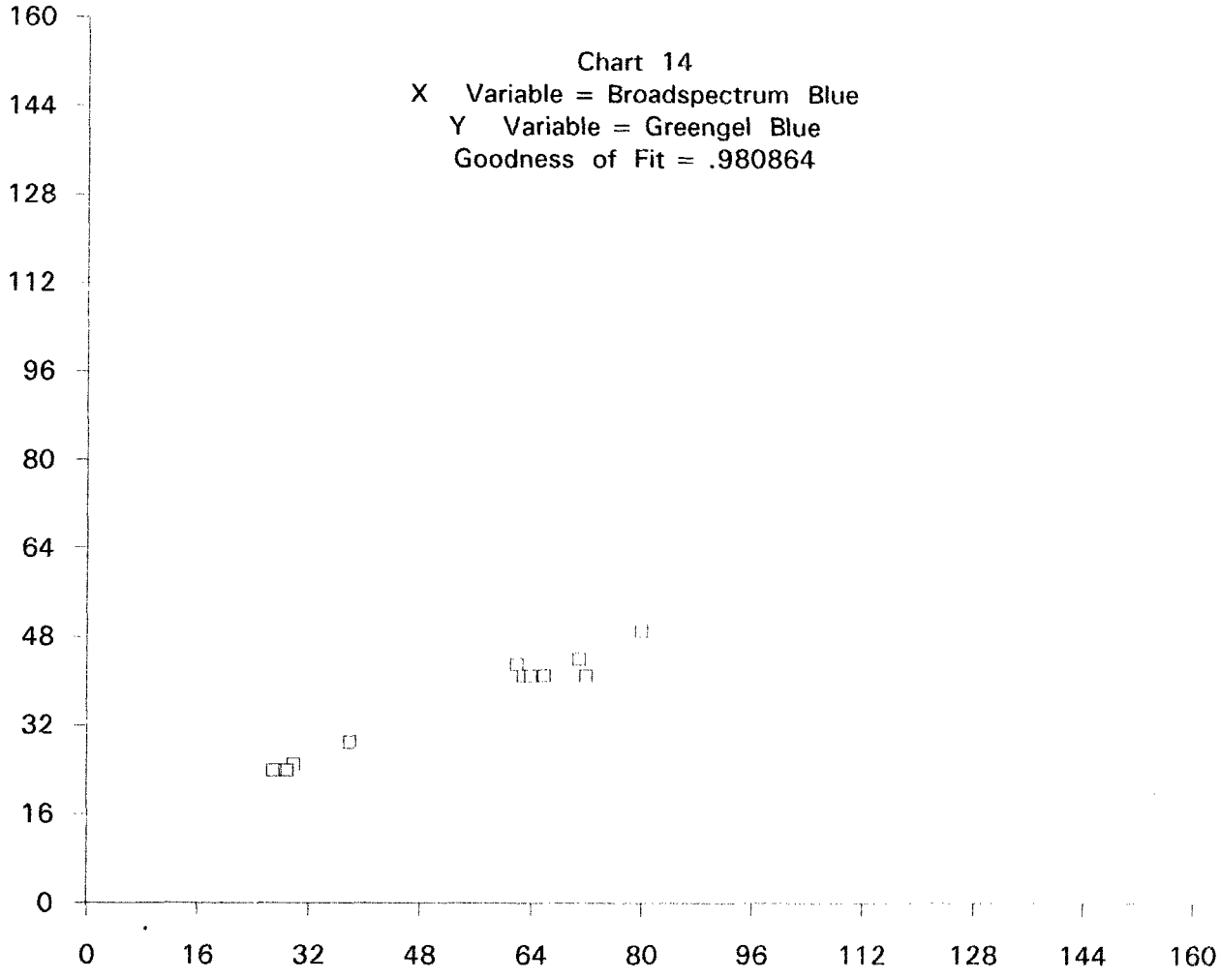
Chart 14
X Variable = Broadspectrum Blue
Y Variable = Greengel Blue
Goodness of Fit = .980864
160
144
128
112
96
80
64
48
32
16
0
0
16
32
48
64
80
96
112
128
144
160

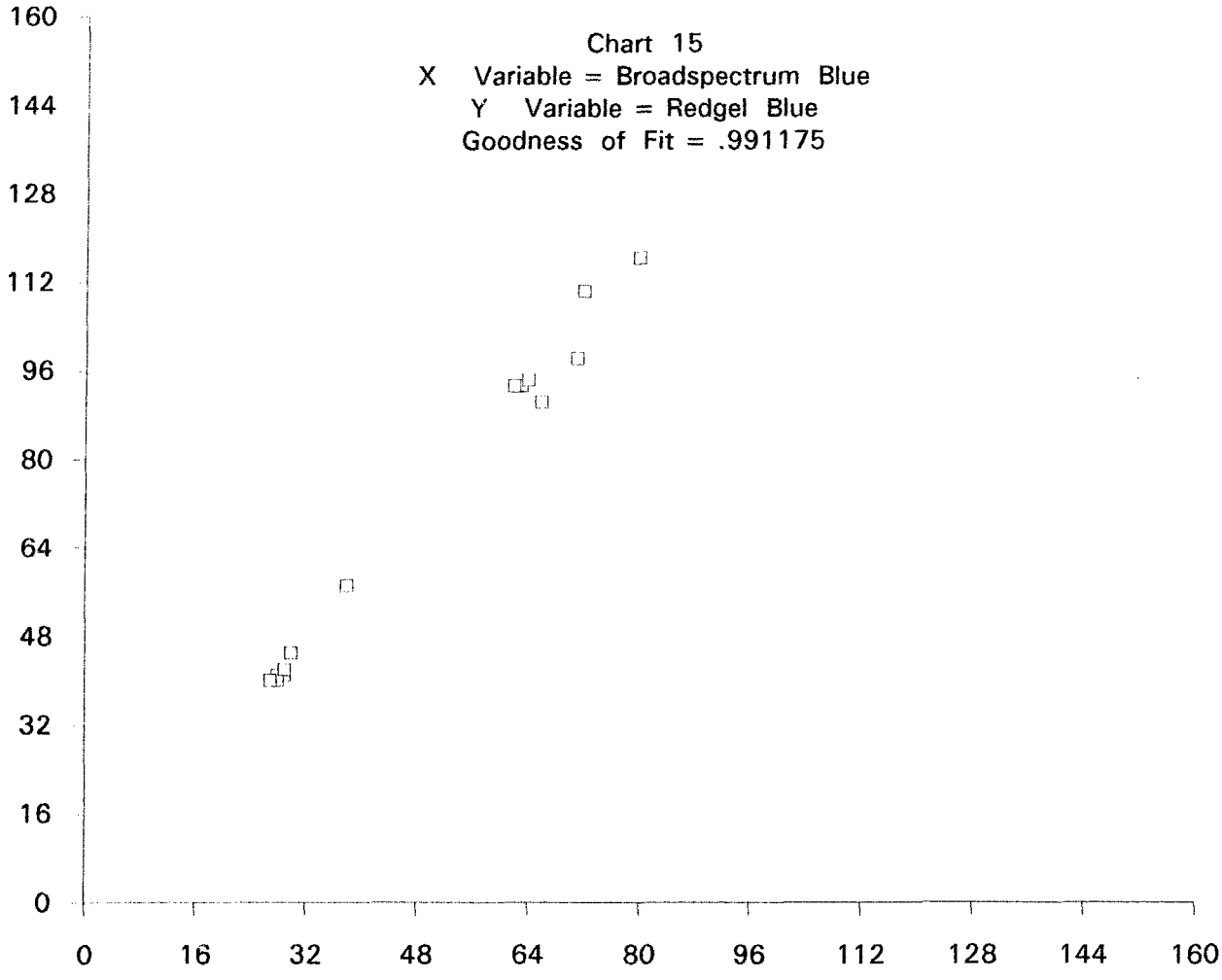
Chart 15
X Variable = Broadspectrum Blue
Y Variable = Redgel Blue
Goodness of Fit = .991175
160
144
128
112
96
80
64
48
32
16
0
0
16
32
48
64
80
96
112
128
144
160

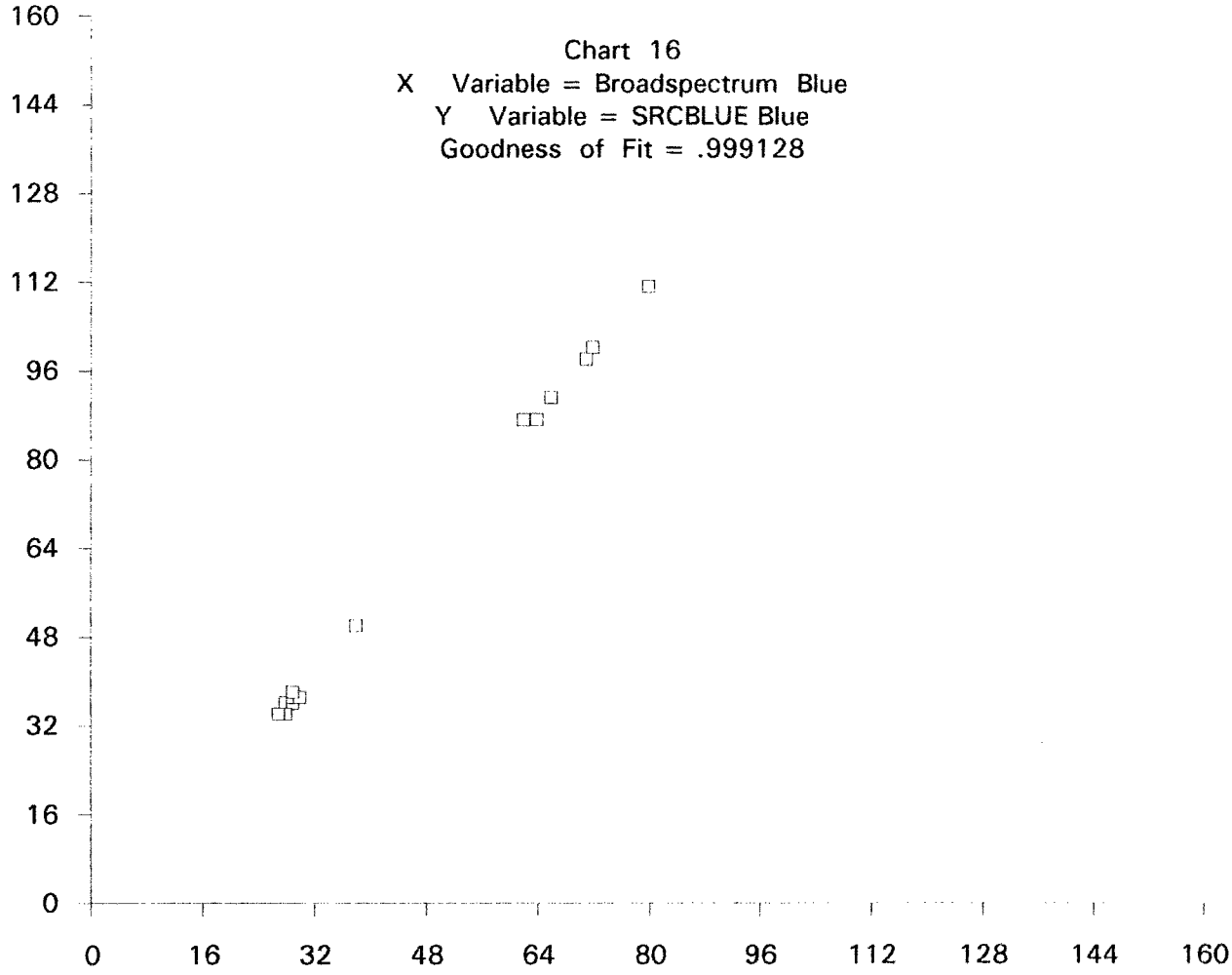
Chart 16
X Variable = Broadspectrum Blue
Y Variable = SRCBLUE Blue
Goodness of Fit = .999128
160
144
128
112
96
80
64
48
32
16
0
0
16
32
48
64
80
96
112
128
144
160

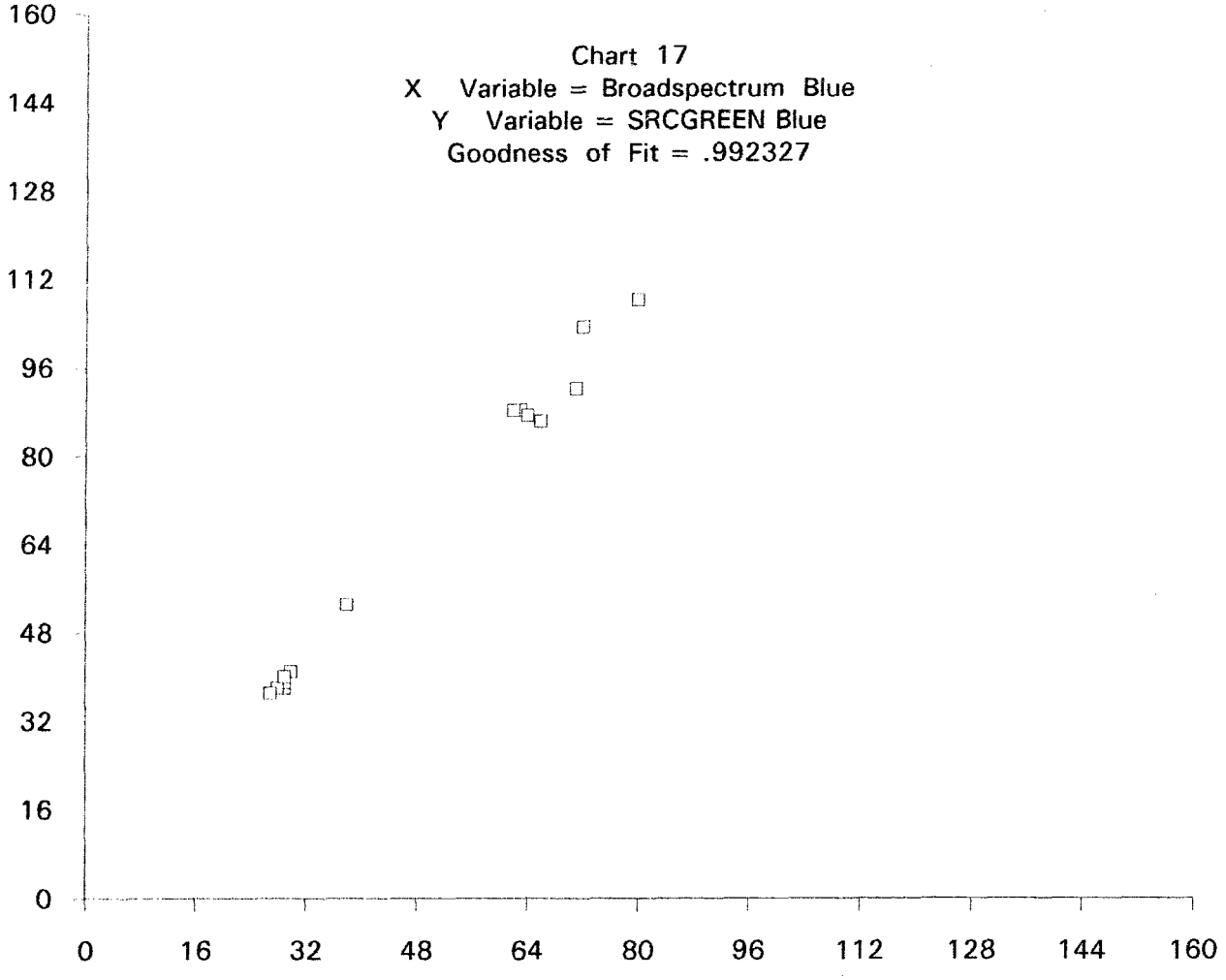
Chart 17
X Variable = Broadspectrum Blue
Y Variable = SRCGREEN Blue
Goodness of Fit = .992327
160
144
128
112
96
80
64
48
32
16
0
0
16
32
48
64
80
96
112
128
144
160

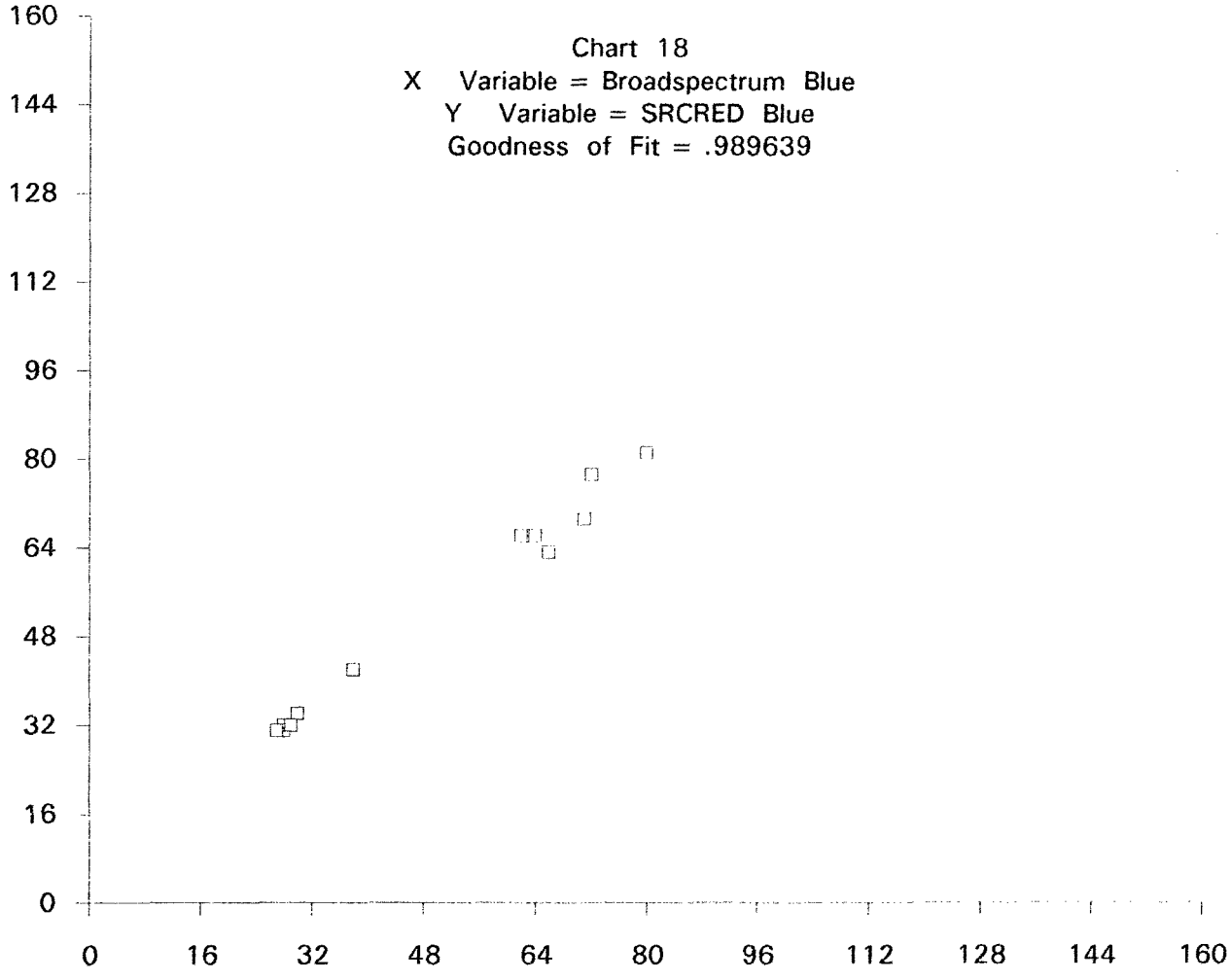
Chart 18
X Variable = Broadspectrum Blue
Y Variable = SRCRED Blue
Goodness of Fit = .989639
160
144
128
112
96
80
64
48
32
16
0
0
16
32
48
64
80
96
112
128
144
160

References

Andelson, E.A., 1982. Saturation and adaptation in the rod system, Vision Research., 22: pg. 1299.

Arend, Lawrence E. Jr., Adam Reeves, James, Schirillo and Robert Goldstein, 1991. J. Opt. Soc. Am., Vol. 8, No. 4., April, pg. 661 - 672.

Aronoff, Stan, 1982. Classification Accuracy: A User Approach: PE&RS, Vol. 48, No. 8, pg. 1299 - 1307.

Aronoff, Stan, 1985. The Minimum Accuracy Value as an Index of Classification Accuracy: PE&RS, Vol. LI, No. 1, pg. 99 - 111.

Barlow, H.B., 1965. Optic Nerve Impulses and Weber's law, Cold Spring Harbor Symposia on Quantitative Biology, Vol. XXX: pg. 539.

Barlow, H.B. and Levick, W.R., 1969, Coding of light intensity by the cat retina, Proc. Intl. Schl. Phys.- Enrico Fermi, pg. 385 - 396.

Barlow, H.B. and Levick, W.R., 1976. Threshold setting by the surround of cat retina ganglion cells, J. Physiol., 259: pg. 737.

Boller, B.K. and C.E. McBride, 1974. Experimental Black-and-White Film for Underwater Photography, Photogrammetric Engineering, 1974: pg. 673 - 681.

Boynton, Robert M., 1979. Human Color Vision. Holt, Rinehart and Winston, New York, U.S.A.

Boynton, R.M. and D.N. Whitten, 1970. Visual adaptation in monkey cones: Recordings of late receptor potentials. Science 170, pg. 1423 - 1426.

Brou, Philippe, Thomas R. Sciascia, Lynette Linden and Jerome Y. Lettvin, 1986. The Color of Things: Scientific American., Sept., pg. 84 - 94.

Brown, P. K. and Wald, G., 1964. Visual pigments in single rods and cones of the human retina: Science, Vol.144, pg. 45 - 52.

Buchsbaum, G., 1980. A spatial processor model for object color perception: J. Opt. Soc. Am., Vol. 72, No. 9, pg. 1225 - 1231.

Congalton, Russell G., 1988. A Comparison of Sampling Schemes Used in Generating Error Matrices for Assessing the Accuracy of Maps Generated from Remotely Sensed Data: PE&RS, Vol. LIV, No. 5, pg. 593 - 600.

Congalton, R.G., *et al.*, 1981. Analysis of Forest Classification Accuracy, Remote Sensing Research Report 81-1, Lyndon B. Johnson Space Center, Houston, Texas.

Cornsweet, Tom N., 1970. Visual Perception: Academic Press, New York, U.S.A.

Davis, John C., 1986. Statistics and Data Analysis in Geology, 2nd. ed. John Wiley and Sons, New York.

Edmund Scientific Company, 1994. Edmund Scientific 1995 Annual Reference Catalog for Optics, Science And Education, Volume 15N1, NJ, U.S.A.

Dekker, A.G., T.J. Malthus, M.M. Wijnen and E. Seyhan, 1992. The Effect of Spectral Bandwidth and Positioning on the Spectral Signature Analysis of Inland Waters: Remote Sensing of the Environment., N0. 41, pg. 211 - 225.

Eastman Kodak Company, 1981. Kodak Filters For Scientific And Technical Uses, Kodak Publication No. B-3, Second Edition, NY., U.S.A.

Finlayson, G.D., 1995. Color in Perspective: Centre For Systems Science, LCCR TR95-02., Simon Fraser University. Burnaby, B.C., Canada.

Finlayson, G.D., B.V. Funt and K Barnard, 1995. Color Constancy Under Varying Illumination: Centre For Systems Science, LCCR TR95-01., Simon Fraser University. Burnaby, B.C., Canada.

Fisher, Peter, F., 1994. Visualization of the Reliability in Classified Remotely Sensed Images: PE&RS, Vol. LX, No. 7, pg. 905 - 910.

Geisler, W.S., 1981.Effects of bleaching and backgrounds on the flash response of the cone system, Journal of Physiology., London., 312: pg. 413.

Gershon, Ron, Allan D. Jepson and John K. Tsotsos, 1987. From [R,G,B] to Surface Reflectance: Computing Color Constant Descriptors in Images: Porcroc. of the 2nd. Int. Conf. on Computer Vision DERCC. Vol. 20, No. 24, pg. 4175 - 4180.

Graham, Clarence H., 1965. Vision and Visual Perception. John Wiley and Sons, Inc., New York, U.S.A.

Hayhoe, M.M., Benimoff, N.I. and Hood, D.D., 1987. The time course of multiplicative and subtractive adaptation process, Vision Research., No. 27 pg. 1981.

Hayhoe, Mary and Peter, Wenderoth, 1991. Adaptation Mechanisms in Color and Brightness: From Pigments to Perception, Edited by A. Valberg and B.B. Lee, Plenum Press, New York.

Heinemann, E.G., 1955. Simultaneous brightness induction as a function- inducing and test-field luminance: J. Exptl. Psychol., Vol. 50, pg. 89 - 96.

Helson, H., 1938. Fundamental principles in color vision. I. The principle governing changes in hue, saturation, and lightness of non-selective samples in chromatic illumination: J. Exp. Psychol., Vol. 23, pg. 439 - 471.

Hilbert, David R., 1987. Color and Color Perception: A Study in Anthropocentric Realism: Centre for the Study of Language and Information, Lecture Notes Number 9., Stanford, CA., U.S.A.

Hita, E., J. Romero, A. Cervantes and L. Jiménez del Barco, 1989. The Influence of Chromatic Adaptation Upon Successive Colour Discrimination: Journal of Optics (Paris), Vol. 20, No. 2, pg. 87 - 94.

Jensen, John, R., 1986. Introductory Digital Image Processing: A Remote Sensing Perspective, Prentice-Hall, Engelwood Cliffs, New Jersey 07632.

Jöreskog, K.G., 1977. Factor analysis by least-squares and maximum-likelihood methods, Statistical methods for digital computers, Vol. 3, K. Enslein *et al* eds., John Wiley and Sons, Inc., New York, pg. 125 - 153.

Judd, D.B., 1940. Hue, saturation and lightness of surface colors with chromatic illumination: J. Opt. Soc. Am., Vol. 30, pg. 2 - 32.

Land, E.H., 1959. Experiments in Color Vision: Scientific American, May, pg. 84 - 99.

Land, E.H., 1964. The Retinex: American Scientist, Vol. 52.

Land, E.H., 1977. The Retinex Theory of Color Vision: Scientific American, Dec., pg. 108 - 128.

Land, E.H., 1983. Recent advances in retinex theory and some implications for cortical computations: color vision and the natural image: Proc. Nat. Acad. Sci., Vol. 80, pg. 5163 - 5169.

Land, E.H. and John J. McCann, 1971. Lightness and Retinex Theory: J. Opt. Soc. Am., Vol. 61, No. 1, pg. 1 - 11.

Lawley, D.N. and A.E. Maxwell, 1971. Factor analysis a statistical method 2nd. ed.: Butterworth and Co., Ltd., London, pg. 153.

Leibovic, K.N., 1990. Visual Information: Structure and Function, Science of Vision. Springer - Verlag, N.Y., pg. 313.

Lillesand, Thomas M. and Ralph W. Kiefer, 1994. REMOTE SENSING AND IMAGE INTERPRETATION.Third Edition, John Wiley and Sons, Inc., New York, U.S.A.

MacAdam, D. L., 1985. Color Measurement: Themes and Variations. Springer - Verlag, Berlin

Mac Donald, J. P., 1989. "Radiometric Corrections Through White Region Normalization", Master's thesis, Simon Fraser University.

Mahowald, Misha A. and Carver Mead, 1991. The Silicon Retina: Scientific American, May, pg. 76-82.

Maloney, Laurence T. and Brian A. Wandell, 1986. Color constancy: a method for recovering surface spectral reflectance: J. Opt. Soc. Am., Vol. 3, No. 1, pg. 29 - 33.

Marks, W.B., Dobelle, W.H. and Macnichol, E.F., 1964. Visual pigments of single primate cones: Science, Vol. 143, pg. 1181.

Marr, David, 1982. Vision: A Computational Investigation into the Human Representation and Processing of Visual Information., W.H. Freeman and Company, New York, U.S.A.

Morrison, D.F., 1976. Multivariate statistical methods, 2nd. ed.: McGraw-Hill, Inc., New York, pg. 415.

Neitz, Maureen, Jay Neitz, and Gerald H. Jacobs,1991. Spectral Tuning of Pigments Underlying Red-Green Color Vision. Science Vol. 252, pg.971-974.

Paritsis, N.C. and D.J. Stewart, 1983. A Cybernetic Approach to Colour Perception. Gordon and Breach Science Publishers, New York, U.S.A.

Peet, F., 1990. RSVGA Remote Sensing Image Analysis System User's Manual RSV1, V3.0, Eidetic Digital Imaging Ltd., 1210 Marin Park Drive, Brentwood Bay, B.C., Canada.

Philpot, William, D., 1991. The Derivative Ratio Algorithm: Avoiding Atmospheric Effects in Remote Sensing: IEEE Transactions on Geoscience and Remote Sensing., Vol. 29, No. 3, pg. 144.

Rosenfield, George H., 1986. Analysis of Thematic Map Classification Error Matrices: PE&RS, Vol. LII, No. 5, pg. 681 - 686.

Rosenfield, George H. and Katherine Fitzpatrick-Lins, 1986. A Coefficient of Agreement as a Measure of Thematic Classification Accuracy: PE&RS, Vol. LII, No. 2, pg. 223 - 227.

Rushton, W.A.H., 1961. The cone pigments of human fovea in colour blind and normal: Visual problems of colour, symp.

Sacks, O., 1995. The Case of the Colorblind Painter, AN ANTHROPOLOGIST ON MARS. Random House Canada Ltd., Mississauga, Ont., pp. 3 - 41.

Shipley, Thorne and Harold Shore, 1990. THE HUMAN TEXTURE VISUAL FIELD: FOVEA-TO-PERIPHERY PATTERN RECOGNITION. Pattern Recognition, Vol.23, No.11: pg. 1215 - 1221.

Story, Michael and Russell G. Congalton, 1986. Accuracy Assessment: A User's Perspective, PE&RS, Vol. LII, No. 3, pg. 397 - 399.

Vora, Poorvi L. and H. Joel Trussell, 1993. Measurement of goodness of a set of color-scanning filters: J. Opt. Soc. Am. A., Vol. 10, No. 7, pp. 1499 - 1508.

Walraven, J. and Valeton, J.M., 1984. Visual adaptation and response saturation,: Limits in Perception, A.J. van Doorn, W.A. van de Grind and J. J. Koenderink, eds., VNU Science Press, Utrecht.

Wandell, Brian A., 1987. The Synthesis and Analysis of Color Images: IEEE Transactions on Pattern Analysis and Machine Intelligence, Vol. PAMI-9, No. 1, pg. 2 - 13.

Wang, Y.F., Nitin, Karandikar and J.K. Aggaewal, 1991. Analysis Of Video Image Sequences Using Point And Line Correspondences: Pattern Recognition, Vol.24, No.11, pg. 1065 - 1084.

Zacharias, Mark, Olaf Niemann and Gary Borstad, 1992. An Assessment and Classification of a Multispectral Bandset for the Remote Sensing of Intertidal Seaweeds: Canadian Journal of Remote Sensing, Vol. 18, No. 4., pg. 263 - 274.